

**A Kinetic Investigation of As and Se Speciation within Coal Combustion Flue
Gases using *ab initio* Methods**

by

David Raymond Urban

A Thesis

Submitted to the Faculty

of the

WORCESTER POLYTECHNIC INSTITUTE

in partial fulfillment of the requirements for the

Degree of Master of Science

in

Chemical Engineering

May 2006

APPROVED:

Dr. Jennifer Wilcox, Major Adviser

Dr. David DiBiasio, Head of Department

Abstract

In the technologically driven information age, the consumption of power is as vital to daily life as food and shelter. The generation of that power comes from a variety of sources of which coal is the predominant provider of electrical energy. Coal combustion is a well-known technology and the United States possesses the most abundant coal deposits on Earth, however, the drawback accompanying this process is the significant emissions which are released during combustion. Over the years, much effort has gone into reducing the emissions of majority constituent elements CO_2 , CO , NO_x , SO_x , etc. but it is only in the last decade or so that much attention has been given to the trace metals present within coal. Most of the work into examining these trace metals has been upon Hg and how it speciates within the flue gas in order to determine the most effective means of removal. In this study, the trace metals arsenic (As) and selenium (Se) will be investigated in a similar manner to evaluate the speciation of these elements. While previous experimental work has been performed in this area, it has been limited to thermodynamic studies which determine the speciation after equilibrium has been reached, this ignores the fact the residence times within the flue are often only several minutes during which time rapid quenching is taking place. This study takes a different approach by examining the speciation using computational chemistry which affords the advantage of being able to perform a kinetic study which is more useful in creating a flue gas model. Using *ab initio* the properties of various As and Se species can be evaluated compared to existing experimental data for validation. After which, a number of reactions may be selected and the structure of the transition state for each identified. Once the properties of the transition structure are known, the appropriate kinetic model, be it Transition State Theory, RRKM Theory, etc. can be applied and the rate constant determined. It is by the determination of these rate constants that the kinetic model of the flue gas can be improved and a more accurate depiction of the speciation of these trace metals created.

Acknowledgements

The completion of this work required a number of individuals and groups contributed invaluable assistance. The following is a list of those whom deserved to be recognized for their efforts:

Thesis Advisor:

Dr. Jennifer Wilcox

Lab Mates:

Michael Brunetti, Chandrashekhar Sonwane, Bihter Padak, Erdem Sasmaz, and Micheal Plummer

Department Administrative Assistants:

Sandra Natale, Joseph Kaupu, and Elaine Brady

Technical Assistance:

Center for Computational Science and the Scientific Computing and Visualization Group at Boston University and the National Science Foundation

In addition, thanks go out to the all the Chemical Engineering faculty, students, and staff for their support.

Table of Contents

List of Figures	6
List of Tables	7
Chapter 1: Introduction	8
Chapter 2: Background	10
2.1 Coal Energy Overview	10
2.2 Environmental	14
2.2.1 Arsenic	14
2.2.2 Selenium	15
Chapter 3: Theory and Methodology	16
3.1 Computational Chemistry	16
3.2 Kinetics and Thermodynamics	18
3.2.1 Potential Energy Surface Development	18
3.2.2 Bimolecular Reactions with True Transition State	19
3.3.3 Unimolecular Reactions with True Transition State	20
3.3.4 Reactions without True Transition State	27
3.3.5 Thermodynamics	29
Chapter 4: Results and Discussion	30
4.1 Theory Validation	30
4.1.1 Species Geometry	30
4.1.2 Vibrational Frequency	36
4.1.3 Reaction Enthalpy	41
4.2 Complete Arsenic Reactions	47
4.2.1 $\text{As} + \text{O}_2 \rightarrow \text{AsO} + \text{O}$	47
4.2.2 $\text{As} + \text{OH} \rightarrow \text{AsO} + \text{H}$	52
4.2.3 $\text{As} + \text{HCl} \rightarrow \text{AsCl} + \text{H}$	57
4.3 Complete Selenium Reactions	60
4.3.1 $\text{Se} + \text{O}_2 \rightarrow \text{SeO} + \text{O}$	60
4.3.2 $\text{Se} + \text{H}_2 \rightarrow \text{SeH}_2$	65
4.4 Incomplete Reactions	69
4.4.1 Reactions to with only a Thermodynamic Study	69
4.4.2 Reactions with Thermodynamic Study and PES	71
4.5 Overall Discussion	82
Chapter 5: Conclusions	85
Appendix A: Basis Sets	91
A.1 Arsenic	92
A.2. Selenium	97
A.3. Chlorine	102
A.4. Hydrogen	105
A.5. Oxygen	106
Appendix B: Raw Data, Bimolecular Reactions using Transition State Theory	109
B.1. $\text{As} + \text{O}_2 \rightarrow \text{AsO} + \text{O}$ (QCISD/ECP28MWB)	110
B.2. $\text{As} + \text{OH} \rightarrow \text{AsO} + \text{H}$ (QCISD(T)/ECP28MWB)	112
B.3. $\text{As} + \text{HCl} \rightarrow \text{AsCl} + \text{H}$ (QCISD(T)/6-311++G(3df,3pd))	114
B.4. $\text{Se} + \text{O}_2 \rightarrow \text{SeO} + \text{O}$ (CCSD/RECP28VDZ)	116

Appendix C: Raw Data, Unimolecular Reactions using RRKM Theory	118
C.1. $\text{Se} + \text{H}_2 \rightarrow \text{SeH}_2$ (CCSD(T)/6-311++G(3df,3pd))	119
Appendix D: Raw Data, Thermodynamic Data	120
D.1. $\text{As} + \text{O}_2 \rightarrow \text{AsO} + \text{O}$ (QCISD/ECP28MWB)	121
D.2. $\text{As} + \text{OH} \rightarrow \text{AsO} + \text{H}$ (QCISD(T)/ECP28MWB)	123
D.3. $\text{As} + \text{HCl} \rightarrow \text{AsCl} + \text{H}$ (QCISD(T)/6-311++G(3df,3pd))	125
D.4. $\text{As} + \text{O} \rightarrow \text{AsO}$ (QCISD(T)/ECP28MWB)	127
D.5. $\text{As} + \text{OH} \rightarrow \text{AsH} + \text{O}$ (QCISD/ECP28MWB).....	129
D.6. $\text{Se} + \text{O}_2 \rightarrow \text{SeO} + \text{O}$ (CCSD/RECP28VDZ).....	131
D.7. $\text{Se} + \text{O} \rightarrow \text{SeO}$ (QCISD(T)/6-311++G(3df,3pd)).....	133
D.8. $\text{Se} + \text{OCl} \rightarrow \text{SeO} + \text{Cl}$ (CCSD/RECP28VDZ)	135
D.9. $\text{Se} + \text{O}_2 \rightarrow \text{SeO}_2$ (QCISD(T)/6-311++G(3df,3pd))	137
D.10. $\text{SeO} + \text{O} \rightarrow \text{SeO}_2$ (QCISD(T)/6-311++G(3df,3pd)).....	139
D.11. $\text{SeO} + \text{O}_2 \rightarrow \text{SeO}_2 + \text{O}$ (QCISD(T)/ECP28MWB).....	141
D.12. $\text{Se} + \text{H}_2 \rightarrow \text{SeH}_2$ (CCSD(T)/6-311++G(3df,3pd)).....	143
Bibliography	145

List of Figures

Figure 1: Coal Consumption by Sector.....	12
Figure 2: Production by Mining Method	12
Figure 3: Energy Production by Source for 2000	13
Figure 4: Electricity Net Generation by Source for 2000.....	13
Figure 5: PED Unimolecular Decomposition Reaction w/ True Transition State.....	25
Figure 6: Barrierless Reaction (No True Transition State).....	28
Figure 7: $\text{As} + \text{O}_2 \rightarrow \text{AsO} + \text{O}$ (PES).....	49
Figure 8: $\text{As} + \text{O}_2 \rightarrow \text{AsO} + \text{O}$ (Contour Plot)	49
Figure 9: Rate Constant as a Function of Temperature ($\text{As} + \text{O}_2 \rightarrow \text{AsO} + \text{O}$)	50
Figure 10: Rate Constant as a Function of Temperature ($\text{AsO} + \text{O} \rightarrow \text{As} + \text{O}_2$)	50
Figure 11: Equilibrium Constant as a Function of Temperature ($\text{As} + \text{O}_2 \rightarrow \text{AsO} + \text{O}$)	51
Figure 12: $\text{As} + \text{OH} \rightarrow \text{AsO} + \text{H}$ (PES)	54
Figure 13: $\text{As} + \text{OH} \rightarrow \text{AsO} + \text{H}$ (Contour Plot).....	54
Figure 14: Rate Constant as a Function of Temperature ($\text{As} + \text{OH} \rightarrow \text{AsO} + \text{H}$).....	55
Figure 15: Rate Constant as a Function of Temperature ($\text{AsO} + \text{H} \rightarrow \text{As} + \text{OH}$).....	55
Figure 16: Equilibrium Constant as a Function of Temperature ($\text{As} + \text{OH} \rightarrow \text{AsO} + \text{H}$).....	56
Figure 17: $\text{As} + \text{HCl} \rightarrow \text{AsCl} + \text{H}$ (PES).....	58
Figure 18: $\text{As} + \text{HCl} \rightarrow \text{AsCl} + \text{H}$ (Contour Plot).....	58
Figure 19: Rate Constant as a Function of Temperature ($\text{As} + \text{HCl} \rightarrow \text{AsCl} + \text{H}$).....	59
Figure 20: Rate Constant as a Function of Temperature ($\text{AsCl} + \text{H} \rightarrow \text{As} + \text{HCl}$).....	59
Figure 21: $\text{Se} + \text{O}_2 \rightarrow \text{SeO} + \text{O}$ (PES).....	62
Figure 22: $\text{Se} + \text{O}_2 \rightarrow \text{SeO} + \text{O}$ (Contour Plot)	62
Figure 23: Rate Constant as a Function of Temperature ($\text{Se} + \text{O}_2 \rightarrow \text{SeO} + \text{O}$)	63
Figure 24: Rate Constant as a Function of Temperature ($\text{SeO} + \text{O} \rightarrow \text{Se} + \text{O}_2$)	63
Figure 25: Equilibrium Constant as a Function of Temperature ($\text{Se} + \text{O}_2 \rightarrow \text{SeO} + \text{O}$)	64
Figure 26: $\text{Se} + \text{H}_2 \rightarrow \text{SeH}_2$ (PES).....	67
Figure 27: $\text{Se} + \text{H}_2 \rightarrow \text{SeH}_2$ (Contour Plot).....	67
Figure 28: Rate Constant as a Function of Temperature ($\text{SeH}_2 \rightarrow \text{Se} + \text{H}_2/\text{Ar bath gas}$)	68
Figure 29: Equilibrium Constant as a Function of Temperature ($\text{Se} + \text{H}_2 \rightarrow \text{SeH}_2$)	68
Figure 30: Equilibrium Constant as a Function of Temperature ($\text{As} + \text{O} \rightarrow \text{AsO}$).....	70
Figure 31: Equilibrium Constant as a Function of Temperature ($\text{SeO} + \text{O}_2 \rightarrow \text{SeO}_2 + \text{O}$).....	70
Figure 32: Equilibrium Constant as a Function of Temperature ($\text{As} + \text{OH} \rightarrow \text{AsH} + \text{O}$).....	75
Figure 33: $\text{As} + \text{OH} \rightarrow \text{AsH} + \text{O}$ (PES)	76
Figure 34: Equilibrium Constant as a Function of Temperature ($\text{As} + \text{OCl} \rightarrow \text{AsO} + \text{Cl}$).....	76
Figure 35: $\text{As} + \text{OCl} \rightarrow \text{AsO} + \text{Cl}$ (PES).....	77
Figure 36: Equilibrium Constant as a Function of Temperature ($\text{Se} + \text{O}_2 \rightarrow \text{SeO}_2$).....	77
Figure 37: Equilibrium Constant as a Function of Temperature ($\text{SeO} + \text{O} \rightarrow \text{SeO}_2$)	78
Figure 38: Equilibrium Constant as a Function of Temperature ($\text{Se} + \text{OCl} \rightarrow \text{SeO} + \text{Cl}$).....	78
Figure 39: Equilibrium Constant as a Function of Temperature ($\text{SeO} + \text{O} \rightarrow \text{SeO}$).....	79
Figure 40: $\text{Se} + \text{O}_2 \rightarrow \text{SeO}_2$ (PES).....	79
Figure 41: $\text{SeO} + \text{O} \rightarrow \text{SeO}_2$ (PES)	80
Figure 42: $\text{Se} + \text{OCl} \rightarrow \text{SeO} + \text{Cl}$ (PES).....	80
Figure 43: $\text{Se} + \text{O} \rightarrow \text{SeO}$ (PED).....	81

List of Tables

Table 1: State Combinations of Example Molecule	26
Table 2: Sum and Average Density of States of Example Molecule.....	26
Table 3: Arsenic Species Geometry (1)	33
Table 4: Arsenic Species Geometry (2)	34
Table 5: Selenium Species Geometry	35
Table 6: Arsenic Species Vibrational Frequencies (1)	38
Table 7: Arsenic Species Vibrational Frequencies (2)	39
Table 8: Selenium Species Vibrational Frequencies	40
Table 9: Arsenic Reaction Enthalpies (1)	43
Table 10: Arsenic Reaction Enthalpies (2)	44
Table 11: Selenium Reaction Enthalpies (1)	45
Table 12: Selenium Reaction Enthalpies (2)	46
Table 13: Thermodynamic Parameters for Reactions w/o PES's	70
Table 14: Thermodynamic Parameters for Reactions w/ PES's	75
Table 15: Completed Reactions Kinetic/Thermodynamic Analysis.....	84
Table 16: Incomplete Reactions Kinetic/Thermodynamic Analysis	84
Table 17: Average Deviations: Oxygen vs. no Oxygen	89
Table 18: Average Deviations by Basis Set.....	89
Table 19: Equilibrium Data, All Reactions.....	90

Chapter 1: Introduction

In today's political climate, the issue of energy independence is one of the most important challenges facing the United States. While crude oil remains the root source of virtually all fuel for transportation and heating, the majority of electricity generation still comes from coal, in fact, roughly 50% of the electricity generated in the US comes from coal combustion. Coal has many advantages which make it an attractive energy source, it is a well-tested technology, it is relatively cheap, and most importantly, the US possesses some of the world's most abundant coal deposits. The major drawback of coal, and the reason why alternative energy sources were first examined, is the particulate matter that is created during its combustion. However, the progress in clean-coal technology has sparked renewed interest in coal as an energy source.

Over the years, many techniques have been developed in trapping these particulates to prevent releases into the atmosphere, and they have been largely successful in removing the major-constituent elements (C, N, S, etc.). However, the most recent concerns have been in regard to the release of species containing trace metals into the environment. The most notable of these is Hg, however, species of As and Se are beginning to be examined to limit their potential release as well. The majority of experimental work into their removal has centered on the use of Ca-based sorbents to adsorb the desired compounds.^{1,2,3}

The difficulty in devising effective removal strategies of trace metal compounds is in knowing which species of each metal is the major constituent. To determine the speciation in the flue gas, knowledge of the kinetic and thermodynamic parameters of all possible reactions involving these elements is required. Although several empirical studies have been conducted,^{4, 5, 6} experimentation has proven to be tremendously problematic; the high temperature of the flue gas makes conditions dangerous to replicate and the nature of many of the species themselves makes accurate analytical detection all but impossible. Fortunately, the progress in computational chemistry techniques and technology affords another option in determining the kinetic and thermodynamic parameters for reactions involving trace metals.

By utilizing computational chemistry, the parameters for any reaction can be determined theoretically. In particular, *ab initio* methodology evaluates molecular properties without any empirical data, being based upon first principles instead. By making use of this technique, even those radical species which are only present for brief periods can be studied and, therefore, a more accurate picture of the flue gas environment can be created. By combining the computational results of the pertinent species with the various theories concerning the determination of reaction kinetics, the parameters important for simulation purposes can be calculated. Both traditional Transition State Theory (TST) and the theory developed by Rice-Ramsperger-Kassel-Marcus (RRKM) are employed in determining the pre-exponential frequency factor and the activation energy of each bimolecular and unimolecular reaction considered, respectively.

In this way, the kinetic parameters of every reaction can be incorporated into a kinetic model of the flue gas which may then be used to ascertain the flue gas composition at any variety of process conditions. The ability to examine, in simulation, the effect that a different coal composition, oxygen ratio, quench rate, etc. will have upon the speciation allows the process operators to predict how a sudden change in an input variable, or combination of variables, will influence output conditions. While some deviation between the model and the real process is to be expected, it would at least provide a sound starting point from which to begin an assessment. By utilizing such a comprehensive model with additional analytical monitoring, it is hoped that a more accurate depiction of the flue gas can be obtained over a variety of conditions, and that this knowledge will assist in the development of more effective strategies for the removal of trace metal species.

Chapter 2: Background

2.1 Coal Energy Overview

The combustion of coal to generate energy has been in practice since the Industrial Revolution, but it was not until 1885 when it became the primary energy source in the United States, a title which it held until 1951 when it was displaced by crude oil and natural gas. It was coal which was the driving force behind the rapid industrialization of the late 19th century, being used to power the manufacturing and residential sectors in the east as well as fueling the railroad and steel industries which were the engine of westward expansion. After World War II, as shipment by rail was replaced by gasoline and diesel fueled trucks and natural gas began taking over the home heating market, the coal industry was forced to change its focus. The ongoing electrification of the country provided the most plausible alternative and, as shown in Figure 1, by 1965 electrical utilities were the largest consumers of coal.

As the demand for electricity increased, the total consumption of coal, likewise, increased. Developments in coal mining technology and techniques have dramatically increased the capacity and productivity of the mining industry. Figure 2 shows how the improvements in surface mining have increased the output from those mines by almost 7 times between 1950 and 2000. Overall, the rate of coal production in the United States increased from 0.7 short tons per hour per miner in 1949 to 6.5 in 1999. These increases in capacity and productivity drove down the price of coal substantially so that the average price of coal in 1999 was 47% lower than in 1949. This steady price decrease, in contrast to the sharp fluctuations in the oil and gas markets, has contributed to the re-emergence of coal as the leading energy source in the US. In 1998, US coal production reached a record 1.12 billion short tons which has since decreased slightly so that in 2000 this number was 1.08 billion. As shown in Figure 3, as of 2000 coal comprised roughly 1/3 of the total energy generated in the United States; more specifically, coal was the source of just over half of the electricity created in that same year (Figure 4).

Examination of both the long and short term trends in coal energy and its competition suggest that the combustion of coal to generate raw energy or create electricity will continue well into the foreseeable future. The unfortunate drawback of coal, the amount of pollutants created during the combustion process, therefore, becomes quite significant. Knowledge of the species emitted during combustion, not just bulk compounds like CO₂ and CH₄ but also trace element constituents, is of great importance.

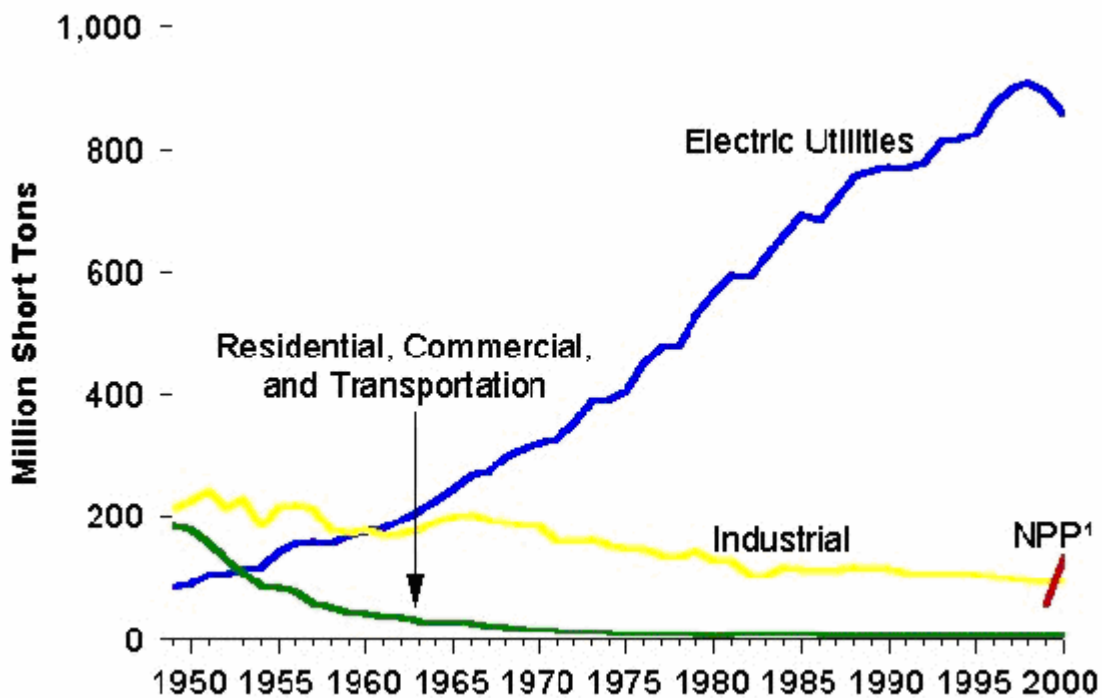


Figure 1: Coal Consumption by Sector
<http://www.eia.doe.gov/emeu/aer/eh/coal.html>

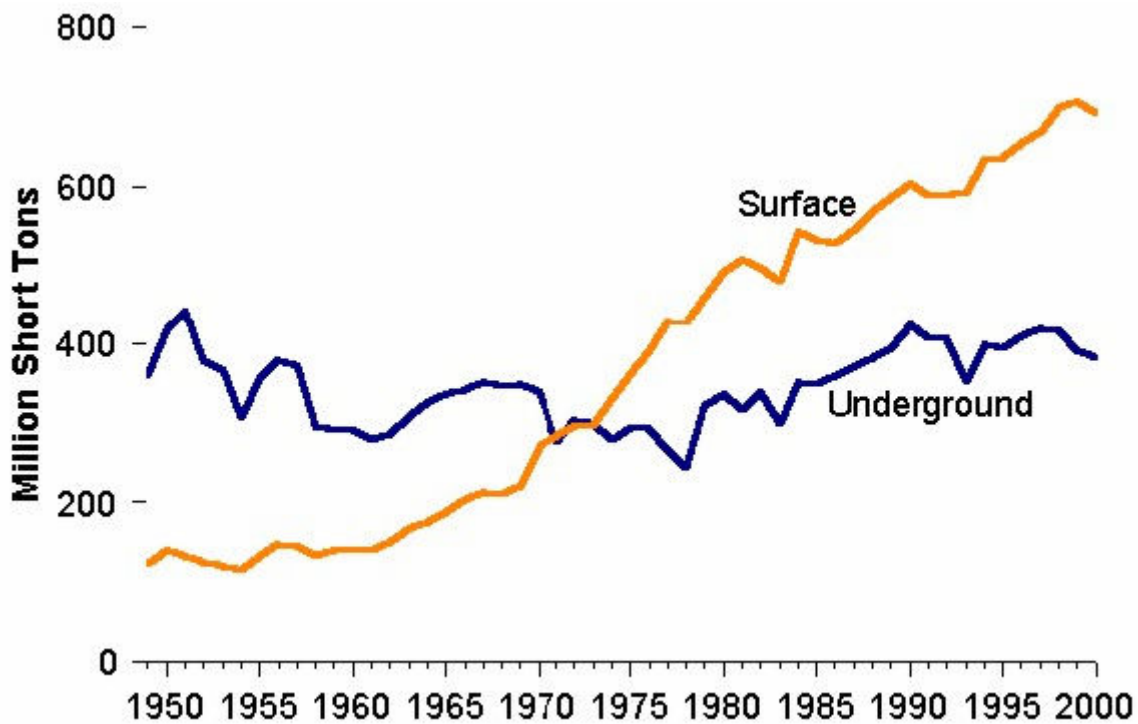


Figure 2: Production by Mining Method
<http://www.eia.doe.gov/emeu/aer/eh/coal.html>

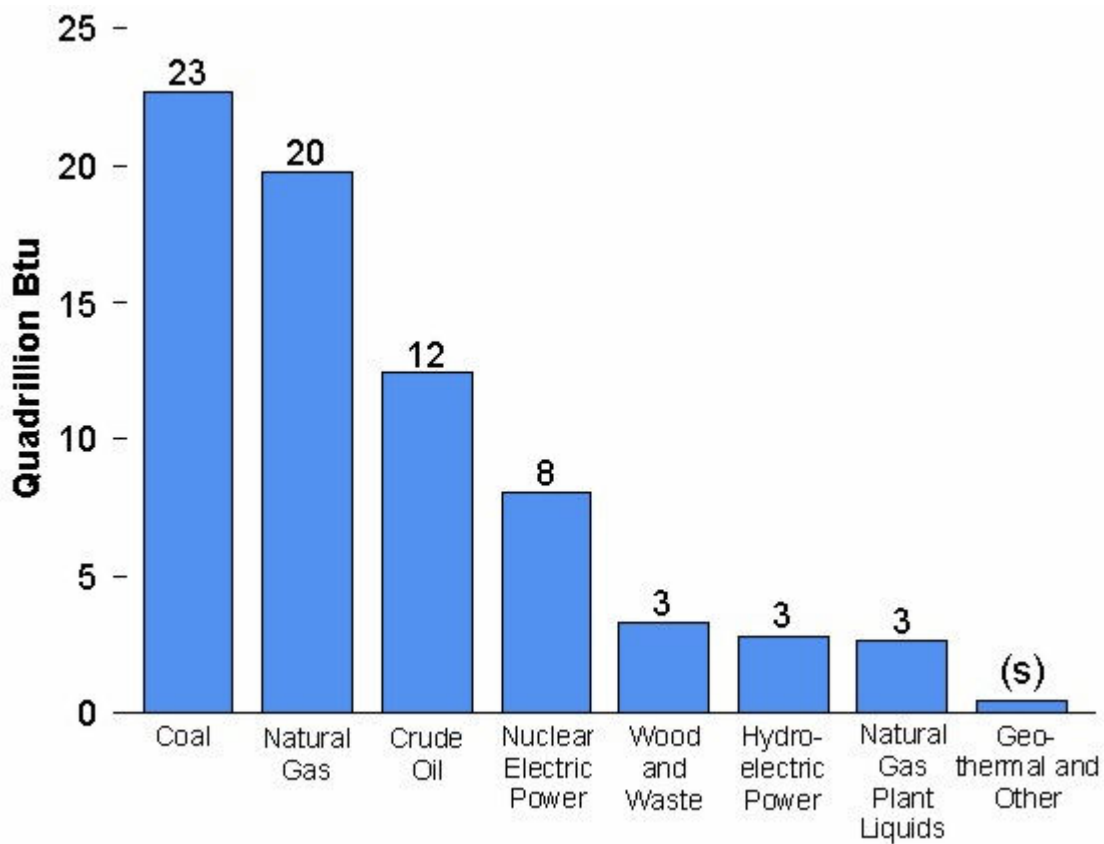


Figure 3: Energy Production by Source for 2000
<http://www.eia.doe.gov/emeu/aer/eh/coal.html>

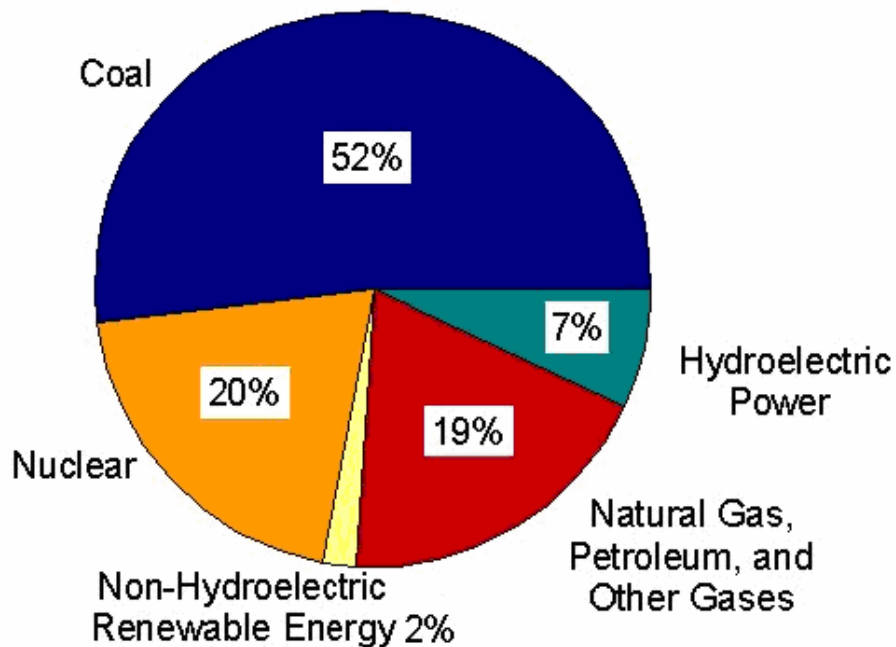


Figure 4: Electricity Net Generation by Source for 2000
<http://www.eia.doe.gov/emeu/aer/eh/coal.html>

2.2 Environmental

2.2.1 Arsenic

One of the most toxic naturally derived metals, arsenic is used in a myriad of industrial manufacturing applications in such products as paints, agricultural products (fungicides, insecticides, pesticides, and herbicides), wood preservatives, semiconductors, metal alloys, and certain types of glass. It can be found in many mineral species, all soils (in various forms), and in all waters (concentrations ranging from 1 to 2 $\mu\text{g/L}$).^{7,8} The most prevalent sources of anthropogenic arsenic production, however, are from mining operations and both coal and petroleum-based power plants. In 2000, the amount of arsenic generated by coal/petroleum was 23.9 thousand tons accounting for about 46% of the annual world gross production, an increase of almost 20 thousand tons since 1900.⁹ The majority of this arsenic gets deposited in the soil rather than in the world's oceans due to the fact that the retention time of arsenic in the atmosphere is only 7-10 days, limiting the transport capacity.¹⁰ This presence in the soil has led to much concern regarding the effect it may have on the surrounding ecosystems.

Of particular concern regarding arsenic is its effect on humans. Long term exposure to arsenic can have adverse effects on areas of the body including the skin, and the gastrointestinal, cardiovascular, and respiratory systems causing conditions such as hyperpigmentation, diarrhea, cardiac arrhythmia, and cardiomyopathy as well as malignancies of the skin, lungs, liver, kidneys, and bladder. The most seriously affected area, however, is the neurological system where the effects of arsenic toxicity manifest as behavioral changes, confusion, and memory loss. The most common source of long term exposure to arsenic is from contamination of drinking water caused by leaching into aquifers from natural geological sources¹¹. In particular areas of the world, such as Bangladesh and West Bengal India, this is of great concern as groundwater arsenic concentrations have been found to be above the World Health Organization's maximum permissible limit of 50 $\mu\text{g/l}$.¹²

2.2.2 Selenium

Selenium has the unique property that its resistance to the flow of electricity is greatly affected by the amount of light shining on it; as the brightness of the light increases, the better selenium is able to conduct electricity. This makes it an ideal component for use in light sensitive devices such as photo cells, electric eyes, light meters in cameras and photocopiers, and solar cells, as well as in semiconductors and steel additives. Anthropogenic selenium in the environment is largely due to the mining, processing, and combustion of coal which releases selenium vapor into the atmosphere where it finds its way into the soil and the hydrosphere.

Selenium is actually a required element for human life, 50-300 µg being the recommended daily dosage for adults. However, too much selenium can be poisonous (5 mg per day is considered the toxic dosage)¹³ and may result in impaired endocrine functionality, hepatotoxicity, and gastrointestinal disturbances¹⁴. Increased selenium levels have also been known to have severe environmental impact as well. In aquatic environments, selenium has been shown to bioaccumulate in fish¹⁵ and to greatly affect the development and reproduction of aquatic birds¹⁶. Similarly, selenium has been linked to population declines in arctic wildlife including several species of eider¹⁷ and is under observation in several others such as Yukon wolves¹⁸.

Chapter 3: Theory and Methodology

3.1 Computational Chemistry

As technology continually improves, the scope and detail of computer modeling becomes much greater. Of particular importance to the world of theoretical chemists is the greater capability of simultaneous mathematical equation solving software because more and more “experimentation” can be conducted without ever needing to purchase supplies, check valves, clean equipment, etc. Even more consequential, is the ability of computational chemistry to determine quantities which cannot be measured experimentally, making the utilization of this resource applicable to virtually every field.

There are several scales in modeling which encompass the relative size of the system under study. Process modeling, for instance, is used in evaluating the operation of a piece of equipment or even an entire plant, while molecular modeling examines processes such as the diffusion of a substance through a membrane. The most recent scale to be explored using computational chemistry, however, is the atomic scale, examining the structure and properties of the electronic bonds formed between atoms. It is this application of computational chemistry which has made the results presented in this study possible.

The technique of determining electronic properties exclusively from theory is known as *ab initio*. The phrase ‘*ab initio*’ means roughly, “from first principles” and refers to the process of solving approximations to the Schrodinger Wave Equation (1); approximations because it has never been solved exactly for any but simple model problems such as atomic H or H₂⁺.¹⁹ The actual computations are performed using the Gaussian '03²⁰ software package with additional inputs, such as effective core potential basis functions, being acquired elsewhere if necessary. In carrying out these computations the required input consists of a method and basis set with which to conduct the calculations.

$$1 \quad H\Psi = E\Psi$$

A method is defined as a mathematical approach to approximating the Schrodinger Wave Equation. The largest concerns in selecting an appropriate method are time and desired accuracy. In an optimal situation, the affect of any electron upon every other in the system would be determined, however, such a calculation would take an extremely long amount of time. The selection of a method, therefore, comes down to a trade-off between these two concerns and a compromise must be reached whereby the calculation is reliable but not overly time consuming. Several types of methods are available, being defined in how they handle the interactions between electrons. The simplest, known as Density Functional Theory (DFT), assumes a different approach than most *ab initio* methods. Rather than calculating the full wavefunction, DFT calculates the total electronic energy and overall electronic density distribution of the system²¹, the idea being based on the relationship between quantities first developed in-depth by Hohenberg and Kohn²². While this makes the computations go very quickly it also generates results which are prone to be in error. A most basic of the traditional *ab initio* methods is Hartree-Fock (HF) which accounts for electron-electron interaction by taking the average potential energy across the field and determining how each electron reacts to that average value. As with DFT, this method is quite expeditious but the accuracy of the calculations are somewhat compromised. More rigorous methods such as Quadratic Configuration Interaction (QCI) or Coupled Cluster (CC) account for these interactions between electrons within the same vicinity and so the force of four or more electrons is calculated for any one within the cloud. These calculations are usually quite accurate but do require substantial amounts of time and computational resources.

The other required input, a basis set, is simply a mathematical description of the molecular orbital space occupied by the electrons. The clearest definition of a basis set is that given in Foresman²³ namely, that a basis set can be interpreted as restricting each electron to a particular region of space; larger basis sets impose fewer constraints on electrons and more accurately approximate exact molecular orbitals. Basis sets fall into two main categories, complete basis sets and Effective Core Potential (ECP) basis sets. A complete basis set is one in which the orbital of every electron present in the system is explicitly accounted for in the calculations. As with the methods, the larger the system is, the more difficult it will be to finish the computations for basis sets which account for every electron. The ECP basis sets are designed to address this

issue by taking advantage of the fact that the orbitals of the core electrons are not altered much when bonds are formed and neglecting the interactions between the core and the valence electrons²⁴. In this way, only the outer s and p orbital electrons, i.e. those that participate in bonding, are fully analyzed. The use of ECP serves to reduce the required computational resources and in most cases still predicts a fairly accurate species geometry and/or reaction enthalpy.

3.2 Kinetics and Thermodynamics

3.2.1 Potential Energy Surface Development

After the best level of theory has been selected for a reaction, the first step in determining the kinetic parameters is the development of a Potential Energy Surface (PES). A PES is nothing more than a 3-Dimensional representation of the energy of the molecule at a particular geometry, but the creation of a surface does require that some restrictions be made. Because the z-axis of a surface represents the energy of the molecule, the remaining degrees of freedom must be limited to two, in order to plot a 3D surface, otherwise a multi-dimensional hyper-surface is created which may be more accurate but is not as effective as a visual aid.

The simplest example of degree of freedom restriction is the reaction $AB + C \rightarrow A + BC$. Here, the system consists of only three atoms and so will remain planar, however, if atom B is taken as the central atom, there will be 3 degrees of freedom: A-B bond distance, B-C bond distance, and A-B-C bond angle. Accounting for all three of these in addition to the energy results in 4 degrees of freedom and so in order to plot the surface one variable must be fixed; in such a reaction the bond angle is most often the fixed value, being held constant at 180°. Another PES scheme created in this study dealt with reactions of the form $A + B_2 \rightarrow AB_2$. Here the final product has a specified bond angle which must be accounted for and so the degree of freedom restriction was that both bond lengths, each being of type A-B, were assumed to be identical. In this way, the definition of the bonds as symmetric provides a reasonable method of reducing the degrees of freedom.

Once a plotting scheme has been defined, the creation of the surface is achieved by defining the geometric degrees of freedom and running a single point energy calculation in Gaussian. Once completed, the two geometric values and the energy value are plotted using MatLab. A fully developed PES gives a fairly precise overview of the important steps of a reaction. The main purpose of a PES is to narrow the search area for particular phenomena, the most important for the purpose of this work being the transition structure. On any PES, the transition structure will show up as a saddle point connecting the reactants to the products along the reaction coordinate. Once found, further computational chemistry calculations must be performed upon the structure at the saddle point geometry to determine if it is, in fact, a true transition state; in such a case the calculation will return a single imaginary frequency value. While a separate calculation may be run which could locate the transition state without the PES, the initial starting point provided from the surface serves to cut down on the required computing time significantly. In addition to the transition state, the PES may also reveal certain reaction intermediates which show up as potential wells on the surface. In this way, it is possible to identify species which may never have been considered as stable structures.

3.2.2 Bimolecular Reactions with True Transition State

After developing a PES and performing the necessary calculations using the Gaussian software, the next step in the determination of kinetic rate constant parameters is the application of the theoretical equation(s) which actually calculate the activation energy and pre-exponential factor of the reaction. For those cases where a true transition state exists in a bimolecular (i.e. single displacement) reaction, standard Transition State Theory (TST) was used. This equation (2)²⁵ was also modified with the tunneling correction factor first developed by Wigner²⁶ (3) to generate the final equation (4).

$$2 \quad k^{TST} = \frac{k_b T}{h} \frac{Q_{TS}}{Q_1 Q_2} e^{\left(\frac{-E_a}{RT}\right)}$$

$$3 \quad k_T = 1 + \frac{1}{24} \left[\frac{hc\nu}{k_b T} \right]^2$$

$$4 \quad k = k^{TST} \cdot k_T$$

For this type of reaction, the hard sphere collision model was also used as a means of comparison. In collision theory, it is assumed that every collision will result in a reaction, which is not always the case. Because of this, collision theory serves as an upper-bound to the rate constant value predicted using TST; in effect, if the frequency factor determined using TST is not smaller than that found using collision theory, there is an error somewhere within the calculations. Equation (5)²⁷ represents the rate constant as determined by collision theory; notice that information about the species is required, meaning that some estimation had to be made where experimental data was lacking, namely, the collision diameter, σ .

$$5 \quad k^{Coll} = \pi\sigma_{12}^2 N_A \sqrt{\frac{8k_b T}{\pi\mu_{12}}} e^{\left(\frac{-E_a}{RT}\right)}$$

The primary technique utilized for this estimation was a traditional approach based upon the critical properties of the reacting species. The value of σ was calculated (6) for each species and then the average was taken to get σ_{12} .

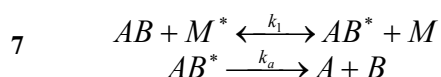
$$6 \quad \sigma = 0.1866V_c^{1/3} Z_c^{-6/5}$$

Unfortunately, the lack of experimental data for many of the examined species also pertains to the critical parameters, and so in several instances, the collision diameter was estimated by summing up the atomic collision diameters of each atom in the species. While this method was not based on any theory, the values obtained for σ_{12} were comparable to those obtained using the primary technique, in instances where there was enough data to use both. In any event, the main goal is the determination of the rate constant and the deviation in collision diameter is unlikely to change that by an order of magnitude. Therefore, the estimated values, while not theoretically precise, are relatively unimportant.

3.3.3 Unimolecular Reactions with True Transition State

For cases in which a true transition state exists in a unimolecular reaction i.e., decomposition, a completely different theoretical approach is necessary. In these instances, the theory developed by Rice, Ramsperger, Kassel, and Marcus, or RRKM theory, is used. In a unimolecular decomposition reaction, the overall reaction is composed of two steps (7); a collision or

activation step and a reaction step. In the first step, the molecule AB is struck by an energized collision partner M^* which may be an inert bath gas molecule such as N_2 or Ar, or another AB molecule at high pressures or high concentrations of AB. This collision imparts the kinetic energy of the collision partner to AB which then becomes “activated”. It then depends upon how the energy is partitioned between the various modes of vibration and rotation of AB to determine if AB^* will proceed to products A and B or if it will remain activated until being struck by another de-energized collision partner and become deactivated. This makes decomposition reactions particularly sensitive to pressure, as a system with high pressure will increase the frequency of collisions and thus decrease the time AB^* can exist before being deactivated. If the correct partitioning of the kinetic energy has not occurred before AB^* is struck again, the decomposition step will not occur.



The rate at which the overall reaction proceeds is then dependent upon the fate of the activated molecule, AB^* . Since the overall reaction may follow two paths, the likelihood of deactivation and decomposition relative to each other must be accounted for, therefore, the overall rate constant expression k_{uni} given in equation (8) includes the summation of the quantity X over all states examined. As shown in equation (9), X is the ratio of the decomposition rate constant k_a (10) over the deactivation rate constant, represented by the $B_c Z_{LJ}[M]$ term, at each state. However, to determine k_a , and consequently X and k_{uni} , the sum of states (W) and the density of states (ρ) must first be determined. Additionally, the parameters L^\ddagger , Q_v^\ddagger , Q_v , and Q_r which represent, respectively, the transition state statistical factor, the total vibrational partition function of the transition state, the total vibrational partition function of the reactant, and the rotational partition function of the reactant. The statistical factor deals with the number of possible ways the products can be reached; CO_2 for instance can decompose into two identical CO molecules and therefore has a statistical factor of 2. The total vibrational partition function is found by plugging each vibrational mode (ν) of a molecule into equation (11) and taking the product while the rotational partition function is taken directly from the Gaussian output.

$$8 \quad k_{uni} = \frac{L' Q'_v}{N_A h Q_v Q_r} e^{\left[\frac{-E_0}{RT} \right]} \Delta E \cdot \sum(X)$$

$$9 \quad X = \frac{W}{1 + \frac{k_a}{B_c Z_{LJ} [M]}} e^{\left[\frac{-(E^* - E_0)}{RT} \right]}$$

$$10 \quad k_a = L' \frac{Q'_v}{Q_v} \frac{W}{N_A h \rho}$$

$$11 \quad Q_v = \left(1 - e^{\left[\frac{-0.9427 hc \nu}{k_b T} \right]} \right)^{-1}$$

Before determining the sum and density of states, it is important to understand what is meant by a ‘state’. In a unimolecular decomposition reaction with a true transition state, the potential energy diagram along the reaction coordinate will exhibit the general trend shown in Figure 5 with the reactant molecule AB at the potential well, the product at the plateau, and the transition state at the maximum in between the two minima. When the collision partner M^* strikes AB its energy is partitioned among the various modes; some may go into altering a particular bond vibration or group rotation, altering the configuration of the molecule. In order to proceed from reactants to products, an amount of energy equal to the difference, $(E_{ab^*} - E_{ab})$, must be transferred, but it may be that more than the required energy is imparted to AB in the collision. In this instance, the excess energy can be partitioned amongst the available modes in a number of different ways giving rise to alternate states.

For an effective illustration, a hypothetical molecule will be used to demonstrate the method of identifying these states and calculating the sum and density of states. A simple, but effective, example molecule is a non-linear, tri-atomic species possessing three modes of vibration: $\nu_1 = 1500 \text{ cm}^{-1}$, $\nu_2 = 1200 \text{ cm}^{-1}$, and $\nu_3 = 600 \text{ cm}^{-1}$. Keeping the generic terms AB and AB^* , when this molecule is struck and becomes energized it will proceed toward the transition state AB^* . If excess energy is transferred, at the transition state the total energy of the molecule can be anywhere from E^* , the ground state energy of AB^* , to E^{\max} , a maximum value which is chosen for the sake of calculations. As shown in Figure 5, there will be a number of steps in between E^* and E^{\max} , which is determined by the step size, ΔE , also a selected quantity.

For this example, the energy values will be set relative to one another so that the value of E^* will be zero and E^{\max} will be set to 3000 cm^{-1} , with a step size of 300 cm^{-1} ; again, these are arbitrary values chosen for illustrative purposes only. The total energy of the molecule can be found by summing the three vibrational energies which, at the ground state, would simply be the sum of ν_1 , ν_2 , and ν_3 . However, excess energy partitioned in the vibrations would result in increasing a particular vibrational energy by an integer multiple so that the total energy at any state is calculated by $1500\nu_1 + 1200\nu_2 + 600\nu_3$. The first step in determining the sum and density of states, then, is finding how many different combinations ν_1 , ν_2 , and ν_3 exist in which the total energy lies between E^* and E^{\max} , in this case 0 and 3000 cm^{-1} .

The first possible combination, in which all integers are 0, results in a total energy of 0 cm^{-1} and is designated as state 'a'. Another possible combination is $\nu_1 = 0$, $\nu_2 = 0$, and $\nu_3 = 1$, giving a total energy of 600 cm^{-1} . This process is repeated until all combinations within the range are accounted for; the entire list of 17 states (a-q) is given in Table 1. Once all of the possible states have been identified, the number of states within each energy range and the average density of states can be found. First, the total energy range is divided into smaller ranges based on the step size previously selected; and so the ranges, in this case, are 0-299, 300-599...2700-2999, 3000-3299 cm^{-1} . Each state is then placed in its proper range based upon its total energy value, and the number of states within that range is noted. The average density of states is, then, simply the number of states within the range divided by the step size while the sum of states is merely a running total of all states having a total energy at or below the energy range examined. For example, in the first energy range, 0-299 cm^{-1} , there is a single state, a, and so the density of states is $1/300\text{ (1/cm}^{-1}\text{)}$ and the sum of states is 1. At the next step, 300-599 cm^{-1} , there are no states and so the density is 0 while the sum of states remains 1. Proceeding to the 600-899 cm^{-1} range, there is only state b, and so the density is again $1/300\text{ (1/cm}^{-1}\text{)}$ but the sum of states is increased to 2. This process is repeated for each range as shown in Table 2, yielding the density and sum of states at each energy range. This direct method of counting the vibrational states of a molecule is known as the Beyer-Swinehart Algorithm²⁸ and when transposed into a software package can be used to find the density and sum of states for any pair of reactant and transition state molecules.

Once the sum and density of states have been determined, the value of k_a at each state can be found which is then incorporated into the equation for determining the quantity X. In this formula the other quantity which must be determined, the rate of deactivation, is found by calculating the Lennard-Jones parameter, Z_{LJ} , the concentration of M, and selecting a collisional deactivation efficiency, B_c . Collisional efficiency is a specified value and the concentration of M is a simple calculation from the system pressure and temperature, but Z_{LJ} requires additional input as shown in equation (12). This formula is very similar to that of the hard sphere collision model in equation (5), the “am” designation of reactant and collision partner replacing the “12” designation of reactants 1 and 2. Those variables which appeared in the previous formula represent the same quantities as before while new variable Ω_{am} is a correction factor, usually close to 1, which is found using either (13) or (14) depending upon which criteria are met. The value of ε/k , the Lennard-Jones well-depth of each species, is in turn found using (15); ε_{am}/k is the average of the two. After determining both the rate of decomposition (k_a) and the rate deactivation $B_c Z_{LJ}[M]$, the overall rate constant (k_{uni}) can be found.

$$12 \quad Z_{LJ} = N_A \sigma_{am}^2 \sqrt{\frac{8RT}{\pi \mu_{am}}} \Omega_{am}$$

$$13 \quad \Omega_{am} = \left[0.636 + 0.567 \log \left(\frac{kT}{\varepsilon_{am}} \right) \right]^{-1} \quad \text{when} \quad 0.3 \leq \frac{kT}{\varepsilon_{am}} \leq 500$$

$$14 \quad \Omega_{am} = \left[0.697 + 0.5185 \log \left(\frac{kT}{\varepsilon_{am}} \right) \right]^{-1} \quad \text{when} \quad 3 \leq \frac{kT}{\varepsilon_{am}} \leq 300$$

$$15 \quad \frac{\varepsilon}{k} = 65.3 T_c Z_c^{\frac{18}{5}}$$

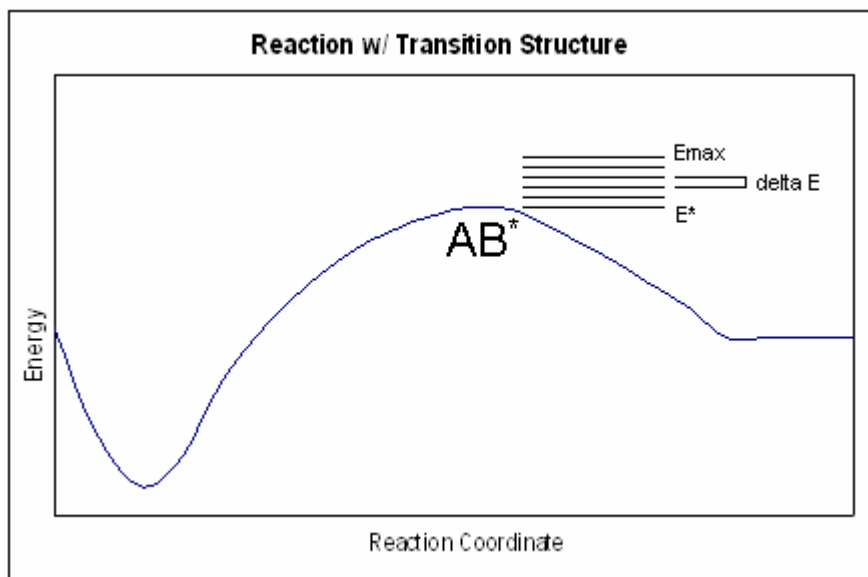


Figure 5: PED Unimolecular Decomposition Reaction w/ True Transition State

Table 1: State Combinations of Example Molecule

v_1	v_2	v_3	Total Energy (cm^{-1})	Label
0	0	0	0	a
0	0	1	600	b
0	0	2	1200	c
0	0	3	1800	d
0	0	4	2400	e
0	0	5	3000	f
0	1	0	1200	g
0	1	1	1800	h
0	1	2	2400	i
0	1	3	3000	j
0	2	0	2400	k
0	2	1	3000	l
1	0	0	1500	m
1	0	1	2100	n
1	0	2	2700	o
1	1	0	2700	p
2	0	0	3000	q

Table 2: Sum and Average Density of States of Example Molecule

Energy Range (cm^{-1})	Label	States in Range	Average Density of States ($1/\text{cm}^{-1}$)	Sum of States
0-299	a	1	1/300	1
300-599	-	0	0	1
600-899	b	1	1/300	2
900-1199	-	0	0	2
1200-1499	c, g	2	2/300	4
1500-1799	m	1	1/300	5
1800-2099	d, h	2	2/300	7
2100-2399	n	1	1/300	8
2400-2699	e, i, k	3	3/300	11
2700-2999	o, p	2	2/300	13
3000-	f, j, l, q	4	4/300	17

3.3.4 Reactions without True Transition State

For bimolecular or unimolecular reactions without true transition structures, the Variational Transition State Theory (VTST) technique must be employed. When no true transition state is present, the potential energy along the reaction coordinate is barrierless and takes on the general form shown in Figure 6. In such a case, the rate constant is calculated for a series of transition state geometries along the asymptote portion of the curve. The value is determined in a manner consistent with the previous reactions, i.e., TST for bimolecular reactions and RRKM theory for unimolecular ones. Beyond a certain value, the deviation in the calculated rate constant should not change by a significant amount, say an order of magnitude, and so the geometry at which this value is calculated is taken as a sufficient transition state.

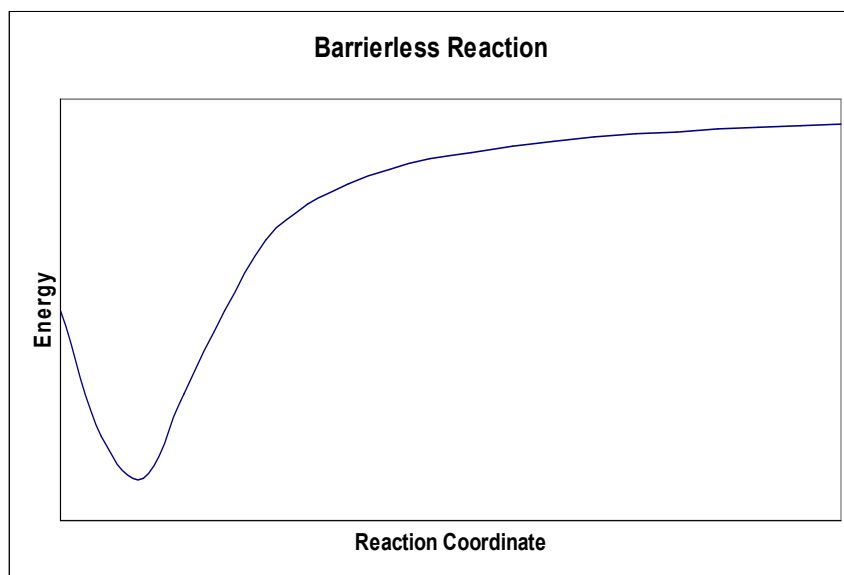


Figure 6: Barrierless Reaction (No True Transition State)

3.3.5 Thermodynamics

The determination of the thermodynamic parameters was more straight-forward than the kinetics due to the fact that the thermodynamics requires knowledge of only the energetics of the products and reactants. The primary reason for examining the thermodynamic parameters of each reaction was the calculation of the equilibrium constants which could then be compared to both experimental data and to the ratio of the forward and reverse rate constants calculated theoretically. In this way, a favorable comparison of theoretical kinetics to theoretical thermodynamics and experimental thermodynamics would provide further validation of the theoretically determined parameters. Finding the K_{eq} of each reaction was accomplished by finding the Gibbs free energy from the reaction enthalpy and entropy as shown in (16) and (17).

$$16 \quad \Delta G = \Delta H - T\Delta S$$

$$17 \quad K_{eq} = e^{\left(\frac{-\Delta G}{RT}\right)}$$

Chapter 4: Results and Discussion

4.1 Theory Validation

Before going through the process of determining a rate constant for a particular As/Se reaction, it is important to assess how reliable the species data is that is being used in those calculations. For instance, if a PES is created using a basis set which is ill-equipped to handle a particular species or using a method which is too simplistic, it is possible that the surface gives a false impression of the location and energy associated with the transition state, if one is present at all. Even if a true transition state were identified using a transition state search algorithm, the partition functions of the transition structure, as well as of the products and reactants, may generate a rate constant that deviates orders of magnitude from the actual value. It is for this reason that before any evaluation of kinetic and thermodynamic parameters is undertaken, each level of theory considered must be validated with regard to reaction enthalpy, species geometry, and vibrational frequency.

Within this study, 19 different levels of theory were examined covering a wide range of methods and basis sets to find the ones which best represented a particular species or reaction. The methods used included the DFT B3LYP along with HF, and QCI and CC at both the double and triple excitations. The basis sets consisted of the built-in models LANL2DZ, SDD, and 6-311++G(3df,3pd) as well as the effective core potential models ECP28MWB and RECP28VDZ. It should also be noted that when the ECP basis sets were used it was only for the trace metal atom in the species, with the remaining light elements were all computed using the 6-311++G(3df,3pd) Pople basis set.

4.1.1 Species Geometry

The data contained in Table 3, Table 4, and Table 5 presents the predicted and experimental species geometry of the primary arsenic and selenium species considered. Notice that the more sophisticated levels of theory could not be completed for the larger species because there were

just too many electrons for the available computing resources to handle. It should also be mentioned that while experimental data was not available for every compound, most species geometries could be located after examining a variety of sources: (SeO, Se₂, SeO₂, AsO, and AsCl₃),²⁹ (SeH₂),³⁰ (SeCl and SeCl₂),³¹ and (AsH, AsH₂, and AsH₃).³²

Through examining the arsenic geometry tables (Table 3 and Table 4), several observations can be made. In regard to AsO, the ECP28MWB basis set performs remarkably well at the double excitation level only, with the CCSD method predicting a geometry within 0.0002 Å of the experimental value. The QCISD/6-311++G(3df,3pd) combination also performs well, unfortunately the CCSD calculation with this method was incomplete. The arsenic hydride species fared well also, though not at these same levels of theory. The best AsH geometry predictions were those using the complete Pople basis set which deviated from experiment by slightly less than 0.005 Å, while the ECP basis sets performed comparatively poorly. A similar situation is seen with the bond lengths in both AsH₂ and AsH₃ where the those levels of theory utilizing this basis set most closely matched experiment, though for AsH₃ the bond length predictions of ECP28MWB are relatively the same. However, in the prediction of the bond angles, the ECP28MWB predictions are slightly more accurate as compared to the 6-311++G(3df,3dp) ones, with a 0.07° deviation as opposed to a 0.4°. In the case of the dihedral angle of AsH₃ all of the calculations produce essentially the same prediction and so there is no clear best in this regard. The arsenic chlorides AsCl and AsCl₂ had no experimental data to compare to, and AsCl₃ was only completed at very low levels of theory and so substantial results are somewhat limited. However, some observations can be made here as well, for instance, notice the consistency of the data within each basis set. Also, this data fit in with the trend seen in each species, which is, the predicted bond lengths for the higher levels of theory are roughly 0.05 Å smaller than those of the less sophisticated models.

Similar observations can be made upon examination of the selenium species data. The most accurate predictions made of the bond distance of SeO are those using the ECP28MWB with the most accurate deviating by only 0.0002 Å while the complete Pople basis set also performed well with a minimum deviation of 0.005 Å. There are not enough complete computations for SeO₂ to get a full picture of its performance but from those that are complete it is clear that the

ECP28MWB is the best in both bond length and angle predictions. A similar situation exists for SeH_2 where only the QCISD method could be complete when using the 6-311++G(3df,3pd). Here, this is the best in terms of bond length prediction by far and is only negligibly worse than other levels of theory in predicting the bond angle. The predictions of the selenium chlorides are also most accurate with the complete Pople basis set, with both bond length calculations falling within 0.005 Å of experiment while the bond angle of SeCl_2 deviates by less than a degree.

From this data one observation stands out; the ECP28MWB basis set performed the best for both the As and Se oxide compounds while the complete Pople basis set was superior for all others. This may suggest that the ECP works well in computing the parameters of oxygen compounds in general. Perhaps because oxygen has the capability of forming multiple bonds with its valence electrons, the core electrons are less important in determining the species geometry than in those atoms which can bond only once. There have not been enough computations performed or experimental data available to state that this is a definitive occurrence, but from the information available this is a development which is worth further investigation.

Table 3: Arsenic Species Geometry (1)

	AsO	AsH	AsCl	As ₂	
Level of Theory	As-O (Å)	As-H (Å)	As-Cl (Å)	As-As (Å)	
Experiment	1.6236	1.528	-	-	
B3LYP/LANL2DZ	1.6883	1.5663	2.3208	2.1927	
HF/SDD	1.6279	1.5385	2.3081	2.1141	
QCISD/SDD	1.7251	1.5762	2.3426	2.2162	
QCISD(T)/SDD	1.7142	1.5767	2.3442	2.2244	
CCSD/SDD	1.6985	1.5763	2.3397	2.2144	
CCSD(T)/SDD	1.7158	1.5768	2.3418	2.2244	
HF/6-311++G(3df,3pd)	1.5788	1.5166	2.1598	2.0596	
QCISD/6-311++G(3df,3pd)	1.6300	1.5316	2.1604	-	
QCISD(T)/6-311++G(3df,3pd)	-	1.5334	-	2.1333	
CCSD/6-311++G(3df,3pd)	-	1.5314	-	-	
CCSD(T)/6-311++G(3df,3pd)	-	1.5333	-	-	
QCISD/ECP28MWB	1.6260	1.5087	2.2003	2.2160	
QCISD(T)/ECP28MWB	1.6395	1.5087	2.2055	2.2241	
CCSD/ECP28MWB	1.6234	1.5086	2.2000	2.2143	
CCSD(T)/ECP28MWB	1.6396	1.5087	2.2050	2.2243	
QCISD/RECP28VDZ	1.6375	1.5013	2.2124	2.2235	
QCISD(T)/RECP28VDZ	1.6512	1.5014	2.2170	2.2317	
CCSD/RECP28VDZ	1.6319	1.5014	2.2120	2.2213	
CCSD(T)/RECP28VDZ	1.6504	1.5014	2.2165	2.2322	
	AsH ₂		AsH ₃		
Level of Theory	As-H (Å)	H-As-H (°)	As-H (Å)	H-As-H (°)	Dihedral (°)
Experiment	1.521	90.7	1.511	92.1	109.4
B3LYP/LANL2DZ	1.5531	91.26	1.5398	92.58	109.43
HF/SDD	1.5261	92.65	1.5146	94.29	109.35
QCISD/SDD	1.5635	91.31	1.5512	92.65	109.43
QCISD(T)/SDD	1.5641	91.36	1.5519	92.63	109.43
CCSD/SDD	1.5636	91.30	1.5512	92.65	109.43
CCSD(T)/SDD	1.5641	91.35	1.5519	92.63	109.43
HF/6-311++G(3df,3pd)	1.5127	93.02	1.5083	94.61	109.33
QCISD/6-311++G(3df,3pd)	1.5253	91.32	1.5208	92.72	109.42
QCISD(T)/6-311++G(3df,3pd)	1.5274	91.11	1.5226	92.48	109.43
CCSD/6-311++G(3df,3pd)	1.5252	91.32	1.5200	92.82	109.42
CCSD(T)/6-311++G(3df,3pd)	1.5274	91.11	1.5226	92.48	109.43
QCISD/ECP28MWB	1.5042	90.62	1.5040	92.20	109.44
QCISD(T)/ECP28MWB	1.5040	90.56	1.5040	92.02	109.45
CCSD/ECP28MWB	1.5042	90.63	1.5040	92.20	109.44
CCSD(T)/ECP28MWB	1.5040	90.56	1.5040	92.02	109.45
QCISD/RECP28VDZ	1.4931	90.48	1.4874	92.38	109.43
QCISD(T)/RECP28VDZ	1.4932	90.37	1.4874	92.24	109.44
CCSD/RECP28VDZ	1.4931	90.49	1.4874	92.39	109.43
CCSD(T)/RECP28VDZ	1.4932	90.37	1.4874	92.24	109.44

Table 4: Arsenic Species Geometry (2)

Level of Theory	AsCl ₂		AsCl ₃		
	As-Cl (Å)	Cl-As-Cl (°)	As-Cl (Å)	Cl-As-Cl (°)	Dihedral (°)
Experiment	-	-	2.165	98.6	108.9
B3LYP/LANL2DZ	2.3183	101.71	2.3185	99.86	108.74
HF/SDD	2.2850	100.48	2.2723	99.13	108.86
QCISD/SDD	2.3326	101.36	2.3277	99.78	108.76
QCISD(T)/SDD	2.3355	101.74	2.3323	100.06	108.71
CCSD/SDD	2.3287	101.27	-	-	-
CCSD(T)/SDD	2.3329	101.66	-	-	-
HF/6-311++G(3df,3pd)	2.1574	100.13	-	-	-
QCISD/ECP28MWB	2.1979	99.84	-	-	-

Table 5: Selenium Species Geometry

	SeO	SeCl	Se ₂	SeH ₂	
Level of Theory	Se-O (Å)	Se-Cl (Å)	Se-Se (Å)	Se-H (Å)	H-Se-H (°)
Experiment	1.639	2.13	2.1660	1.46	90.6
B3LYP/LANL2DZ	1.7480	2.3263	2.3323	1.4981	92.17
HF/SDD	1.6819	2.3138	2.2335	1.4663	93.72
QCISD/SDD	2.1281	2.3605	2.3204	1.5014	92.20
QCISD(T)/SDD	1.7688	2.3622	2.3274	1.5016	92.21
CCSD/SDD	1.7601	2.3554	2.3187	1.5014	92.19
CCSD(T)/SDD	1.7650	2.3544	2.3266	1.5016	92.20
HF/6-311++G(3df,3pd)	1.5925	2.1277	2.1368	1.4528	93.26
QCISD/6-311++G(3df,3pd)	1.6362	2.1355	-	1.4650	91.50
QCISD(T)/6-311++G(3df,3pd)	1.6484	2.1410	-	-	-
CCSD/6-311++G(3df,3pd)	1.6338	2.1341	-	-	-
CCSD(T)/6-311++G(3df,3pd)	1.6463	-	-	-	-
QCISD/ECP28MWB	1.6423	2.1733	2.3204	1.4237	90.81
QCISD(T)/ECP28MWB	1.6492	2.1788	2.3274	1.4228	90.74
CCSD/ECP28MWB	1.6392	2.1726	2.3187	1.4236	90.83
CCSD(T)/ECP28MWB	1.6477	2.1780	2.3266	1.4228	90.74
QCISD/RECP28VDZ	1.6756	2.1875	2.3244	1.4256	90.41
QCISD(T)/RECP28VDZ	1.6837	2.1936	2.3301	1.4249	90.33
CCSD/RECP28VDZ	1.6718	2.1868	2.3230	1.4255	90.43
CCSD(T)/RECP28VDZ	1.6822	2.1927	2.3295	1.4249	90.33
	SeO ₂		SeCl ₂		
Level of Theory	Se-O (Å)	O-Se-O (°)	Se-Cl (Å)	Cl-Se-Cl (°)	
Experiment	1.6076	113.83	2.157	99.6	
B3LYP/LANL2DZ	1.7164	110.97	2.3442	102.18	
HF/SDD	1.6473	111.34	2.2887	100.11	
QCISD/SDD	1.7477	112.12	2.3619	101.07	
QCISD(T)/SDD	1.7627	112.28	2.3677	101.45	
CCSD/SDD	1.7248	111.42	2.3600	100.87	
CCSD(T)/SDD	1.7530	111.68	2.3666	101.31	
HF/6-311++G(3df,3pd)	1.5549	114.08	2.1389	100.45	
QCISD/6-311++G(3df,3pd)	1.6009	114.29	2.1551	100.36	
QCISD(T)/6-311++G(3df,3pd)	-	-	-	-	
CCSD/6-311++G(3df,3pd)	-	-	-	-	
CCSD(T)/6-311++G(3df,3pd)	-	-	-	-	
QCISD/ECP28MWB	1.6023	113.21	2.1922	99.93	
QCISD(T)/ECP28MWB	-	-	-	-	
CCSD/ECP28MWB	-	-	-	-	
CCSD(T)/ECP28MWB	-	-	-	-	
QCISD/RECP28VDZ	1.6173	110.94	2.2038	99.97	
QCISD(T)/RECP28VDZ	-	-	-	-	
CCSD/RECP28VDZ	-	-	2.2036	99.93	
CCSD(T)/RECP28VDZ	-	-	-	-	

4.1.2 Vibrational Frequency

As with the species geometries, the vibrational frequencies predicted were also evaluated against the experimentally determined values. Experimental data on the vibrational frequencies was as difficult to come by as the experimental geometry data, if not more so, but data for most of the species was located: (SeO and AsO),²⁹ (AsCl),³³ (SeO₂),³⁴ (SeCl₂),³⁵ and (SeH₂ and AsCl₃).³⁶ As before, several larger species are incomplete at the higher levels of theory but a comparison can be drawn on the existing data.

From the data presented in Table 6 and Table 7 several assessments can be made. Firstly, the only species which have experimental and high level computational data are AsO and AsCl; looking at these species it can be seen that those calculations using the 6-311++G(3df,3pd) basis set produce the most accurate results, deviating by 9 and 2 cm⁻¹, respectively. Also, the pattern observed in the geometry data appears again, the ECP28MWB basis set predicts fairly reliable vibrational frequencies for the oxide compound but not for the chloride, further strengthening the theory of a link between the use of ECP's and multiple bonds. From the tables, it is also clear that those calculations sharing a common basis set produce results with excellent precision, rarely deviating by more than a few wave numbers. This holds true for all As species, but the data, while certainly precise, cannot be described as accurate until further experimental results are confirmed.

The Se-containing species have a bit more experimental data and so more valuable insight can be gained by examining them. The data for these compounds, shown in Table 8, present a somewhat different picture than in the previous data tables. The SeO data is similar to previous results in that the complete Pople basis set and the ECP28MWB basis set produce results which have approximately the same variance and deviate from the experimental value by only a few wave numbers. Also, the best level of theory for SeH₂ is that which uses the 6-311++G(3df,3pd) basis set, however, while the predicted value differs from the experimental for ν_1 by a few cm⁻¹, the difference between the values for ν_2 and ν_3 is on the order of a few hundred cm⁻¹. Further, the level of theory which most closely matches experiment for both SeO₂ and SeCl₂ is QCISD/ECP28MWB. This goes against the previous observed trend that this ECP basis set is

inferior to the complete Pople basis set for non-oxide compounds. Unfortunately, there are few computations completed for these molecules at the higher levels of theory and so additional calculations may present results more in-line with the previous data, or they may reinforce the data currently observed. In either case additional computations at high levels of theory would be beneficial.

In general, several evaluations can be made regarding the vibrational frequency data. In some instances, the lower levels of theory actually do perform well, the predictions of SeH₂ using B3LYP/LANL2DZ for example, however there is little consistency in these and the results may be due to a cancellation of error in the calculations more than a true convergence. Secondly, the theoretical data for the As compounds within a particular basis set appear to be more precise than in the Se compounds. The reason for this is unknown, although this could also be a consequence of the electronic structure of the atoms and the way in which they bond. Finally, in the case of many of the molecules larger than two atoms, each vibrational frequency may be most accurately predicted by a different level of theory. To determine the exact reason for this, many more compounds would need to be investigated along with the nature of the vibrational modes themselves. It may be that a particular method or basis set is better equipped to handle a scissors-type vibration than others. Again, at this stage this is only speculation but it may provide a good starting point for further examination of these findings.

Table 6: Arsenic Species Vibrational Frequencies (1)

	AsO	AsH	AsH₂		
Level of Theory	ν_1 (cm ⁻¹)	ν_1 (cm ⁻¹)	ν_1 (cm ⁻¹)	ν_2 (cm ⁻¹)	ν_3 (cm ⁻¹)
Experiment	967.08	-	-	-	-
B3LYP/LANL2DZ	877.99	2036.25	1031.53	2072.02	2100.00
HF/SDD	1019.97	2145.44	1115.79	2214.83	2226.67
QCISD/SDD	713.27	1940.99	996.48	1988.76	2013.57
QCISD(T)/SDD	818.95	1937.51	992.93	1984.16	2009.80
CCSD/SDD	834.24	1940.43	996.61	1988.42	2013.08
CCSD(T)/SDD	791.28	1937.12	992.98	1983.85	2009.40
HF/6-311++G(3df,3pd)	1156.90	2282.70	1092.88	2306.12	2307.58
QCISD/6-311++G(3df,3pd)	978.04	2171.02	1019.22	2205.43	2209.65
QCISD(T)/6-311++G(3df,3pd)	-	2158.65	1008.41	2190.18	2195.57
CCSD/6-311++G(3df,3pd)	-	2172.39	1019.76	2206.79	2211.04
CCSD(T)/6-311++G(3df,3pd)	-	2158.46	1008.74	2190.54	2196.08
QCISD/ECP28MWB	861.32	2236.82	1075.80	2266.30	2267.07
QCISD(T)/ECP28MWB	906.40	2235.66	1071.60	2266.35	2266.98
CCSD/ECP28MWB	1004.34	2236.60	1076.38	2266.08	2266.73
CCSD(T)/ECP28MWB	959.52	2235.52	1071.85	2266.16	2266.80
QCISD/RECP28VDZ	836.58	2151.31	1087.60	2204.90	2206.99
QCISD(T)/RECP28VDZ	836.52	2149.97	1082.36	2202.10	2202.62
CCSD/RECP28VDZ	921.97	2150.66	1088.12	2204.40	2206.78
CCSD(T)/RECP28VDZ	871.83	2149.58	1082.55	2201.71	2202.42
	As₂	AsCl	AsCl₂		
Level of Theory	ν_1 (cm ⁻¹)	ν_1 (cm ⁻¹)	ν_1 (cm ⁻¹)	ν_2 (cm ⁻¹)	ν_3 (cm ⁻¹)
Experiment	-	424	-	-	-
B3LYP/LANL2DZ	400.36	363.37	127.95	353.91	361.90
HF/SDD	466.24	363.29	146.23	381.41	384.24
QCISD/SDD	364.83	346.66	128.75	350.42	352.54
QCISD(T)/SDD	355.65	347.22	127.61	349.42	350.64
CCSD/SDD	366.35	349.03	130.26	354.11	354.80
CCSD(T)/SDD	354.80	350.26	127.32	352.59	353.21
HF/6-311++G(3df,3pd)	512.25	432.44	179.32	420.49	443.29
QCISD/6-311++G(3df,3pd)	-	426.24	-	-	-
QCISD(T)/6-311++G(3df,3pd)	-	425.58	-	-	-
CCSD/6-311++G(3df,3pd)	-	-	-	-	-
CCSD(T)/6-311++G(3df,3pd)	-	-	-	-	-
QCISD/ECP28MWB	364.96	391.94	158.66	380.02	399.97
QCISD(T)/ECP28MWB	355.88	388.04	-	-	-
CCSD/ECP28MWB	366.51	392.46	-	-	-
CCSD(T)/ECP28MWB	354.88	388.51	-	-	-
QCISD/RECP28VDZ	362.70	386.71	-	-	-
QCISD(T)/RECP28VDZ	353.63	383.31	-	-	-
CCSD/RECP28VDZ	364.69	387.31	-	-	-
CCSD(T)/RECP28VDZ	352.04	384.14	-	-	-

Table 7: Arsenic Species Vibrational Frequencies (2)

AsH₃						
Level of Theory	ν_1 (cm ⁻¹)	ν_2 (cm ⁻¹)	ν_3 (cm ⁻¹)	ν_4 (cm ⁻¹)	ν_5 (cm ⁻¹)	ν_6 (cm ⁻¹)
Experiment	-	-	-	-	-	-
B3LYP/LANL2DZ	970.16	1056.54	1056.54	2112.59	2150.08	2150.08
HF/SDD	1039.08	1140.49	1140.49	2269.09	2285.73	2285.73
QCISD/SDD	952.12	1015.67	1015.67	2035.69	2068.18	2068.18
QCISD(T)/SDD	948.81	1012.58	1012.67	2030.82	2063.79	2063.91
CCSD/SDD	952.40	1015.91	1015.91	2036.06	2068.22	2068.22
CCSD(T)/SDD	948.83	1012.54	1012.82	2031.04	2063.81	2063.94
HF/6-311++G(3df,3pd)	1001.07	1106.97	1106.97	2330.56	2330.56	2334.05
QCISD/6-311++G(3df,3pd)	937.39	1034.95	1034.95	2230.22	2233.98	2233.98
QCISD(T)/6-311++G(3df,3pd)	925.92	1024.62	1024.91	2216.08	2221.18	2221.32
CCSD/6-311++G(3df,3pd)	936.96	1035.22	1035.31	2234.25	2238.21	2238.63
CCSD(T)/6-311++G(3df,3pd)	926.08	1024.89	1025.17	2216.60	2221.65	2221.80
QCISD/ECP28MWB	989.04	1069.63	1069.63	2277.55	2277.55	2286.60
QCISD(T)/ECP28MWB	981.76	1063.18	1063.60	2273.48	2273.66	2283.63
CCSD/ECP28MWB	989.29	1070.00	1070.00	2277.33	2277.33	2286.42
CCSD(T)/ECP28MWB	981.82	1063.34	1063.76	2273.31	2273.48	2283.42
QCISD/RECP28VDZ	983.25	1076.84	1076.84	2237.62	2237.62	2263.54
QCISD(T)/RECP28VDZ	975.39	1069.91	1070.33	2232.95	2233.20	2260.35
CCSD/RECP28VDZ	983.70	1077.32	1077.32	2237.59	2237.59	2263.38
CCSD(T)/RECP28VDZ	975.52	1070.11	1070.53	2232.83	2233.09	2260.12
AsCl₃						
Level of Theory	ν_1 (cm ⁻¹)	ν_2 (cm ⁻¹)	ν_3 (cm ⁻¹)	ν_4 (cm ⁻¹)	ν_5 (cm ⁻¹)	ν_6 (cm ⁻¹)
Experiment	154	159	193	370	404	410
B3LYP/LANL2DZ	122.59	122.86	154.11	349.14	349.59	357.12
HF/SDD	143.68	143.73	181.70	394.22	394.34	394.58
QCISD/SDD	124.38	124.39	157.37	350.24	355.35	355.36
QCISD(T)/SDD	122.11	122.19	154.56	346.97	350.96	351.06

Table 8: Selenium Species Vibrational Frequencies

Level of Theory	SeO			SeH ₂		
	ν_1 (cm ⁻¹)	ν_2 (cm ⁻¹)	ν_3 (cm ⁻¹)			
Experiment	914.69	-	-	1074	2260	2350
B3LYP/LANL2DZ	797.44	372.82	327.27	1089.85	2268.40	2312.66
HF/SDD	891.36	308.58	387.37	1180.20	2451.29	2478.12
QCISD/SDD	685.03	340.37	321.62	1062.04	2198.13	2234.37
QCISD(T)/SDD	717.91	333.48	315.98	1058.48	2195.95	2232.83
CCSD/SDD	730.61	337.15	323.37	1062.25	2198.08	2234.28
CCSD(T)/SDD	736.63	341.30	316.75	1059.26	2196.24	2232.90
HF/6-311++G(3df,3pd)	1090.55	463.45	442.33	1157.72	2581.68	2587.34
QCISD/6-311++G(3df,3pd)	958.86	446.30	-	1075.99	2465.53	2474.65
QCISD(T)/6-311++G(3df,3pd)	920.24	438.81	-	-	-	-
CCSD/6-311++G(3df,3pd)	965.54	447.86	-	-	-	-
CCSD(T)/6-311++G(3df,3pd)	927.66	-	-	-	-	-
QCISD/ECP28MWB	902.64	408.92	321.62	1162.13	2566.24	2596.41
QCISD(T)/ECP28MWB	891.57	403.43	315.97	1155.30	2569.17	2599.46
CCSD/ECP28MWB	918.53	409.94	323.37	1163.59	2567.15	2597.11
CCSD(T)/ECP28MWB	898.37	404.99	316.75	1155.93	2569.49	2599.78
QCISD/RECP28VDZ	830.55	405.56	326.48	1153.86	2529.78	2543.03
QCISD(T)/RECP28VDZ	823.94	399.59	321.83	1147.60	2532.52	2544.39
CCSD/ RECP28VDZ	848.38	406.56	328.00	1155.18	2530.15	2543.88
CCSD(T)/RECP28VDZ	831.25	401.23	322.39	1148.14	2532.56	2544.73
	SeO₂			SeCl₂		
Level of Theory	ν_1 (cm ⁻¹)	ν_2 (cm ⁻¹)	ν_3 (cm ⁻¹)	ν_1 (cm ⁻¹)	ν_2 (cm ⁻¹)	ν_3 (cm ⁻¹)
Experiment	368	923	968	153	377	415
B3LYP/LANL2DZ	301.37	797.32	817.79	121.63	347.97	355.57
HF/SDD	361.20	908.73	934.78	144.64	396.61	399.79
QCISD/SDD	277.07	334.21	669.79	119.96	335.43	341.84
QCISD(T)/SDD	270.65	595.64	653.80	117.51	330.20	334.48
CCSD/SDD	299.68	754.92	772.05	120.85	337.00	342.31
CCSD(T)/SDD	278.83	678.77	686.97	118.01	330.96	334.44
HF/6-311++G(3df,3pd)	443.81	1154.90	1192.19	181.50	447.83	461.85
QCISD/6-311++G(3df,3pd)	380.68	988.49	1031.65	165.99	420.44	434.30
QCISD/ECP28MWB	385.78	941.24	975.63	157.10	388.21	402.35
QCISD/RECP28VDZ	392.14	885.99	970.52	153.52	387.05	397.88
CCSD/ RECP28VDZ	-	-	-	153.76	386.63	398.08

4.1.3 Reaction Enthalpy

In contrast to the geometry and vibrational frequencies of individual species, the total energy predictions can not be directly compared to the experimental heats of formation. However, the differences in these quantities within a reaction are analogous and so can be evaluated against one another. In this way, the level of theory which best represents a particular reaction, though not necessarily the species involved, can be determined. The relevant experimental data, the heats of formation, come from a variety of sources: (AsCl, AsCl₂, and AsCl₃),³⁷ (As, AsO, AsCl, and AsCl₃),³⁸ (SeO₂),³⁹ and (Se, SeO, SeH₂, and SeCl₂).⁴⁰ Additionally, the heat of formation data for those species not containing arsenic or selenium is taken entirely from the NIST Laboratories.⁴¹

Table 9 and Table 10 show the data for each arsenic reaction investigated. For the majority of the reactions, the ECP28MWB basis set generates the most accurate reaction enthalpy prediction compared to experimental data; interestingly, these are all those reactions which contain oxygen or oxide compounds. The other reactions are best represented by the 6-311++G(3df,3pd) basis set, the exception being the reaction $\text{AsH}_2 + \text{H}_2 \rightarrow \text{AsH}_3 + \text{H}$ which is best represented by the RECP28VDZ basis set. In most reactions, while either ECP28MWB or 6-311++G(3df,3pd) does perform best, the other is usually not much worse, deviating from the experimental value by only a few more kcal/mol than the best basis set. The RECP28VDZ basis set usually lags behind the other higher levels of theory with the exception of the previously mentioned reaction and the reaction, $\text{As} + \text{OH} \rightarrow \text{AsH} + \text{O}$, where it performs just as well as the ECP28MWB basis set. One observation that stands out is that when oxygen is present in a reaction, the ECP28MWB basis set is superior, regardless of which other elements are present. However, in the absence of oxygen, those reactions which include chlorine are best handled using the complete Pople basis set while those which include only arsenic and hydrogen are better carried out using RECP28VDZ. Another observation is that, while in most reactions the difference between a double and triple excitation method for any given basis is minimal, 1-3 kcal/mol, in a few cases the difference is more pronounced. The reaction, $\text{As} + \text{OH} \rightarrow \text{AsO} + \text{H}$, using the complete Pople basis set has a difference of 6-8 kcal/mol between the double and triple excitation

methods, while in the reaction, $\text{As} + \text{O} \rightarrow \text{AsO}$, the difference is almost 10 kcal/mol. The reason for this occurrence is currently unknown and for a full examination, additional reactions of all types should be included.

The reaction enthalpy data tabulated for the selenium reactions exhibits a similar characteristic. The values presented in Table 11 and Table 12 show that the vast majority of these reactions are best represented using either the ECP28MWB or the 6-311++G(3df,3pd) basis set. With the exception of a few reactions, these two basis sets predict a theoretical change in energy that is within 3 kcal/mol of the experimental value. The issue of the difference between double and triple excitations is also significant here, with most of these reactions having a gap of 5-9 kcal/mol between the two computations for both sets. While all the reactions which follow this pattern are selenium oxide formation reactions, not all of this type of reaction follows this behavior. The reactions, $\text{Se} + \text{O}_2 \rightarrow \text{SeO} + \text{O}$, and $\text{Se} + \text{OCl} \rightarrow \text{SeO} + \text{Cl}$, are best represented by the RECP28VDZ basis set and show very little deviation, less than 2 kcal/mol, between the double and triple excitation calculations. Finally, those reactions which don't include oxygen, namely, $\text{Se} + \text{H}_2 \rightarrow \text{SeH}_2$, and $\text{Se} + \text{Cl}_2 \rightarrow \text{SeCl}_2$, are best predicted by the complete Pople basis set, again with very good consistency throughout a single basis set.

Overall, a common theme can be observed among all the reactions considered; the presence of oxygen in a reaction will almost always produce a situation in which the ECP28MWB basis set will accurately predict the reaction enthalpy. This proves to be a particularly significant observation because if the accuracy of this basis set is just as good, if not better than, the complete Pople basis set, the determination of kinetic rate constants can be carried out in a much shorter time-span and at much less computational expense. Additionally, the issue of the double and triple excitation computations is an interesting one. The reason as to why some reactions have a large difference while others have essentially none warrants further investigation; perhaps the effect of including quadruple excitations would provide supplemental insight.

Table 9: Arsenic Reaction Enthalpies (1)

Level of Theory		ΔH_{rxn} (kcal/mol)		ΔH_{rxn} (kcal/mol)		ΔH_{rxn} (kcal/mol)
Experiment		0.98		-15.78		29.87
B3LYP/LANL2DZ		8.23		6.23		31.65
HF/SDD		-11.96		48.97		37.88
QCISD/SDD		-6.26		3.10		28.49
QCISD(T)/SDD		-4.89		1.68		27.92
CCSD/SDD		2.04		11.99		33.90
CCSD(T)/SDD		0.16		6.93		33.13
HF/6-311++G(3df,3pd)		8.06		37.66		33.79
QCISD/6-311++G(3df,3pd)		7.43		-0.60		36.61
QCISD(T)/6-311++G(3df,3pd)		6.75		-6.88		34.87
CCSD/6-311++G(3df,3pd)		9.10		1.72		36.86
CCSD(T)/6-311++G(3df,3pd)		7.37		-5.95		35.03
QCISD/ECP28MWB		5.05		-2.99		38.06
QCISD(T)/ECP28MWB		5.33		-8.31		37.09
CCSD/ECP28MWB		6.00		-1.39		38.17
CCSD(T)/ECP28MWB		5.67		-7.64		37.15
QCISD/RECP28VDZ		11.31		3.28		39.94
QCISD(T)/RECP28VDZ		11.43		-2.20		38.95
CCSD/RECP28VDZ		12.25		4.86		40.04
CCSD(T)/RECP28VDZ		11.75		-1.56		39.02
Level of Theory		ΔH_{rxn} (kcal/mol)		ΔH_{rxn} (kcal/mol)		ΔH_{rxn} (kcal/mol)
Experiment		-118.12		-53.77		33.58
B3LYP/LANL2DZ		-84.93		-49.63		29.21
HF/SDD		0.28		-0.02		17.92
QCISD/SDD		-72.54		-50.66		23.81
QCISD(T)/SDD		-74.06		-51.24		23.81
CCSD/SDD		-63.60		-43.55		28.73
CCSD(T)/SDD		-68.80		-46.93		28.78
HF/6-311++G(3df,3pd)		-26.00		-20.96		22.32
QCISD/6-311++G(3df,3pd)		-99.55		-45.56		37.79
QCISD(T)/6-311++G(3df,3pd)		-107.31		-48.55		38.74
CCSD/6-311++G(3df,3pd)		-97.11		-44.43		37.73
CCSD(T)/6-311++G(3df,3pd)		-106.32		-48.07		38.71
QCISD/ECP28MWB		-101.94		-47.94		33.50
QCISD(T)/ECP28MWB		-108.74		-49.98		34.59
CCSD/ECP28MWB		-100.22		-47.54		33.43
CCSD(T)/ECP28MWB		-108.01		-49.77		34.54
QCISD/RECP28VDZ		-95.67		-41.68		34.66
QCISD(T)/RECP28VDZ		-102.63		-43.88		35.74
CCSD/RECP28VDZ		-93.97		-41.29		34.59
CCSD(T)/RECP28VDZ		-101.93		-43.69		35.69

Table 10: Arsenic Reaction Enthalpies (2)

Level of Theory		ΔH_{rxn} (kcal/mol)		ΔH_{rxn} (kcal/mol)		ΔH_{rxn} (kcal/mol)
Experiment		-87.30		-15.31		31.17
B3LYP/LANL2DZ		-77.27		-24.31		33.82
HF/SDD		-44.62		-25.66		37.33
QCISD/SDD		-63.65		-21.90		32.16
QCISD(T)/SDD		-64.36		-21.44		31.22
CCSD/SDD		-57.95		-16.57		32.53
CCSD(T)/SDD		-58.96		-16.25		31.42
HF/6-311++G(3df,3pd)		-63.17		-21.70		31.98
QCISD/6-311++G(3df,3pd)		-81.25		-15.10		34.05
QCISD(T)/6-311++G(3df,3pd)		-83.74		-14.28		32.20
CCSD/6-311++G(3df,3pd)		-80.96		-14.93		34.18
CCSD(T)/6-311++G(3df,3pd)		-83.55		-14.17		32.28
QCISD/ECP28MWB		-77.45		-13.65		36.40
QCISD(T)/ECP28MWB		-78.77		-12.06		34.95
CCSD/ECP28MWB		-77.36		-13.63		36.47
CCSD(T)/ECP28MWB		-78.72		-12.05		34.99
QCISD/RECP28VDZ		-72.98		-11.77		39.00
QCISD(T)/RECP28VDZ		-74.33		-10.19		37.52
CCSD/RECP28VDZ		-72.89		-11.75		39.07
CCSD(T)/RECP28VDZ		-74.28		-10.18		37.57
Level of Theory		ΔH_{rxn} (kcal/mol)		ΔH_{rxn} (kcal/mol)		ΔH_{rxn} (kcal/mol)
Experiment		27.89		25.17		-20.01
B3LYP/LANL2DZ		33.93		36.27		-19.70
HF/SDD		30.38		34.95		-28.60
QCISD/SDD		32.40		30.87		-19.52
QCISD(T)/SDD		32.24		29.78		-19.58
CCSD/SDD		16.68		30.95		-19.52
CCSD(T)/SDD		32.25		29.84		-19.54
HF/6-311++G(3df,3pd)		27.05		30.21		-25.28
QCISD/6-311++G(3df,3pd)		30.48		-		-
QCISD(T)/6-311++G(3df,3pd)		29.76		-		-
CCSD/6-311++G(3df,3pd)		30.52		-		-
CCSD(T)/6-311++G(3df,3pd)		29.77		-		-
QCISD/ECP28MWB		26.65		-		-
QCISD(T)/ECP28MWB		25.95		-		-
CCSD/ECP28MWB		26.66		-		-
CCSD(T)/ECP28MWB		25.95		-		-
QCISD/RECP28VDZ		28.22		-		-
QCISD(T)/RECP28VDZ		27.56		-		-
CCSD/RECP28VDZ		28.22		-		-
CCSD(T)/RECP28VDZ		27.56		-		-

Table 11: Selenium Reaction Enthalpies (1)

Level of Theory		ΔH_{rxn} (kcal/mol)		ΔH_{rxn} (kcal/mol)		ΔH_{rxn} (kcal/mol)
Experiment		18.20		1.44		-36.55
B3LYP/LANL2DZ		17.36		15.36		-40.50
HF/SDD		-12.09		48.84		-0.16
QCISD/SDD		-1.41		7.94		-45.82
QCISD(T)/SDD		7.84		14.41		-38.52
CCSD/SDD		7.24		17.19		-38.36
CCSD(T)/SDD		8.13		14.89		-38.96
HF/6-311++G(3df,3pd)		3.17		32.76		-25.85
QCISD/6-311++G(3df,3pd)		14.21		6.18		-38.78
QCISD(T)/6-311++G(3df,3pd)		14.11		0.47		-41.20
CCSD/6-311++G(3df,3pd)		14.56		7.17		-38.98
CCSD(T)/6-311++G(3df,3pd)		14.38		1.07		-41.06
QCISD/ECP28MWB		9.61		1.58		-43.38
QCISD(T)/ECP28MWB		11.64		-1.99		-43.67
CCSD/ECP28MWB		9.71		2.33		-43.83
CCSD(T)/ECP28MWB		11.71		-1.61		-43.74
QCISD/RECP28VDZ		17.51		9.48		-35.48
QCISD(T)/RECP28VDZ		19.49		5.85		-35.82
CCSD/RECP28VDZ		17.64		10.25		-35.90
CCSD(T)/RECP28VDZ		19.55		6.23		-35.89
Level of Theory		ΔH_{rxn} (kcal/mol)		ΔH_{rxn} (kcal/mol)		ΔH_{rxn} (kcal/mol)
Experiment		-100.90		-82.05		-100.25
B3LYP/LANL2DZ		-75.80		-28.37		-45.73
HF/SDD		0.14		4.64		16.73
QCISD/SDD		-67.69		-29.68		-28.27
QCISD(T)/SDD		-61.33		-37.92		-45.76
CCSD/SDD		-58.41		-22.86		-30.10
CCSD(T)/SDD		-60.84		-35.40		-43.53
HF/6-311++G(3df,3pd)		-30.89		-12.46		-15.63
QCISD/6-311++G(3df,3pd)		-92.77		-73.18		-87.39
QCISD(T)/6-311++G(3df,3pd)		-99.96		-82.32		-96.43
CCSD/6-311++G(3df,3pd)		-91.65		-70.85		-85.41
CCSD(T)/6-311++G(3df,3pd)		-99.30		-81.13		-95.51
QCISD/ECP28MWB		-97.37		-75.40		-85.01
QCISD(T)/ECP28MWB		-102.42		-83.73		-95.37
CCSD/ECP28MWB		-96.50		-73.82		-83.53
CCSD(T)/ECP28MWB		-101.98		-82.89		-94.59
QCISD/RECP28VDZ		-89.47		-63.35		-80.86
QCISD(T)/RECP28VDZ		-94.58		-71.89		-91.37
CCSD/RECP28VDZ		-88.58		-61.64		-79.28
CCSD(T)/RECP28VDZ		-94.14		-70.99		-90.54

Table 12: Selenium Reaction Enthalpies (2)

Level of Theory		ΔH_{rxn} (kcal/mol)		ΔH_{rxn} (kcal/mol)		ΔH_{rxn} (kcal/mol)
Experiment	SeO + O ₂ → SeO ₂ + O	18.85	SeO + OH → SeO ₂ + H	2.09	SeO + OCl → SeO ₂ + Cl	-35.90
B3LYP/LANL2DZ		47.43		45.43		-10.43
HF/SDD		4.50		65.43		16.43
QCISD/SDD		38.01		47.367		-6.39
QCISD(T)/SDD		23.41		29.98		-22.94
CCSD/SDD		35.54		45.49		-10.05
CCSD(T)/SDD		25.44		32.20		-21.65
HF/6-311++G(3df,3pd)		18.43		48.03		-10.59
QCISD/6-311++G(3df,3pd)		19.59		11.56		-33.39
QCISD(T)/6-311++G(3df,3pd)		17.64		4.01		-37.67
CCSD/6-311++G(3df,3pd)		20.80		13.41		-32.74
CCSD(T)/6-311++G(3df,3pd)		18.17		4.85		-37.27
QCISD/ECP28MWB		21.97		13.94		-31.02
QCISD(T)/ECP28MWB		18.70		5.06		-36.61
CCSD/ECP28MWB		22.68		15.29		-30.86
CCSD(T)/ECP28MWB		19.09		5.78		-36.35
QCISD/RECP28VDZ		26.12		18.09		-26.87
QCISD(T)/RECP28VDZ		22.69		9.06		-32.62
CCSD/RECP28VDZ		26.93		19.55		-26.61
CCSD(T)/RECP28VDZ	23.14	9.83	-32.30			
Level of Theory		ΔH_{rxn} (kcal/mol)		ΔH_{rxn} (kcal/mol)		
Experiment	Se + H ₂ → SeH ₂	-49.25	Se + Cl ₂ → SeCl ₂	-64.25		
B3LYP/LANL2DZ		-35.94		-48.26		
HF/SDD		-8.12		-16.20		
QCISD/SDD		-25.12		-36.56		
QCISD(T)/SDD		-25.36		-37.44		
CCSD/SDD		-40.84		-36.21		
CCSD(T)/SDD		-25.36		-37.21		
HF/6-311++G(3df,3pd)		-26.20		-35.73		
QCISD/6-311++G(3df,3pd)		-48.00		-59.69		
QCISD(T)/6-311++G(3df,3pd)		-49.95		-62.99		
CCSD/6-311++G(3df,3pd)		-47.96		-59.54		
CCSD(T)/6-311++G(3df,3pd)		-49.94		-62.89		
QCISD/ECP28MWB		-59.95		-52.39		
QCISD(T)/ECP28MWB		-61.19		-53.67		
CCSD/ECP28MWB		-59.80		-52.24		
CCSD(T)/ECP28MWB		-61.12		-53.61		
QCISD/RECP28VDZ		-56.52		-49.39		
QCISD(T)/RECP28VDZ		-57.75		-50.61		
CCSD/RECP28VDZ		-56.36		-49.24		
CCSD(T)/RECP28VDZ	-57.68	-50.56				

4.2 Complete Arsenic Reactions

4.2.1 $\text{As} + \text{O}_2 \rightarrow \text{AsO} + \text{O}$

In the selection of a level of theory for calculating the kinetic rate constant parameters, the performance in predicting the geometry and vibrational frequencies of each species was taken into account, but was of secondary consideration to the reaction enthalpy prediction. In this reaction the best level of theory was found to be QCISD/ECP28MWB, predicting a reaction enthalpy of 5.05 kcal/mol to the experimental value of 0.98 kcal/mol. While other levels of theory were closer in their prediction of this, their geometry and vibrational frequency predictions were far less accurate and so it was decided that this method and basis set combination would be the best choice.

In the creation of the PES for this reaction, as for all bimolecular tri-atomic reactions studied, the structure of the transition state was assumed to be linear, thereby eliminating one degree of freedom and allowing a three-dimensional surface to be constructed. The degrees of freedom accounted for were the As-O₍₁₎ and O₍₁₎-O₍₂₎ bond distances; the single point energy of the system was then calculated after changing one or both bond lengths. These single point energy values were then used to create the PES shown in Figure 7 and the contour plot shown in Figure 8. These figures provide a vicinity in which two possible transition states exist, (1.25, 2.1) and (1.6, 1.7); with the exact value to be determined through further Gaussian computations. The surface geometry is used as the initial geometry of a transition state optimization calculation using Gaussian software package which determines the precise transition state configuration. This geometry, highlighted in Figure 7 (O₍₁₎-O₍₂₎: 1.78, As-O₍₁₎: 1.95), is then used in the frequency calculation to determine the values of the partition functions, so long as a single imaginary frequency is present in the output. Once this calculation is complete, the kinetic rate constant and equilibrium parameters can be investigated.

As previously mentioned, rate constant values were found using both TST and the Hard Sphere Collision Model, with the expectation that the pre-exponential factor of the collision model

would be several orders of magnitude higher than that of the TST. The plots created using both methods are shown in Figure 9 (forward reaction) and Figure 10 (reverse reaction). The evaluation of the trendlines associated with each method generates the Arrhenius expressions shown in (18-21). As expected, the collision model frequency factors are several orders of magnitude greater than those found using TST.

$$18 \quad k_f^{TST} = 6.96 \times 10^{11} e^{\left(\frac{41.92}{RT}\right)} \frac{cm^3}{mol \cdot s}$$

$$19 \quad k_f^{Coll} = 2.95 \times 10^{15} e^{\left(\frac{42.17}{RT}\right)} \frac{cm^3}{mol \cdot s}$$

$$20 \quad k_r^{TST} = 2.12 \times 10^{11} e^{\left(\frac{-36.77}{RT}\right)} \frac{cm^3}{mol \cdot s}$$

$$21 \quad k_f^{TST} = 5.07 \times 10^{15} e^{\left(\frac{-37.28}{RT}\right)} \frac{cm^3}{mol \cdot s}$$

A comparison was also made between the theoretically predicted equilibrium constant and that determined experimentally from existing thermodynamic data on the reactant and product species. This comparison, shown in Figure 11, clearly illustrates that the two curves are completely different, suggesting that, perhaps, the theoretical calculations were in error. However, as additional data concerning other reactions shows, the problem may lie in the available experimental data for the species AsO. It is quite possible that the experimentally determined thermodynamic properties of this species are incorrect as only reactions which include this species have theoretical-experimental disagreement. Despite, the drastic differences, the predicted thermodynamic properties of the reaction are present in (22) and (23).

$$22 \quad \begin{aligned} \Delta H^{Th} &= 5.27 \frac{kcal}{mol} \\ \Delta S^{Th} &= 1.53 \frac{cal}{molK} \end{aligned}$$

$$23 \quad \begin{aligned} \Delta H^{Exp} &= -22.33 \frac{kcal}{mol} \\ \Delta S^{Exp} &= 4.19 \frac{cal}{molK} \end{aligned}$$

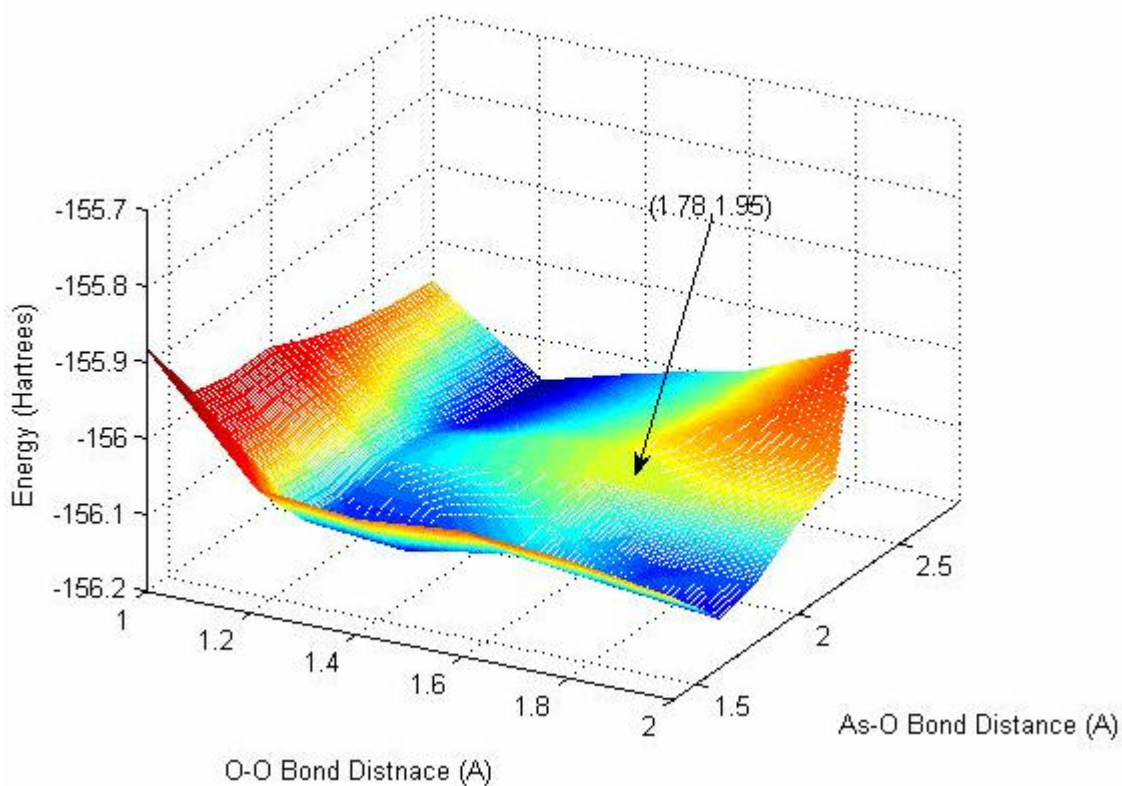


Figure 7: $\text{As} + \text{O}_2 \rightarrow \text{AsO} + \text{O}$ (PES)

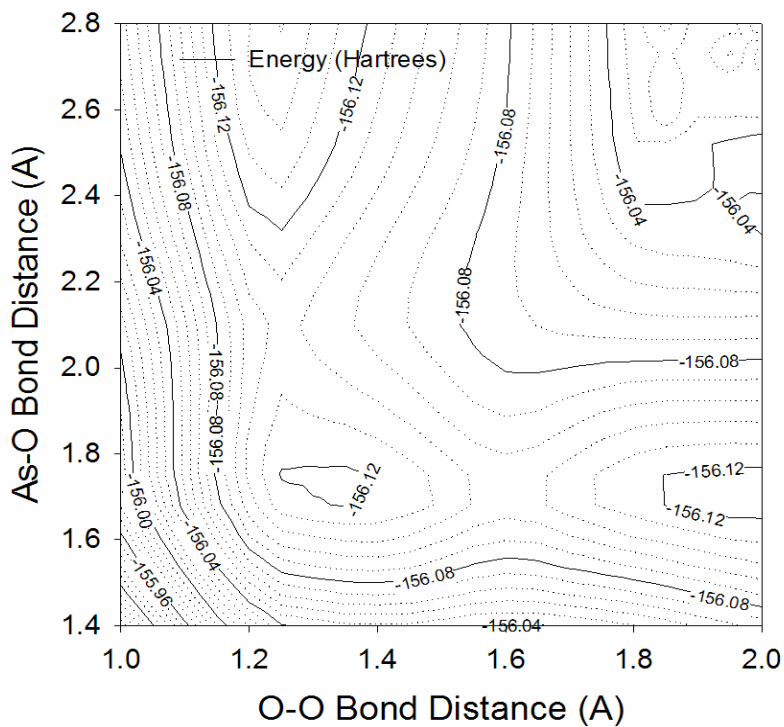


Figure 8: $\text{As} + \text{O}_2 \rightarrow \text{AsO} + \text{O}$ (Contour Plot)

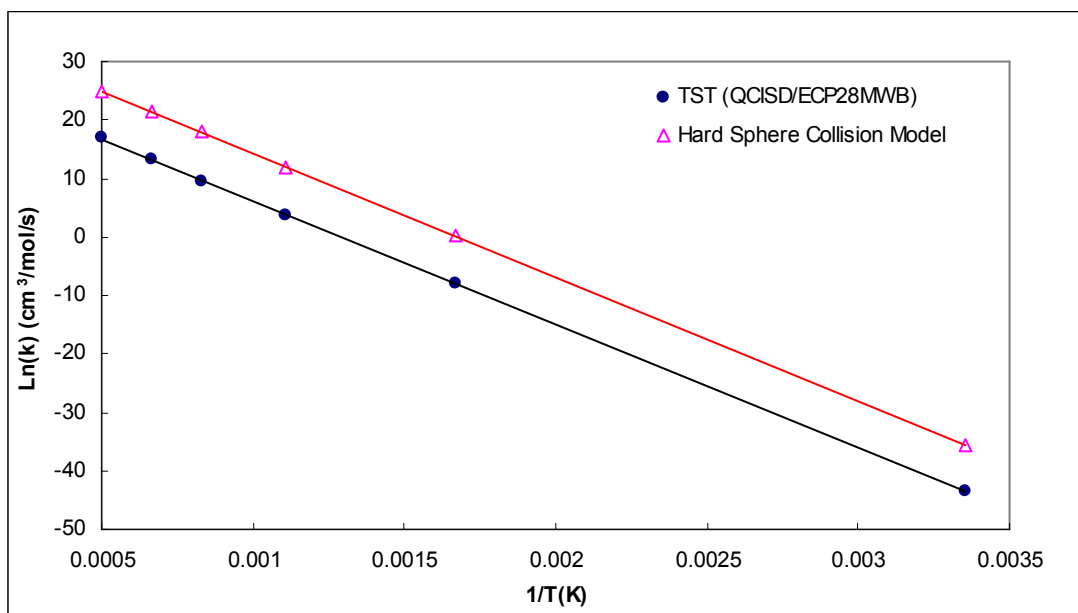


Figure 9: Rate Constant as a Function of Temperature ($\text{As} + \text{O}_2 \rightarrow \text{AsO} + \text{O}$)

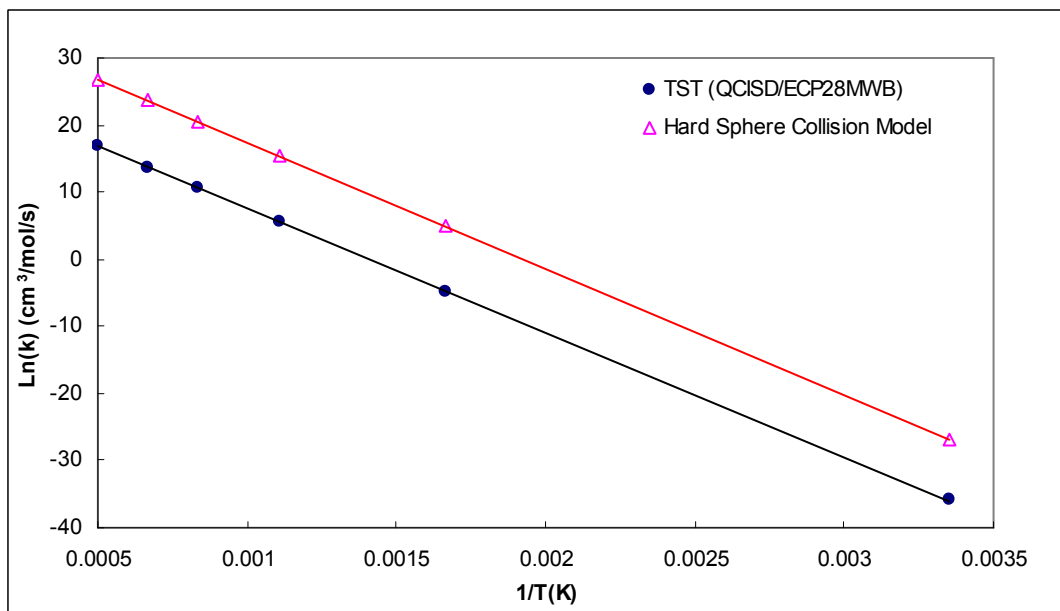


Figure 10: Rate Constant as a Function of Temperature ($\text{AsO} + \text{O} \rightarrow \text{As} + \text{O}_2$)

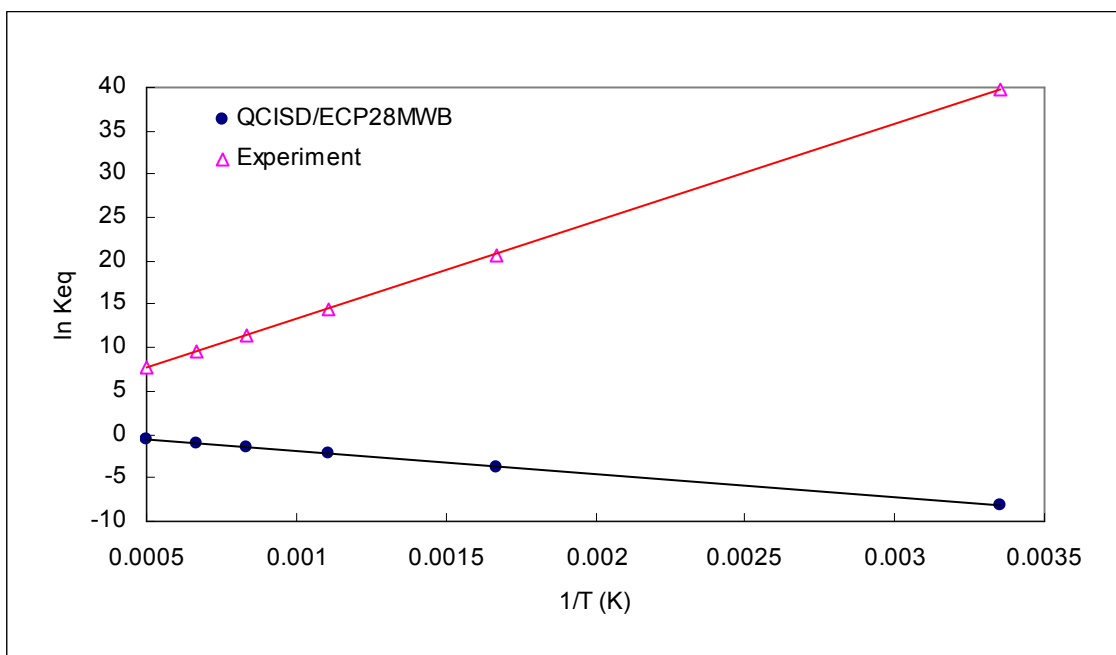


Figure 11: Equilibrium Constant as a Function of Temperature ($\text{As} + \text{O}_2 \rightarrow \text{AsO} + \text{O}$)

4.2.2 As + OH → AsO + H

The best level of theory determined for this reaction was found to be QCISD(T)/ECP28MWB, which gave a reaction enthalpy deviation from experiment of 7.47 kcal/mol. As with the previous reaction, the transition structure created during the reaction of elemental arsenic with the hydroxide radical is assumed to be linear in structure. Here again the active degrees of freedom are the two bond distances (As-O and O-H); and again, from the single point energy data collected at the varying geometries a PES (Figure 12) and a contour plot (Figure 13) were created. Examination of these figures reveals that two possible transition structures exist on the saddle points located at (1.0, 2.6) and (1.75, 1.6), however, calculations performed using the Gaussian software package identify a single transition structure nowhere near a saddle point on the surface. Additionally, this surface shows that an intermediate AsOH species exists, represented by the large potential well and confirmed by energy optimization calculations, and is more stable than either the products or reactants. This casts some suspicion on the results obtained using the transition state optimization calculations as the surface shows that the reaction would be most likely to proceed from reactants to the intermediate through an association reaction and this would then decompose into products, in effect creating two separate steps. However, the modeling of these separate steps requires some experimental knowledge of the intermediate, which does not exist, and the optimization of the transition structure was begun at the points most resembling a saddle on the graph yet the computation still arrived at the listed coordinates from both initial points. Certainly, this reaction requires further examination, but the values obtained are for a valid reaction path, only perhaps not the most likely.

After determining the transition state geometry using a transition state search algorithm, the values of the forward and reverse rate constants at each temperature were calculated and plotted as shown in Figure 14 and Figure 15, respectively. As can be seen, the TST predictions meet the condition that they be smaller than that determined using the hard sphere collision model. From these figures the rate constant expressions for the forward and reverse reactions over the examined temperature range were determined and are provided in 24-27.

$$24 \quad k_f^{TST} = 6.78 \times 10^{13} e^{\left(\frac{-56.83}{RT}\right)} \frac{cm^3}{mol \cdot s}$$

$$25 \quad k_f^{Coll} = 3.71 \times 10^{15} e^{\left(\frac{-56.34}{RT}\right)} \frac{cm^3}{mol \cdot s}$$

$$26 \quad k_r^{TST} = 1.74 \times 10^{14} e^{\left(\frac{-65.09}{RT}\right)} \frac{cm^3}{mol \cdot s}$$

$$27 \quad k_r^{Coll} = 2.57 \times 10^{16} e^{\left(\frac{-65.02}{RT}\right)} \frac{cm^3}{mol \cdot s}$$

The theoretical and experimental thermodynamic results for this reaction are drastically different, as has been observed for all reactions in which AsO is involved. The equilibrium curves shown in Figure 16 clearly show a tremendous discrepancy between the two methods which must be addressed. The parameters for the theory and experiment are provided in 28 and 29.

$$28 \quad \begin{aligned} \Delta H^{Th} &= -7.94 \frac{kcal}{mol} \\ \Delta S^{Th} &= -0.71 \frac{cal}{molK} \end{aligned}$$

$$29 \quad \begin{aligned} \Delta H^{Exp} &= -38.97 \frac{kcal}{mol} \\ \Delta S^{Exp} &= -1.44 \frac{cal}{molK} \end{aligned}$$

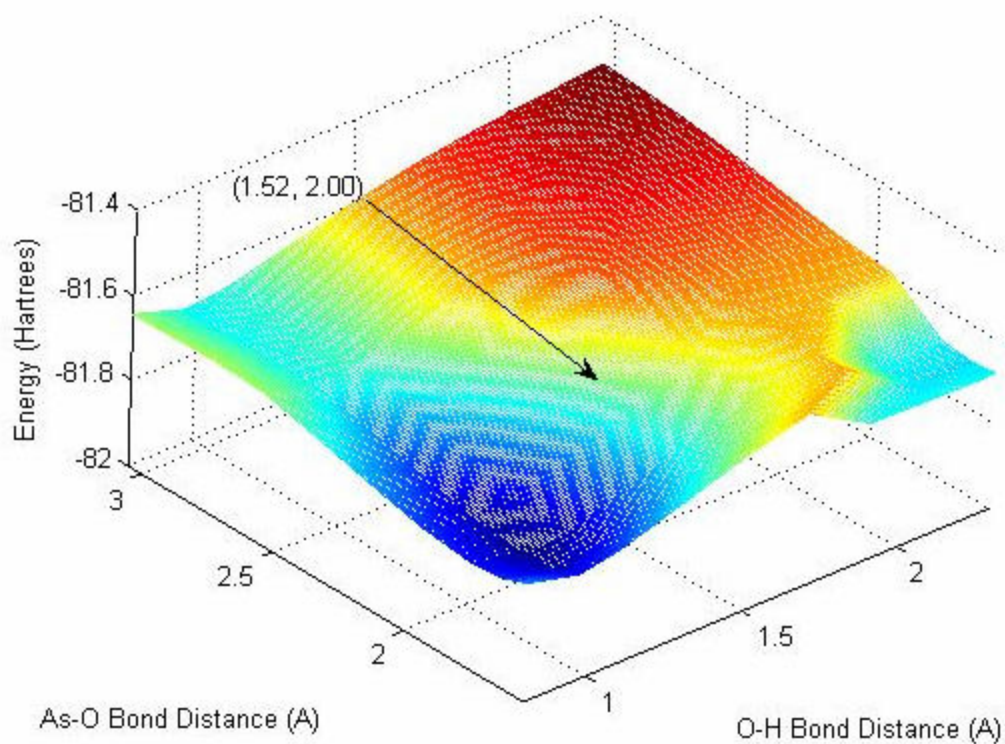


Figure 12: $\text{As} + \text{OH} \rightarrow \text{AsO} + \text{H}$ (PES)

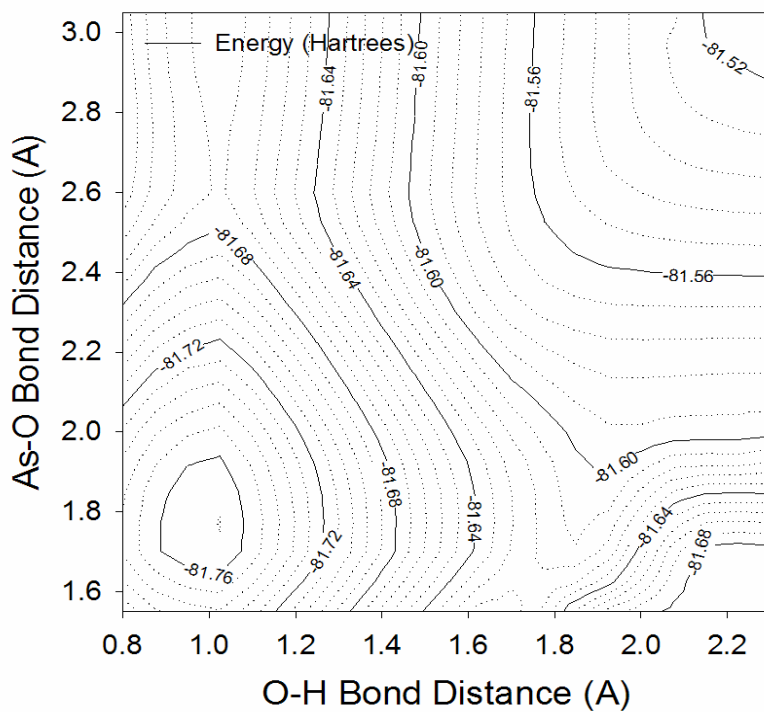


Figure 13: $\text{As} + \text{OH} \rightarrow \text{AsO} + \text{H}$ (Contour Plot)

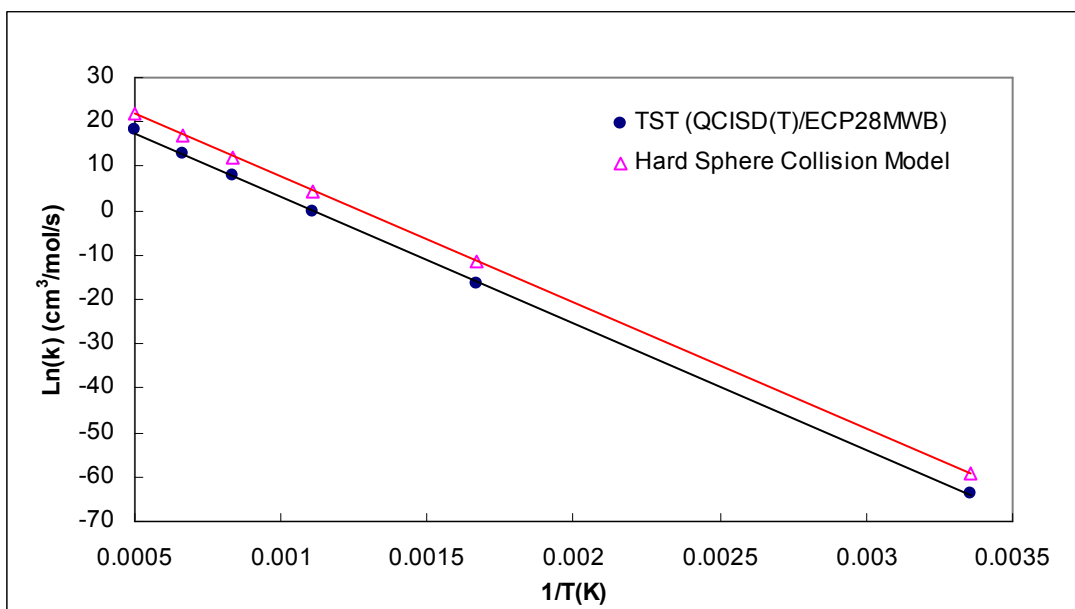


Figure 14: Rate Constant as a Function of Temperature ($\text{As} + \text{OH} \rightarrow \text{AsO} + \text{H}$)

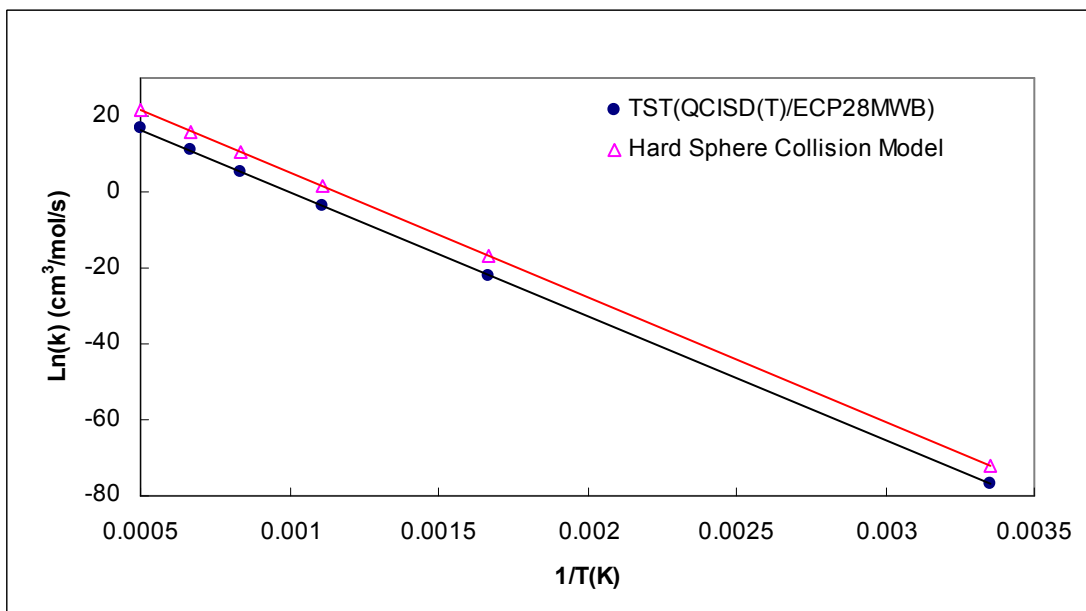


Figure 15: Rate Constant as a Function of Temperature ($\text{AsO} + \text{H} \rightarrow \text{As} + \text{OH}$)

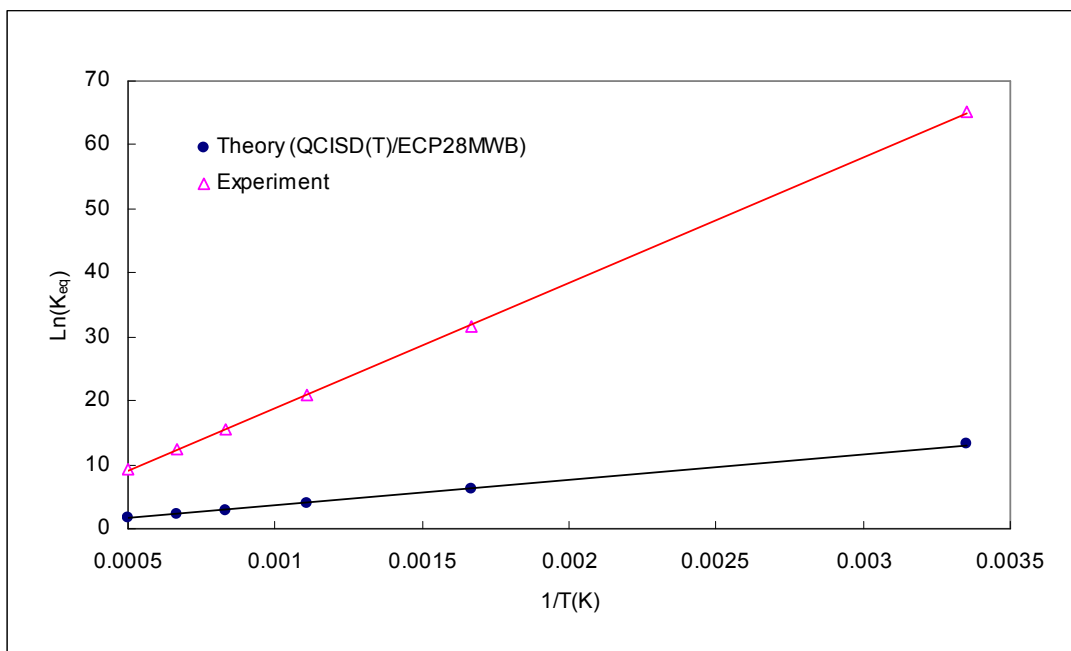


Figure 16: Equilibrium Constant as a Function of Temperature ($\text{As} + \text{OH} \rightarrow \text{AsO} + \text{H}$)

4.2.3 As + HCl → AsCl + H

The best level of theory was found to be QCISD(T)/6-311++G(3df,3pd) having a reaction enthalpy differing from experiment by 5.00 kcal/mol. Again, the transition state of this reaction was assumed to be linear. The PES and the contour plot are provided in Figure 17 and Figure 18, respectively. Using these surfaces as a first approximation, the transition structure geometry was identified, which agreed well with the graphical representation. The values of the rate constant over the temperature range were calculated and plotted in Figure 19, the forward reaction, and Figure 20, the reverse. The determination of the transition state and subsequent computations led to the derivation of the rate constant expressions shown in 30-33.

$$30 \quad k_f^{TST} = 3.35 \times 10^{13} e^{\left(\frac{-40.94}{RT}\right)} \frac{cm^3}{mol \cdot s}$$

$$31 \quad k_f^{Coll} = 1.12 \times 10^{15} e^{\left(\frac{-40.03}{RT}\right)} \frac{cm^3}{mol \cdot s}$$

$$32 \quad k_r^{TST} = 2.27 \times 10^{13} e^{\left(\frac{-5.77}{RT}\right)} \frac{cm^3}{mol \cdot s}$$

$$33 \quad k_r^{Coll} = 1.08 \times 10^{16} e^{\left(\frac{-5.56}{RT}\right)} \frac{cm^3}{mol \cdot s}$$

The lack of experimental data for AsCl meant that no experimental equilibrium constant curve could be generated. Because there is no basis for comparison of the theoretically determined equilibrium curve, the plot has not been included here. However, the theoretical parameters are given in (34) and the values of K_{eq} at each temperature are listed and discussed in the overall discussions section.

$$34 \quad \begin{aligned} \Delta H^{Th} &= 35.39 \frac{kcal}{mol} \\ \Delta S^{Th} &= 2.13 \frac{cal}{molK} \end{aligned}$$

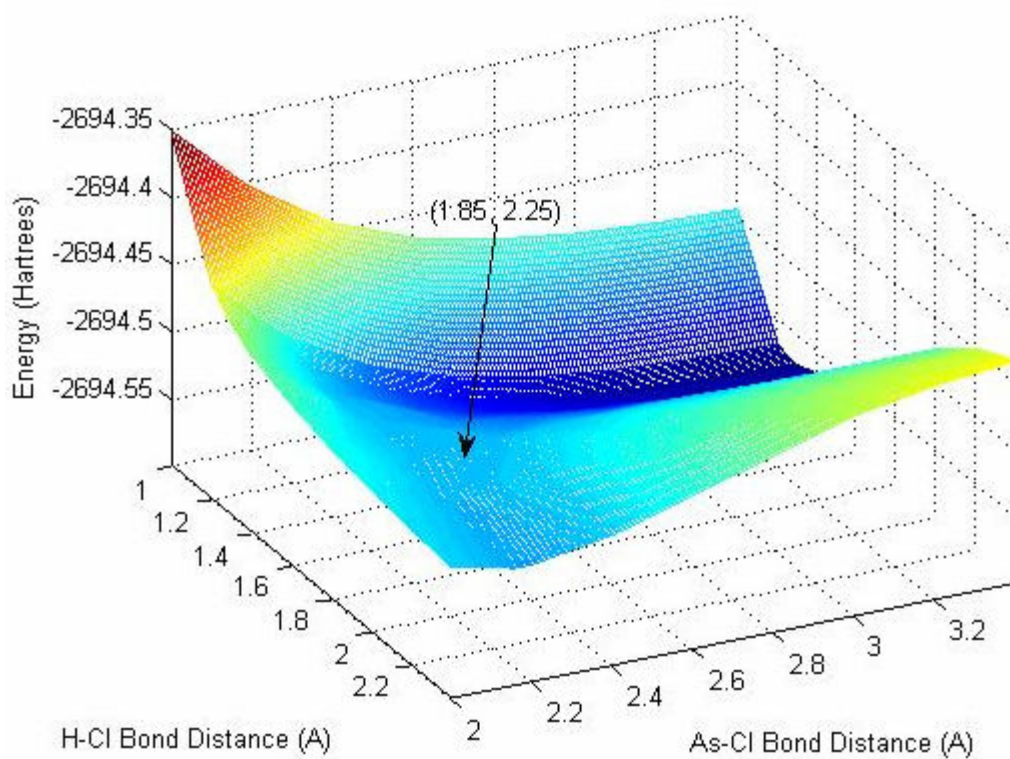


Figure 17: $\text{As} + \text{HCl} \rightarrow \text{AsCl} + \text{H}$ (PES)

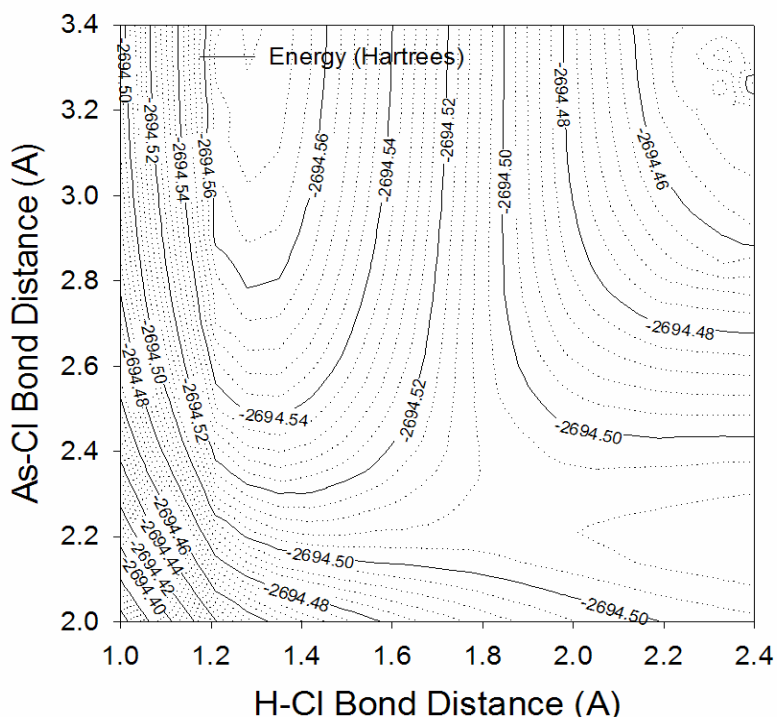


Figure 18: $\text{As} + \text{HCl} \rightarrow \text{AsCl} + \text{H}$ (Contour Plot)

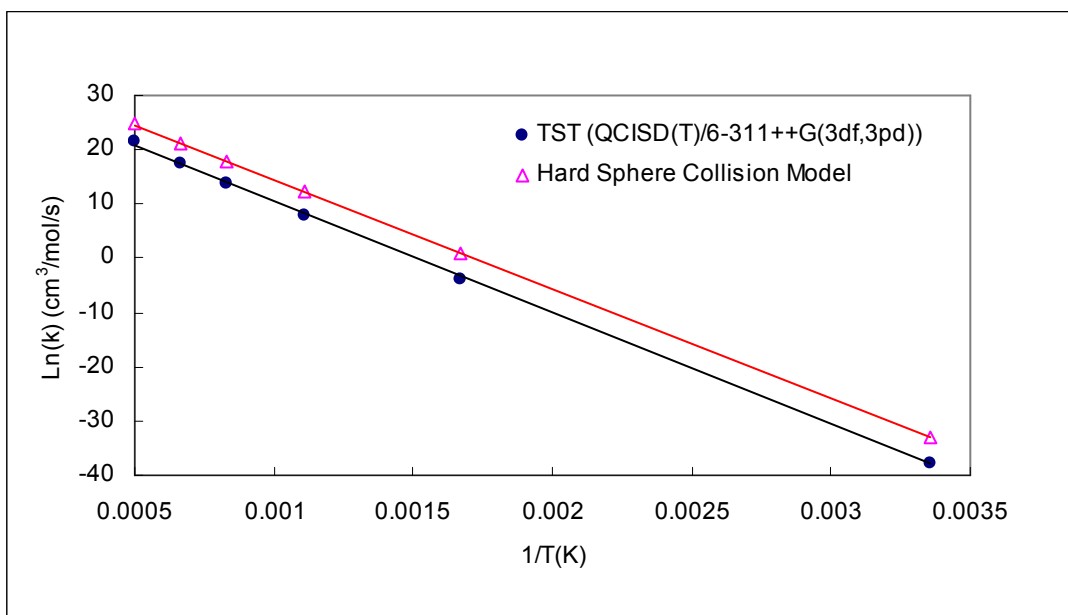


Figure 19: Rate Constant as a Function of Temperature ($\text{As} + \text{HCl} \rightarrow \text{AsCl} + \text{H}$)

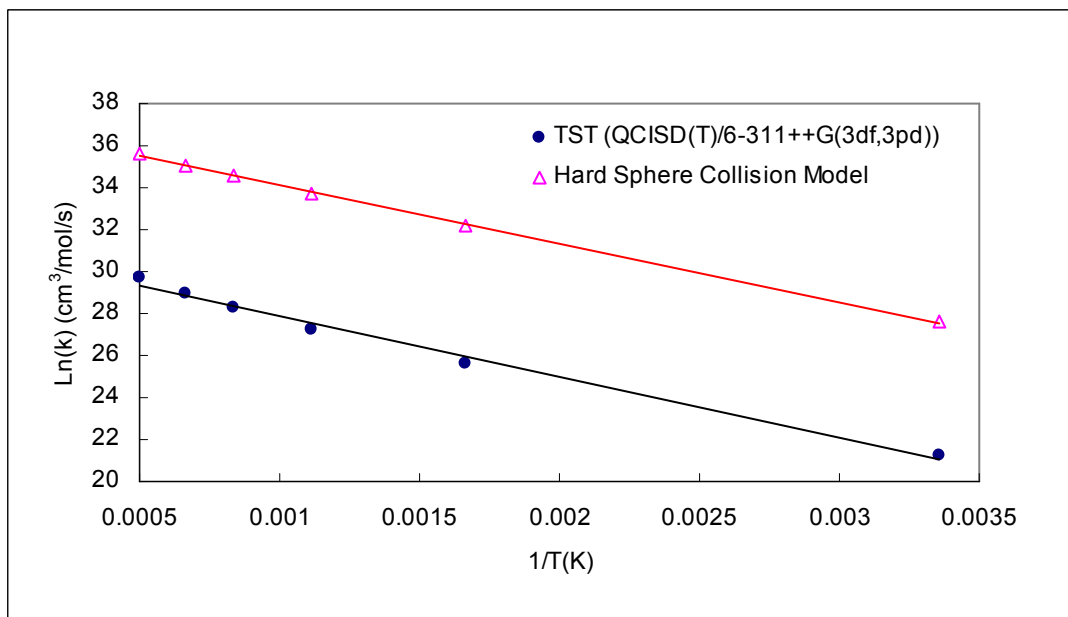


Figure 20: Rate Constant as a Function of Temperature ($\text{AsCl} + \text{H} \rightarrow \text{As} + \text{HCl}$)

4.3 Complete Selenium Reactions

4.3.1 Se + O₂ → SeO + O

The best level of theory for this reaction was found to be CCSD/RECP28VDZ, predicting a reaction enthalpy only 0.15 kcal/mol different from the experimental value. Additionally, this level of theory came within 0.01 Å of the experimental value of the selenium monoxide species. In determining the transition structure the linearity assumption was made once again, limiting the variables to Se-O₍₁₎ and O₍₁₎-O₍₂₎ bond distances. The single point energy values of the structure were then used to create the PES shown in Figure 21 and the contour plot shown in Figure 22. From these figures, the general area in which the transition state falls is quite clear. They provided an initial geometry which was used in a transition state optimization calculation which generated the geometry highlighted in Figure 21 (O₍₁₎-O₍₂₎: 1.53, Se-O₍₁₎: 1.90). After the geometry had been identified, the frequency calculation performed in Gaussian confirmed the presence of a single imaginary frequency which is indicative of a true transition state. After verifying that this geometry was a true transition state, the kinetic rate and equilibrium parameters were then determined.

The rate constant values found using TST and the Hard Sphere Collision Model at each temperature across the entire range were plotted for both the forward and reverse reactions in Figure 23 and Figure 24, respectively. Evaluating the trendlines associated with each method reveals the Arrhenius expressions shown in (35-38). Again, the frequency factors found using the collision model are several orders of magnitude above their TST counterparts while the activation energies remain nearly identical since they are extracted from the same PES.

$$35 \quad k_f^{TST} = 2.32 \times 10^{13} e^{\left(\frac{-55.15}{RT}\right)} \frac{cm^3}{mol \cdot s}$$

$$36 \quad k_f^{Coll} = 1.55 \times 10^{14} e^{\left(\frac{-54.49}{RT}\right)} \frac{cm^3}{mol \cdot s}$$

$$37 \quad k_r^{TST} = 3.32 \times 10^{12} e^{\left(\frac{-37.39}{RT}\right)} \frac{cm^3}{mol \cdot s}$$

$$38 \quad k_r^{Coll} = 2.71 \times 10^{14} e^{\left(\frac{-37.02}{RT}\right)} \frac{cm^3}{mol \cdot s}$$

Figure 25 presents the theoretical and experimental equilibrium constant plots as a function of temperature. Notice how well the curves match one another, suggesting that the equilibrium data collected from theoretical calculations, and by association the calculations themselves, are accurate. Analysis of the trendlines of both plots generates the thermodynamic data shown in 39 and 40.

$$39 \quad \begin{aligned} \Delta H^{Th} &= 17.87 \frac{kcal}{mol} \\ \Delta S^{Th} &= 3.05 \frac{cal}{molK} \end{aligned}$$

$$40 \quad \begin{aligned} \Delta H^{Exp} &= 18.32 \frac{kcal}{mol} \\ \Delta S^{Exp} &= 3.55 \frac{cal}{molK} \end{aligned}$$

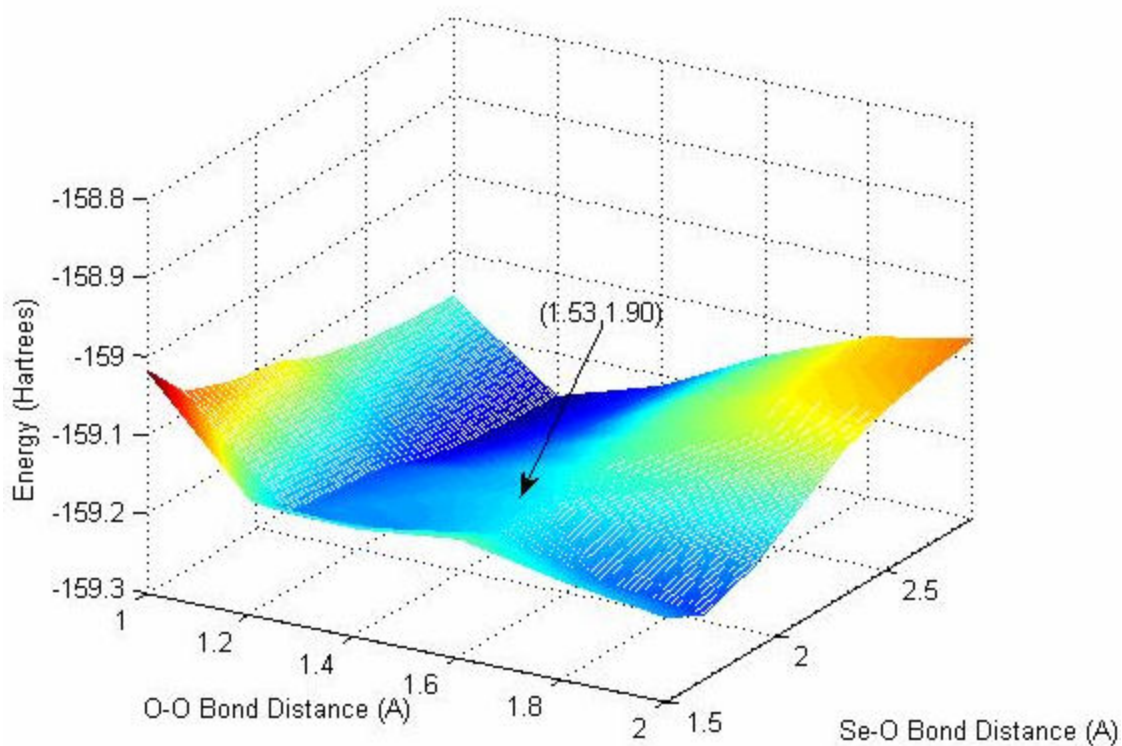


Figure 21: $\text{Se} + \text{O}_2 \rightarrow \text{SeO} + \text{O}$ (PES)

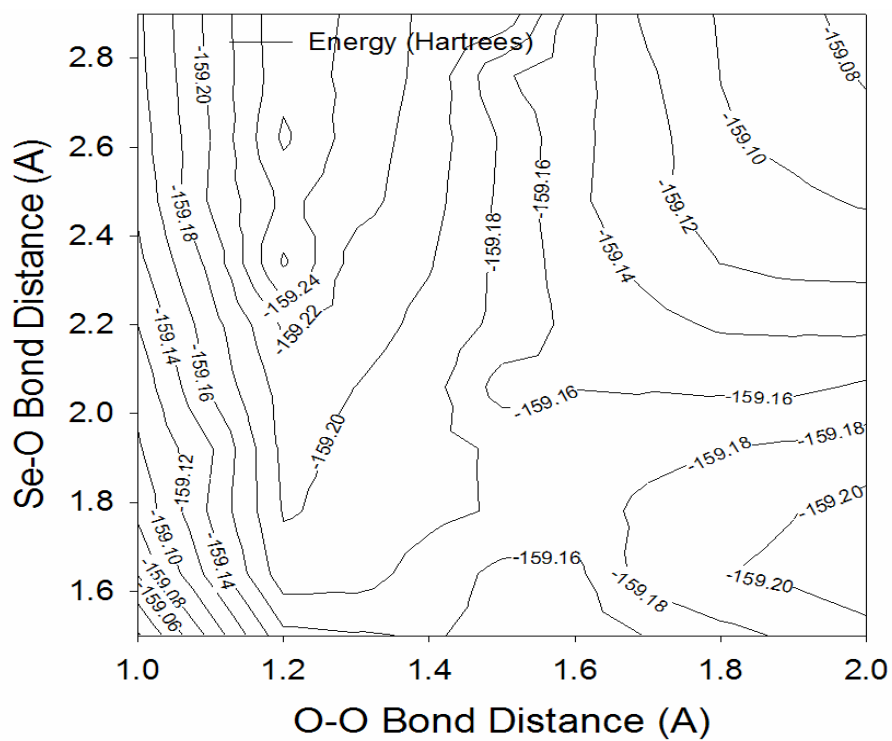


Figure 22: $\text{Se} + \text{O}_2 \rightarrow \text{SeO} + \text{O}$ (Contour Plot)

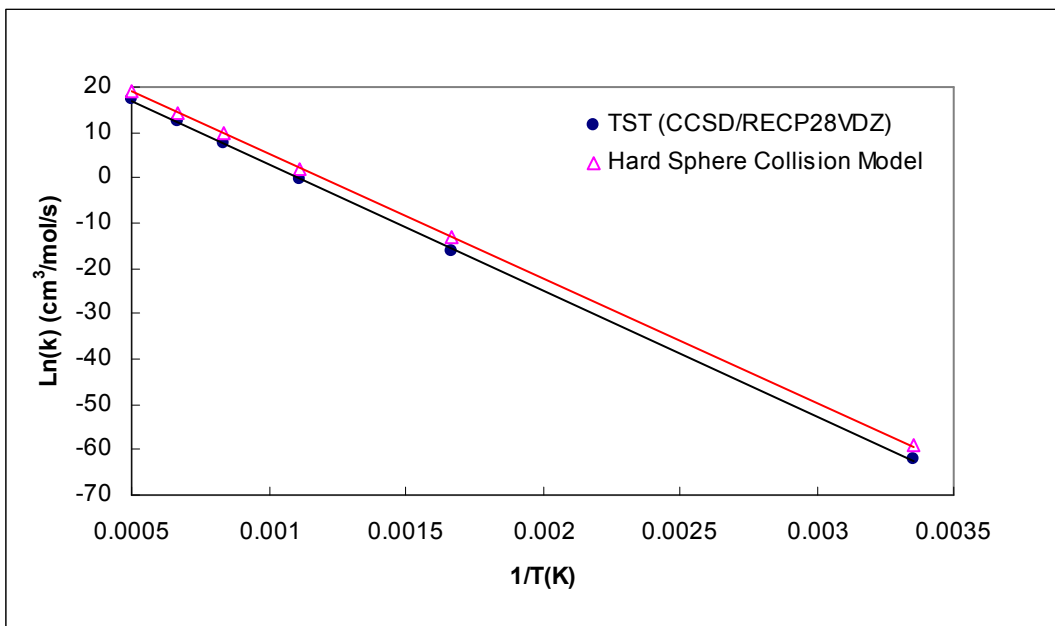


Figure 23: Rate Constant as a Function of Temperature ($\text{Se} + \text{O}_2 \rightarrow \text{SeO} + \text{O}$)

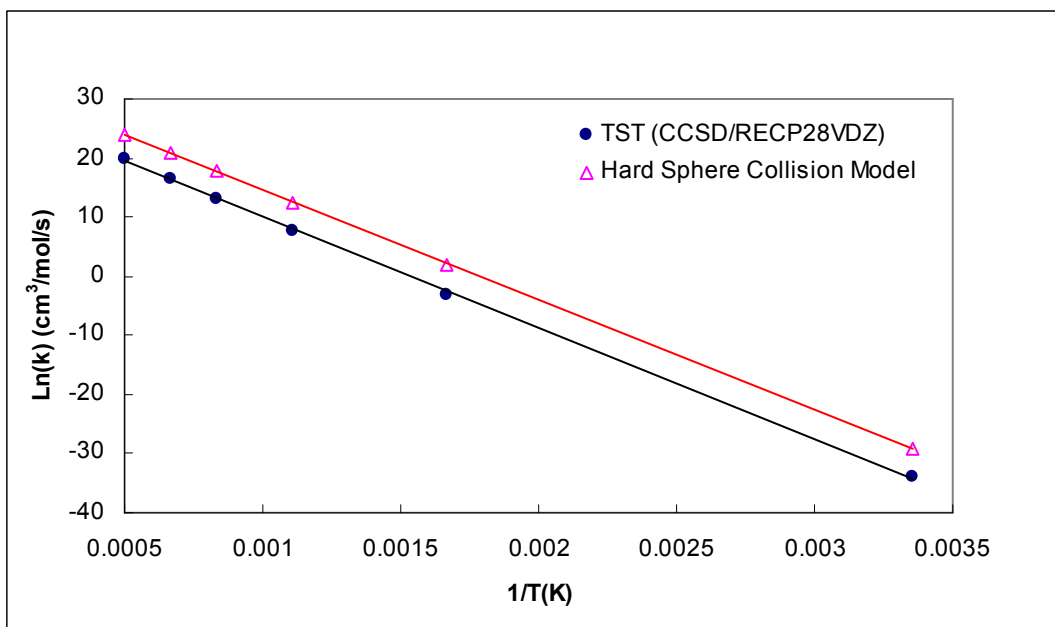


Figure 24: Rate Constant as a Function of Temperature ($\text{SeO} + \text{O} \rightarrow \text{Se} + \text{O}_2$)

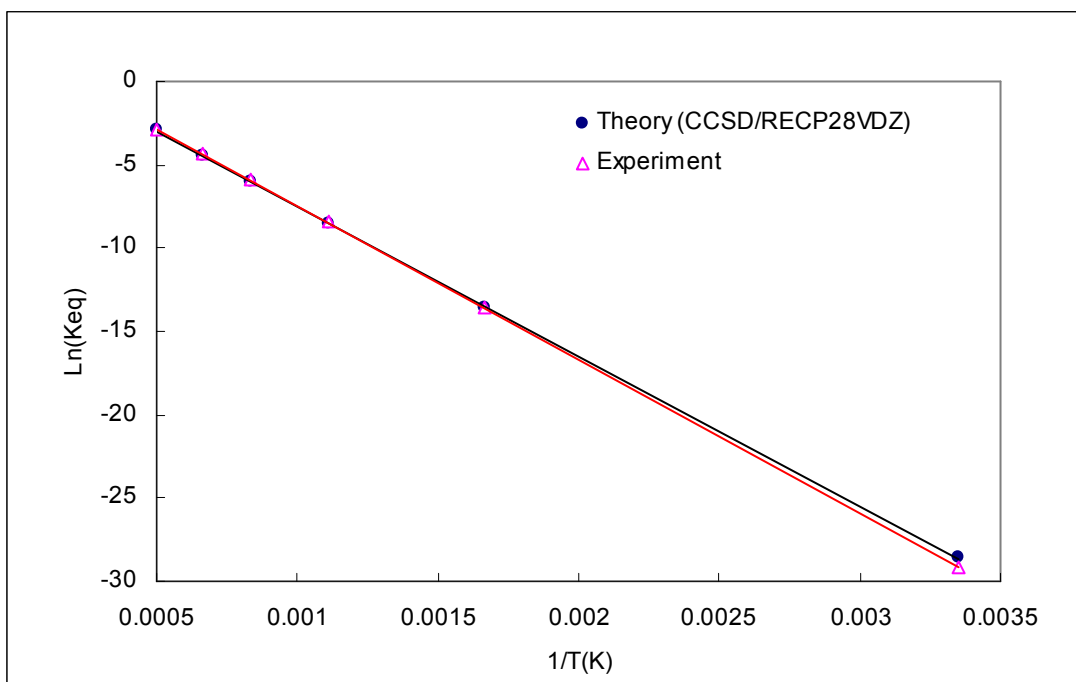


Figure 25: Equilibrium Constant as a Function of Temperature ($\text{Se} + \text{O}_2 \rightarrow \text{SeO} + \text{O}$)

4.3.2 Se + H₂ → SeH₂

In evaluating the unimolecular decomposition reaction, the best level of theory was found to be CCSD(T)/6-311++G(3df,3pd), predicting a reaction enthalpy which deviated from experiment by only 0.69 kcal/mol, however, this value is based upon an optimization of SeH₂ at the lower QCISD/6-311++G(3df,3pd) level of theory. This was done because the geometry optimization of this species could not be completed at the initial level of theory and so the energetics were calculated using an optimized geometry from a lower level of theory. In determining the transition structure, the linearity assumption was impractical and so instead the assumption was made that the distance of both H atoms from Se was equal. By imposing a symmetrical nature on the reaction, the variables could be limited to the Se-H bond length and the H-Se-H bond angle. In this way the PES shown in Figure 26 and the contour plot in Figure 27 were created. Inspection of these surfaces shows the transition state to exist at a bond distance of roughly 2.15 Å and a bond angle of about 25°. Transition state optimizations and complete energetics calculations confirmed this as the true transition state and the kinetic parameters were determined from there using RRKM Theory.

The decomposition rate constant at each temperature was plotted for two collisional efficiency values as shown in Figure 28. The expression in 41, presents the rate of decomposition of the SeH₂ molecule assuming a collisional efficiency of 0.1, that is, only 10% of collisions will result in a complete reaction; a 100% efficiency coefficient increases the pre-exponential factor by one order of magnitude with no change in E_a. It should also be noted that the collision partner used in this calculation, the generic species M, is argon (Ar).

$$41 \quad k_r^{RRKM} = 6.66 \times 10^9 e^{\left(\frac{-69.40}{RT}\right)} \frac{cm^3}{mol \cdot s}$$

While TST is insufficient for predicting the rate of the forward reaction, it is possible to determine this parameter by back calculating it from the reverse rate and the equilibrium constant. In this manner the rate constant expression for the association reaction of Se and H₂ was found using the decomposition kinetics and the equilibrium data calculated from the thermodynamic parameters given below. The forward rate constant is thus given by 42.

$$42 \quad k_f = 1.88 \times 10^{10} e^{\left(\frac{-20.12}{RT}\right)} \frac{\text{cm}^3}{\text{mol} \cdot \text{s}}$$

The thermodynamic predictions of this reaction compare very well to experiment. Figure 29 shows both plots, with only a slight divergence at low temperatures; the parameter values calculated from these plots are given in 43 and 44.

$$43 \quad \begin{aligned} \Delta H^{Th} &= -51.35 \frac{\text{kcal}}{\text{mol}} \\ \Delta S^{Th} &= -24.40 \frac{\text{cal}}{\text{molK}} \end{aligned}$$

$$44 \quad \begin{aligned} \Delta H^{Exp} &= -50.12 \frac{\text{kcal}}{\text{mol}} \\ \Delta S^{Exp} &= -23.79 \frac{\text{cal}}{\text{molK}} \end{aligned}$$

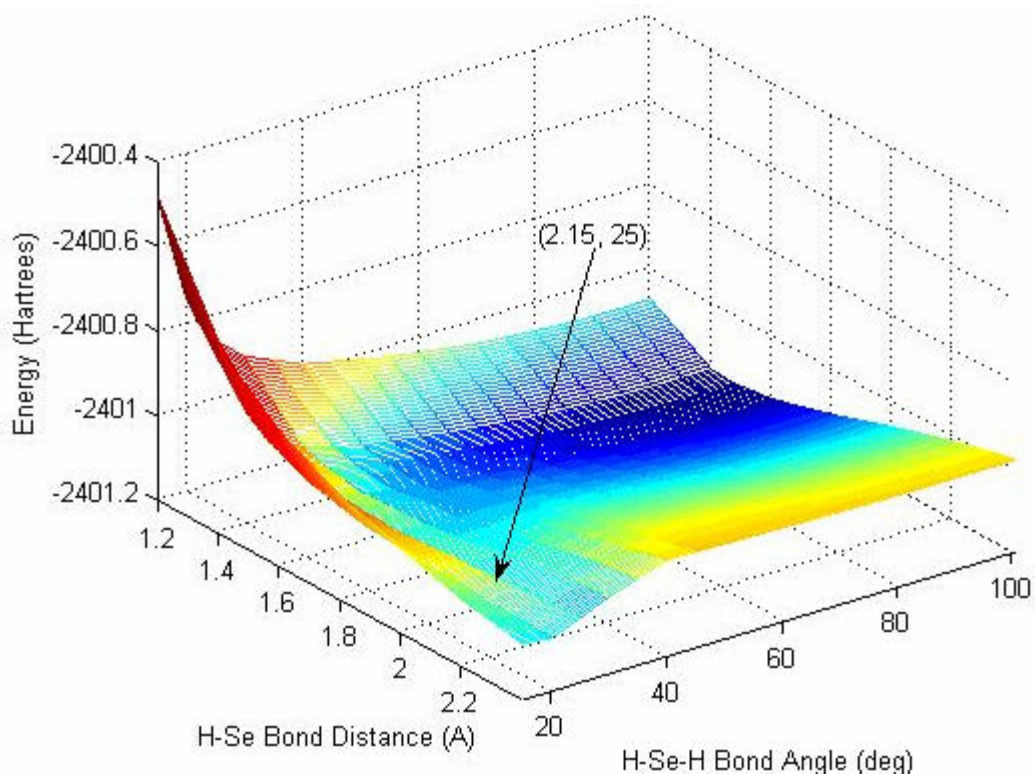


Figure 26: $\text{Se} + \text{H}_2 \rightarrow \text{SeH}_2$ (PES)

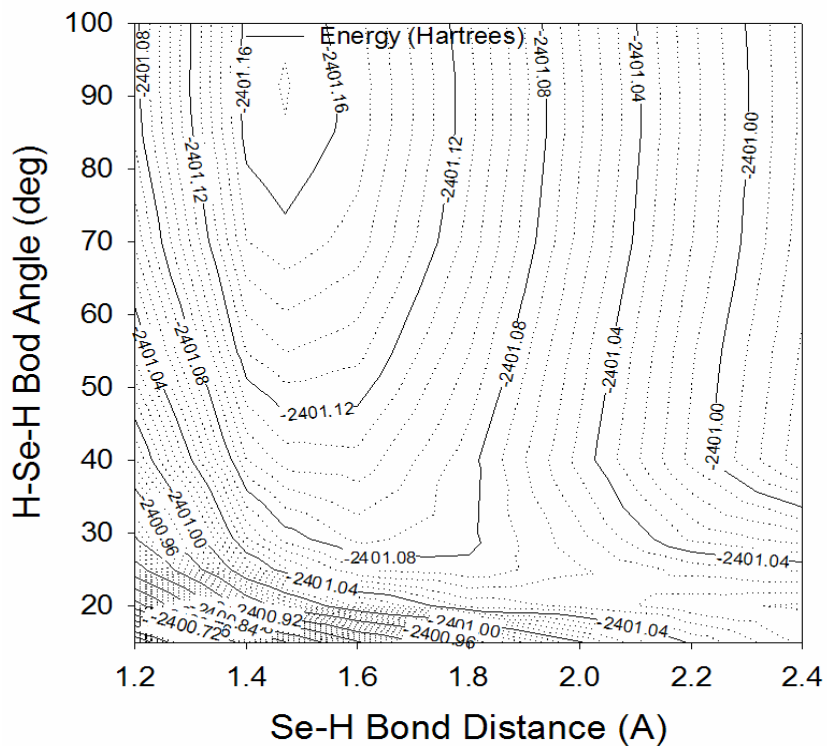


Figure 27: $\text{Se} + \text{H}_2 \rightarrow \text{SeH}_2$ (Contour Plot)

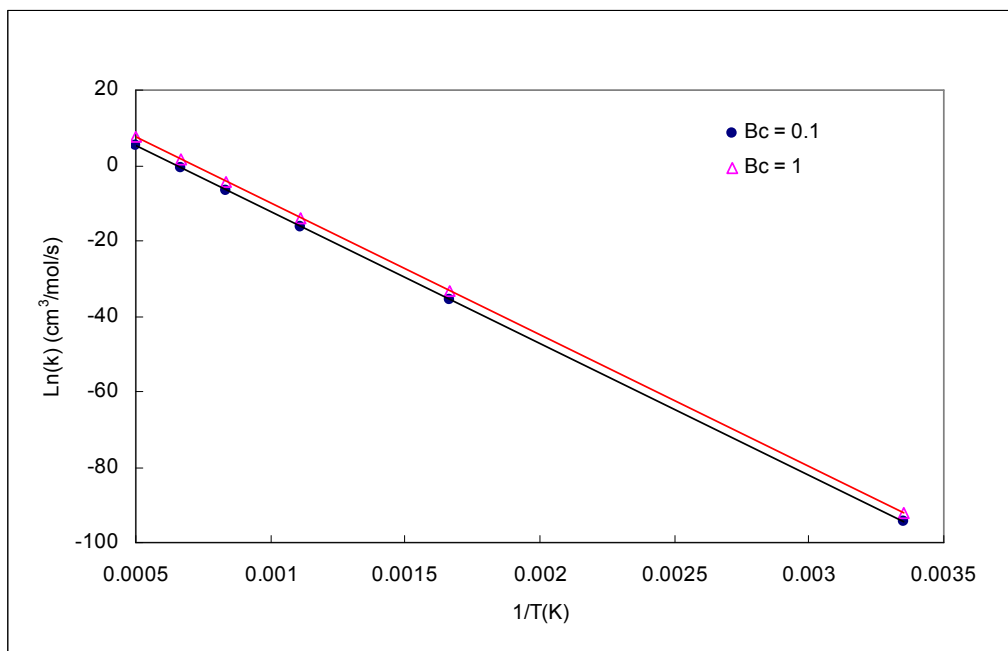


Figure 28: Rate Constant as a Function of Temperature ($\text{SeH}_2 \rightarrow \text{Se} + \text{H}_2/\text{Ar}$ bath gas)

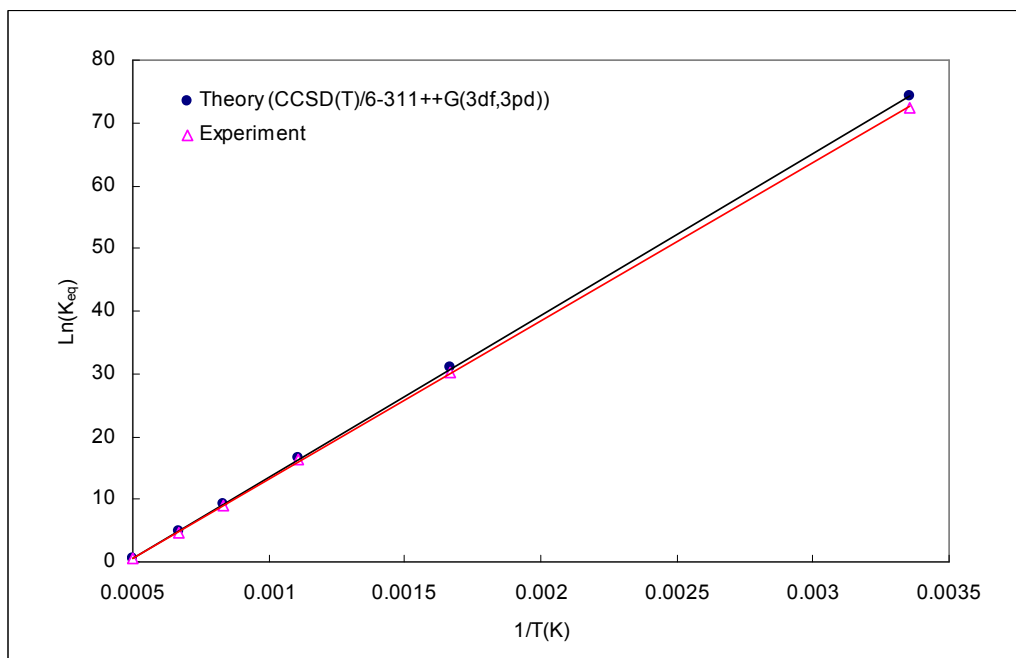


Figure 29: Equilibrium Constant as a Function of Temperature ($\text{Se} + \text{H}_2 \rightarrow \text{SeH}_2$)

4.4 Incomplete Reactions

The reactions included in this section were among those under investigation but were incomplete as of the writing of this thesis. The reactions included herein are those for which a level of theory validation was accomplished but no kinetic rate data could be obtained due to a lack of computed transition structures. While a full analysis could not be given, a thermodynamic study and PES were completed for some reactions while for others only the thermodynamics could be completed. The data for these reactions is presented according to the furthest progress made in the process with a discussion or comparison included when applicable.

4.4.1 Reactions to with only a Thermodynamic Study

Table 13 presents a list of the reactions which have defined thermodynamic properties but no PES. The reaction enthalpy and entropy values were extracted from the equilibrium plots which follow.

Figure 30 presents the equilibrium curve for the reaction, $\text{As} + \text{O} \rightarrow \text{AsO}$. The previously mentioned issue dealing with the experimental values of AsO is present here as well. Because this is the most basic reaction involving AsO, its formation from atomic constituents, and there is tremendous deviance between experiment and theory, a more solid case is made for the re-examination of the validity of experimentally determined values for this species.

The equilibrium curve for the reaction, $\text{SeO} + \text{O}_2 \rightarrow \text{SeO}_2 + \text{O}$ is presented in Figure 31. Notice that the experimental and theoretical plots run parallel to one another for the entire temperature range, meaning that the slopes, i.e., the quantities related to the reaction enthalpy are nearly identical while there is a slight difference in the displacement created by different entropy predictions, which can be seen clearly in the table. The reason for this slight discrepancy is most likely due to a minor tabulation error of some kind, perhaps the standard entropy value was taken at 300 K instead of 298.15 K; in any case the comparison shows the difference between each method to be minimal.

Table 13: Thermodynamic Parameters for Reactions w/o PES's

Reaction	Theoretical Parameters		Experimental Parameters	
	ΔH_{rxn} (kcal/mol)	ΔS_{rxn} (cal/molK)	ΔH_{rxn} (kcal/mol)	ΔS_{rxn} (cal/molK)
$\text{As} + \text{O} \rightarrow \text{AsO}$	-109.91	-24.78	-142.25	-26.26
$\text{SeO} + \text{O}_2 \rightarrow \text{SeO}_2 + \text{O}$	19.09	-4.59	18.89	-2.40

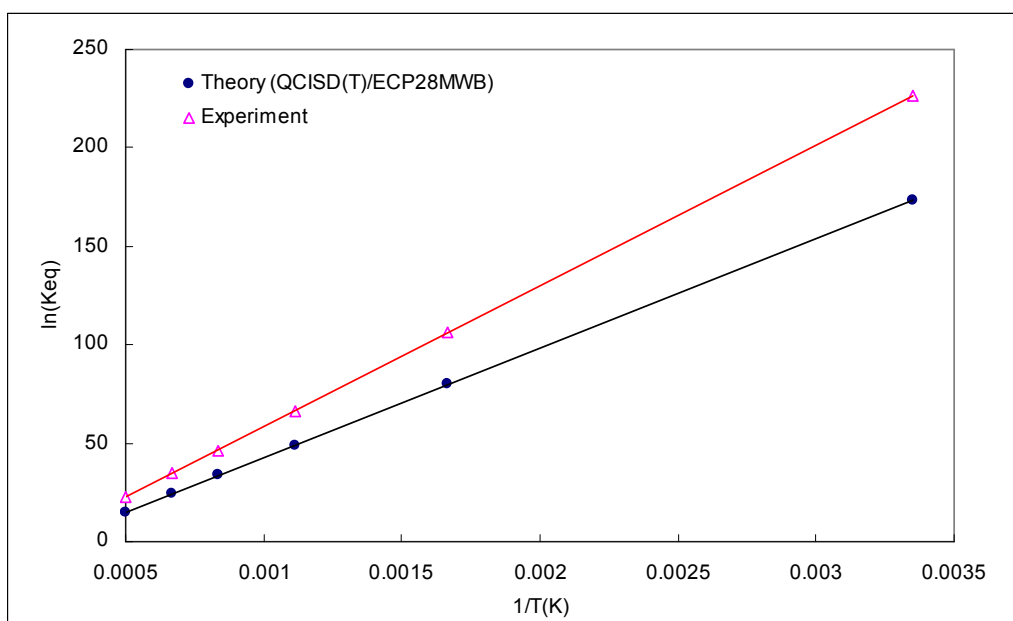


Figure 30: Equilibrium Constant as a Function of Temperature ($\text{As} + \text{O} \rightarrow \text{AsO}$)

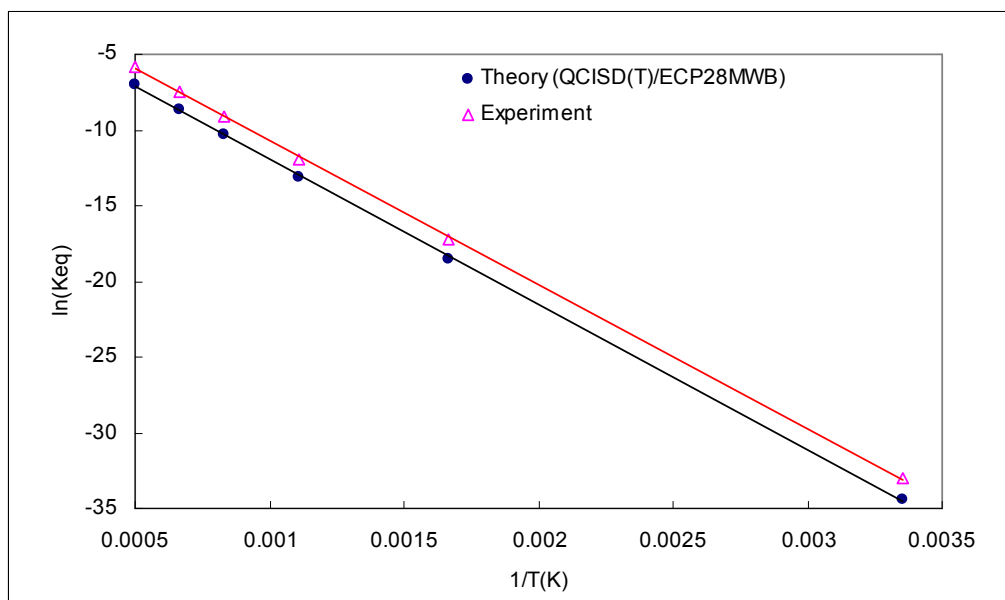


Figure 31: Equilibrium Constant as a Function of Temperature ($\text{SeO} + \text{O}_2 \rightarrow \text{SeO}_2 + \text{O}$)

4.4.2 Reactions with Thermodynamic Study and PES

In the case of several reactions, a PES was constructed but further computations yielded no information regarding the transition structure. In these instances, the information obtained on the reactants and products was still useful in determining the equilibrium constant and a full thermodynamic study could be accomplished. Table 14 shows the thermodynamic parameters of each reaction for both the theoretical and experimental approaches. Additionally, the completed PES and equilibrium curves for each reaction are included and discussed below.

As the data in Table 14 clearly shows, each reaction, with the exception of that including AsO, has fairly good agreement between the theoretical and experimental thermodynamic parameters with deviations of only a few kcal/mol for the enthalpy and <3 cal/molK for the entropy. It is worth mentioning again that AsO is the species present in the other reactions which possess drastically different theoretical and experimental values, lending credence to the suspicion that the experimentally tabulated data is in error. In any event, the equilibrium constant plot for the other arsenic reaction, $\text{As} + \text{OH} \rightarrow \text{AsH} + \text{O}$, is shown in Figure 32. It is important to note that the data is only tabulated up to 1500K ($\sim 6.67 \times 10^{-4}$ 1/K) since no experimental data existed for AsH above this temperature. From the figure, the largest deviation occurs at lower temperatures; the reason for this is unknown, but because the AsH radical would more likely appear at higher temperatures, it may be calculating its properties accurately at ambient conditions is more difficult. Further experimental analysis would be required to make a definitive statement. The PES of this reaction, presented in Figure 33, shows the typical elements of a complete surface, the reactants are represented by the dark blue region in the rear left while the products are located in the light green region in the near right. However, the product energy is never quite reached in this region, the transition structure potential energy along the optimum product geometry line (As-H = 1.51 Å) approaches the total product energy asymptotically, therefore, there is no transition state for this reaction. The kinetics for this reaction would have to be solved using the VTST method which has not yet been employed.

The reaction of As with the OCl radical to form AsO and Cl also follows the trend of divergent theoretical and experimental equilibrium curves as seen in Figure 34. As before, the largest

deviation occurs at lower temperatures, perhaps due to the stability of the radical. The PES for this reaction, shown in Figure 35, presents a two-stage reaction with a somewhat stable AsOCl radical species. While there appears to be two points on the surface which resemble a saddle point, the energetic calculations performed thus far have not been able to verify this, although this may be a computational resource issue. In the future, re-examining this reaction with a lower level of theory may reveal the exact nature of the process.

The theoretical equilibrium constant plots for the selenium reactions match up much more closely with the experimental data. These comparisons are given for the following reactions: $\text{Se} + \text{O}_2 \rightarrow \text{SeO}_2$ (Figure 36), $\text{SeO} + \text{O} \rightarrow \text{SeO}_2$ (Figure 37), $\text{Se} + \text{OCl} \rightarrow \text{SeO} + \text{Cl}$ (Figure 38), and $\text{Se} + \text{O} \rightarrow \text{SeO}$ (Figure 39). Upon examining these plots it is immediately clear that the theoretical and experimental curves are nearly identical across the entire temperature range. The fact that there is such close agreement means that each method serves to independently validate the other thus helping to legitimize both the experimental methodology and the theoretical computations.

The PES's are also presented for these same reactions. Figure 40 presents the PES for the insertion reaction, $\text{Se} + \text{O}_2 \rightarrow \text{SeO}_2$, in a similar manner to that of Figure 26, in which both Se-O bonds are considered symmetrical and the second degree of freedom is the bond angle. In creating this surface, the absence of the reactant molecules was very conspicuous, no matter what configuration was considered, the total energy was never found to match that of the independent reactants Se and O_2 . In fact, the entire region of the graph around which the reactants would most likely appear, the bottom center, had several convergence issues and unpredicted behavior. In contrast, the area of the graph around the product, SeO_2 , behaved exactly as expected, a broad flat region representing the potential well of the stable species. The surface also shows a low energy region in the truncated right corner which most likely represents the separation of the atoms to a point at which they have little influence upon each other and so exist as independent atoms. The issue of surface crossing may have a tremendous impact upon the behavior of this surface due to the fact that the overall spin-multiplicity of the reactants at ground state is 5 while that of the product is 1. This forming of bonds between previously unbonded electrons would be most likely to occur in the regions of the surfaces in which the reactants would be located and so

the issue of overlapping surfaces may be the main cause of the uncertainty surrounding this reaction.

The surface shown in Figure 41 presents a unique view of what appears to be a two-stage reaction. In this reaction an oxygen atom approaches a molecule of SeO to form SeO₂. The bond angle is held constant at the optimum SeO₂ geometry (114.29°) so that the only degrees of freedom are each of the Se-O bond distances. The reactants appear on the surface in the region of the plot near (1.65 Å, 3.00 Å), on the high ridge while the product exists in the valley near the coordinates (1.6 Å, 1.65 Å). The presence of the middle valley is what suggests the two-staged reaction mechanism as it represents an intermediate structure of some kind. It is suspected that the middle valley is caused by the Se-O double bond; as the free oxygen atom approaches the SeO molecule it initially forms a single bond with selenium which causes a dramatic decrease in the potential energy of the system. In order for it to form the second bond, however, it must move even closer, which increases the repulsive forces causing the middle ridge on the surface to be created. Once it moves close enough to achieve the double bond, the energy again decreases and the product is formed. This particular surface does not lend itself to data interpretation very well since the narrow bond length range and wide potential energy difference makes identification difficult. This reaction would most likely be better served by identifying the intermediate structure, if possible, and dividing the surface into two separate figures.

The behavior of the surface shown in Figure 42, for the reaction of Se and OCl, presents several questions. Both the total product and reactant energies were identified on the surface, the products SeO and Cl in the lower central region and the reactants in the potential well in the upper central section. The broad, near uniform area at the product coordinates is expected to be a potential minimum, but the behavior surrounding the reactant coordinates is strange because this region should have a similar uniformity. The reactant total energy is found at the coordinates (1.57 Å, 2.7 Å) and it is expected that as the distance between Se and O increases through movement along the y-axis, the energy should decrease, though only slightly from that of the optimal configuration. However, the surface shows just the opposite, that as this distance is increased the energy increases as well. Additionally, this valley runs nearly parallel to x-axis for almost the entire length of the surface, being interrupted by a rise at x-values of 1.65 and 1.7.

This situation is unlike that seen in any other PES's studied so far and it is unclear as to the reason for this behavior; this is a three-atom system with no surface crossings near the suspicious areas. Further, while there appears to be somewhat of a saddle point between the reactants and products at approximately (1.65 Å, 2.5 Å), transition state optimization calculations have yet to elucidate this phenomenon.

The reaction of Se and O to form SeO is a slightly different situation than the other Se reactions. The only reaction coordinate is the Se-O bond distance and so a potential energy diagram is created rather than a potential energy surface as shown in Figure 43. The diagram presents complications similar to those seen in Figure 41 in that the formation of a single then a double Se-O bond creates a surface crossing due to spin multiplicity change which makes calculations more difficult. The asymptotic plateau on the far right is typical of all PED's, as is the valley where the product resides, however, the barrier shown in between these features is a creation of the transition from a single to a double bond. Because the exact bond length at which the crossover is made is unknown, it is difficult to know if the barrier is real or if it is only an illusion caused by the inability of computing potential energy values at or near the surface crossing. This reaction, therefore, may or may not have an intermediate structure which may or may not be a significant factor in determining the kinetics of the system.

Table 14: Thermodynamic Parameters for Reactions w/ PES's

Reaction	Theoretical Parameters		Experimental Parameters	
	ΔH_{rxn} (kcal/mol)	ΔS_{rxn} (cal/molK)	ΔH_{rxn} (kcal/mol)	ΔS_{rxn} (cal/molK)
As + OH \rightarrow AsH + O	33.56	2.11	37.35	2.99
As + OCl \rightarrow AsO + Cl	-50.01	-1.53	-77.20	-0.34
Se + O ₂ \rightarrow SeO ₂	-83.12	-30.08	-82.71	-29.30
SeO + O \rightarrow SeO ₂	-97.41	-30.88	-101.03	-32.84
Se + OCl \rightarrow SeO + Cl	-36.55	-0.98	-36.08	-0.50
Se + O \rightarrow SeO	-101.14	-23.40	-101.60	-26.90

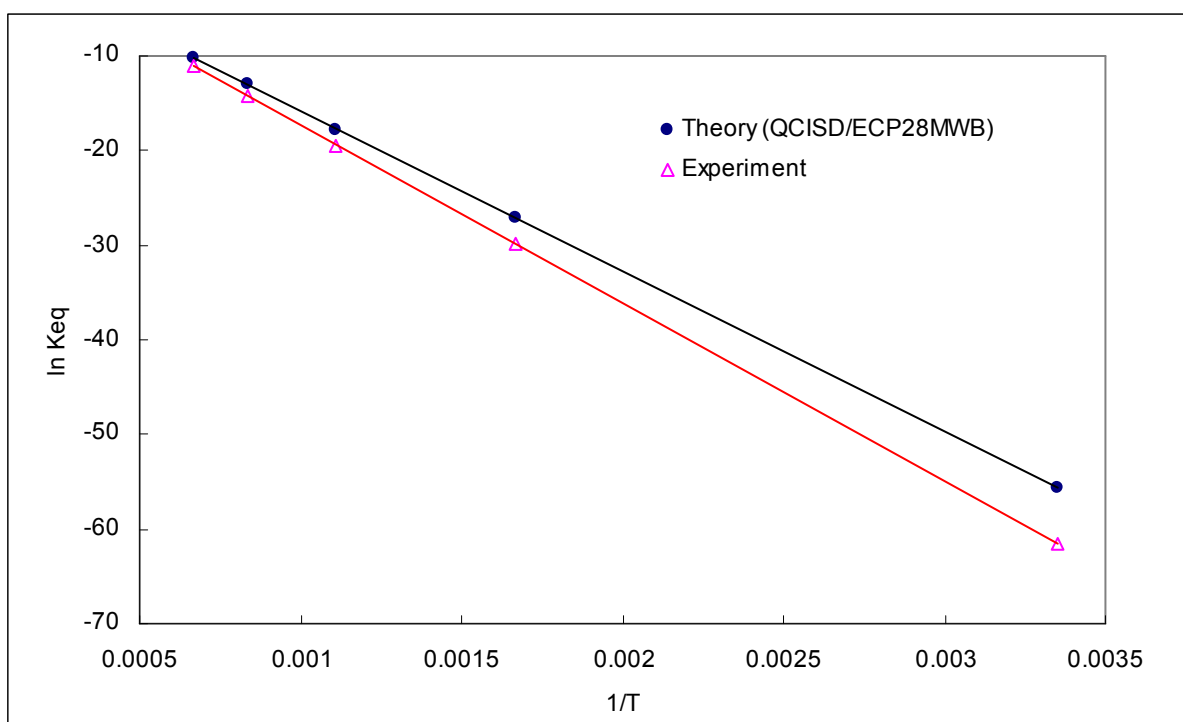


Figure 32: Equilibrium Constant as a Function of Temperature (As + OH \rightarrow AsH + O)

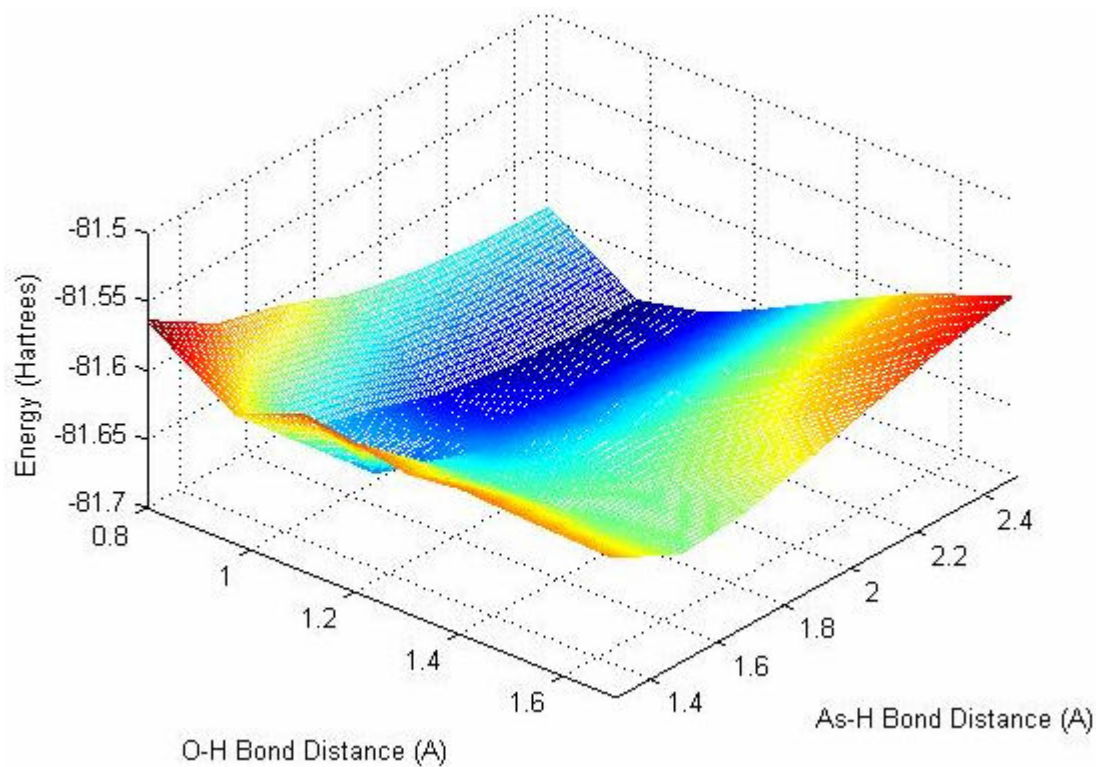


Figure 33: $\text{As} + \text{OH} \rightarrow \text{AsH} + \text{O}$ (PES)

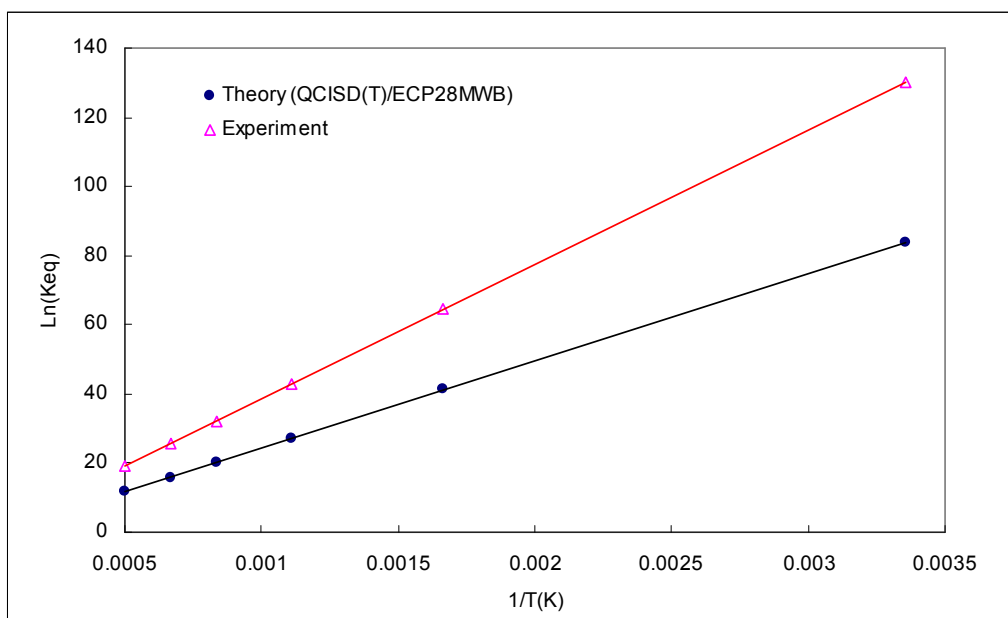


Figure 34: Equilibrium Constant as a Function of Temperature ($\text{As} + \text{OCl} \rightarrow \text{AsO} + \text{Cl}$)

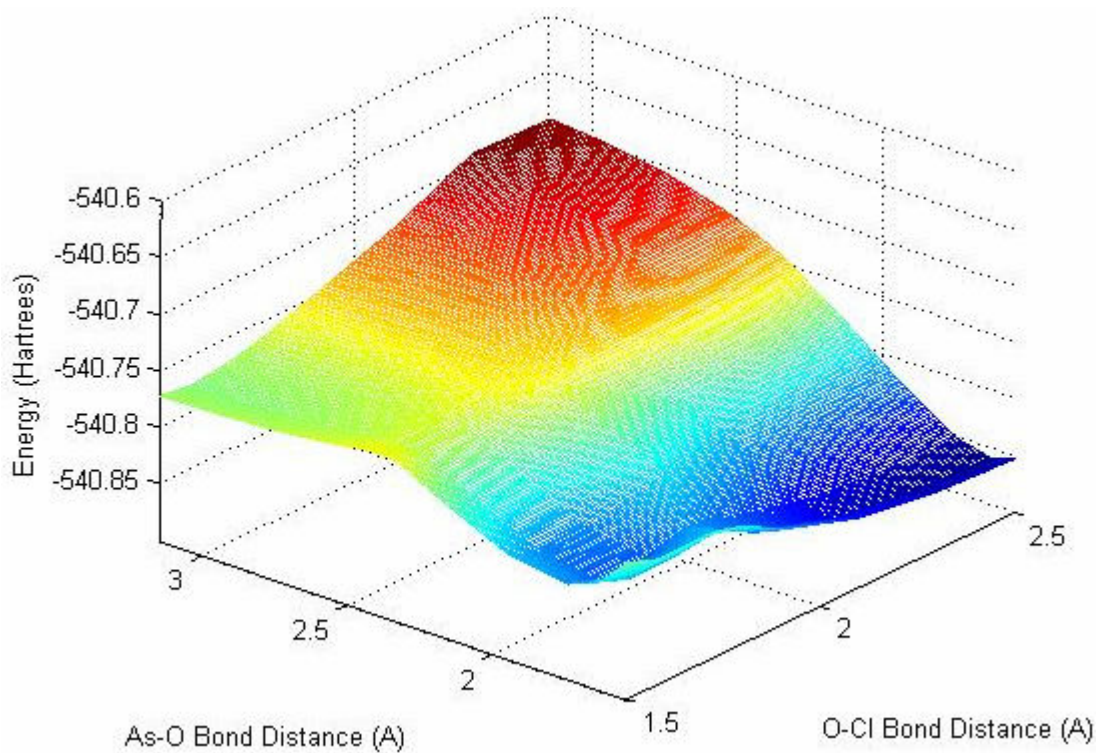


Figure 35: $\text{As} + \text{OCl} \rightarrow \text{AsO} + \text{Cl}$ (PES)

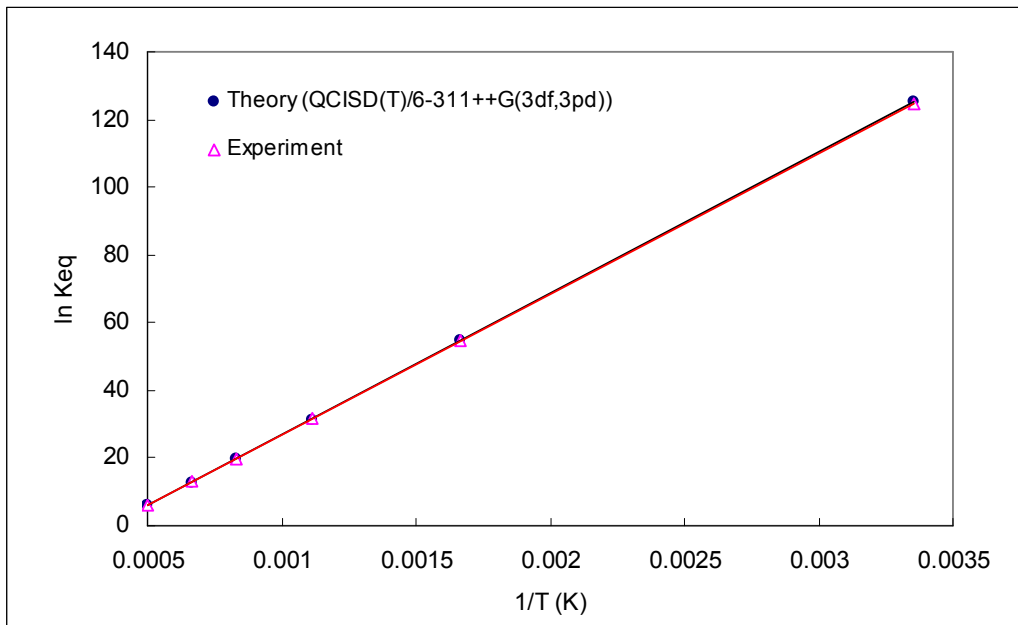


Figure 36: Equilibrium Constant as a Function of Temperature ($\text{Se} + \text{O}_2 \rightarrow \text{SeO}_2$)

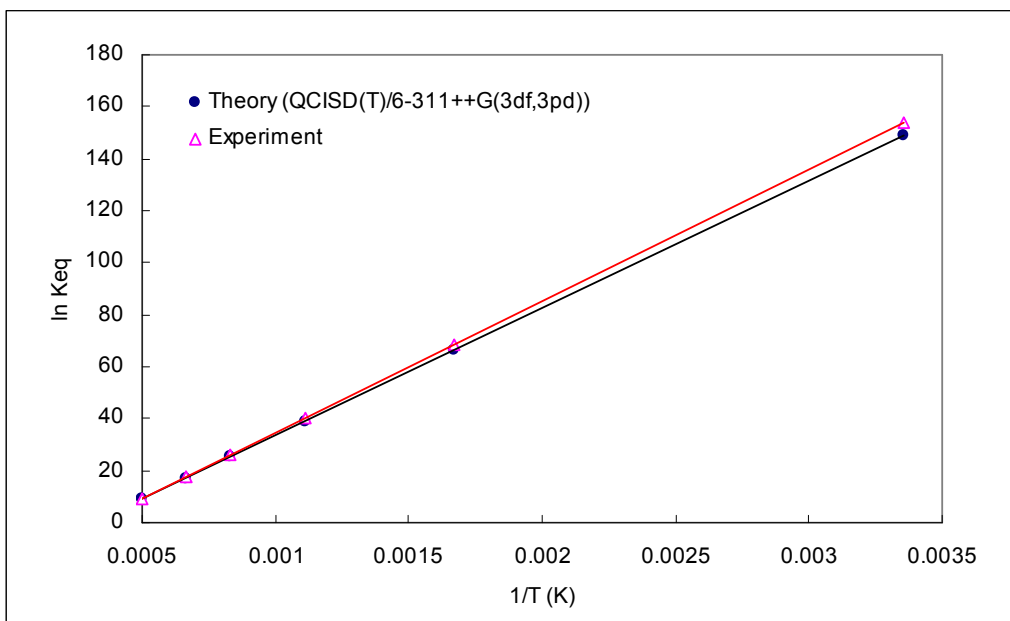


Figure 37: Equilibrium Constant as a Function of Temperature ($\text{SeO} + \text{O} \rightarrow \text{SeO}_2$)

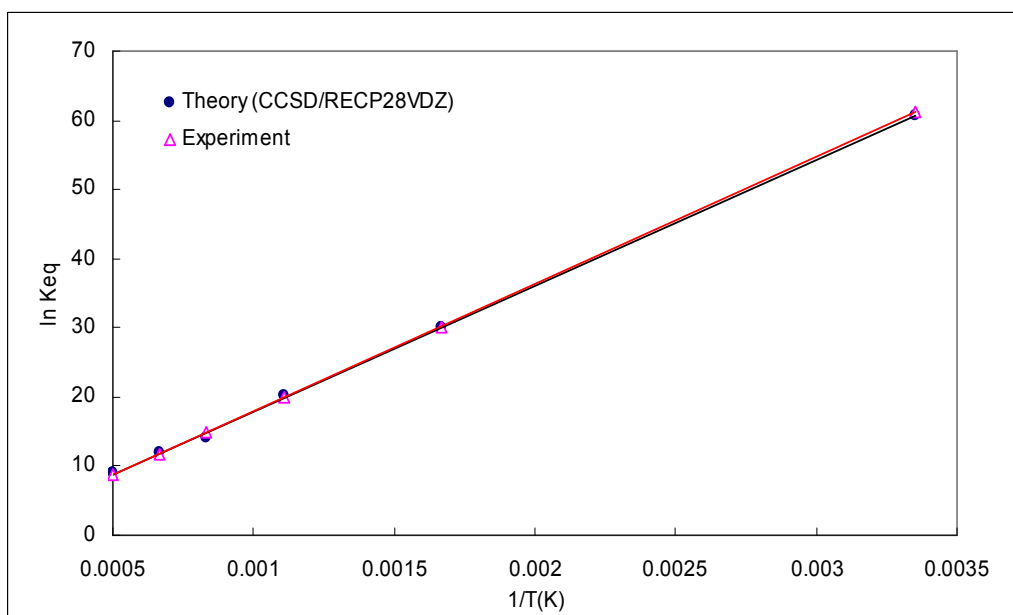


Figure 38: Equilibrium Constant as a Function of Temperature ($\text{Se} + \text{OCl} \rightarrow \text{SeO} + \text{Cl}$)

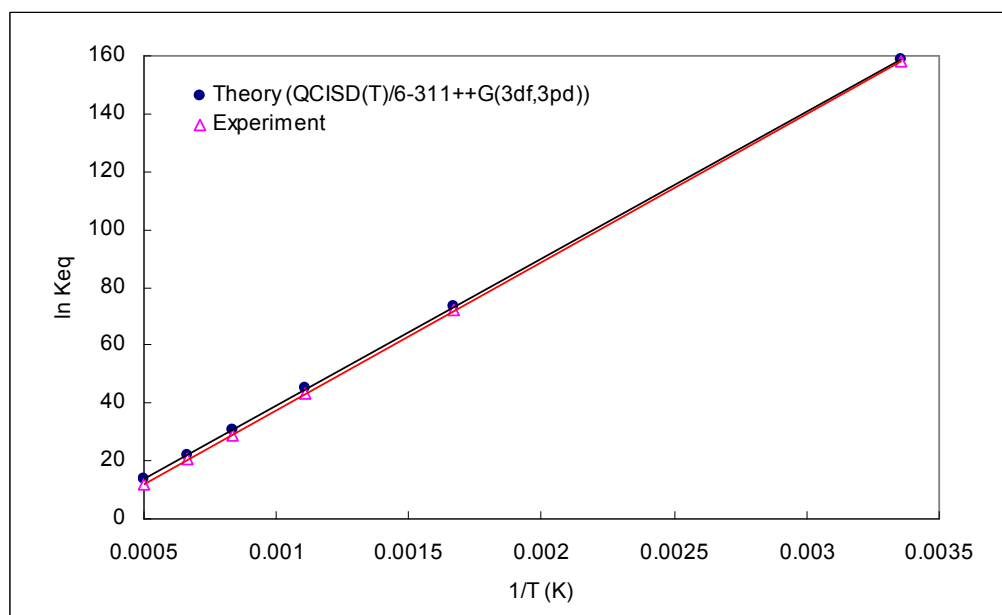


Figure 39: Equilibrium Constant as a Function of Temperature ($\text{SeO} + \text{O} \rightarrow \text{SeO}$)

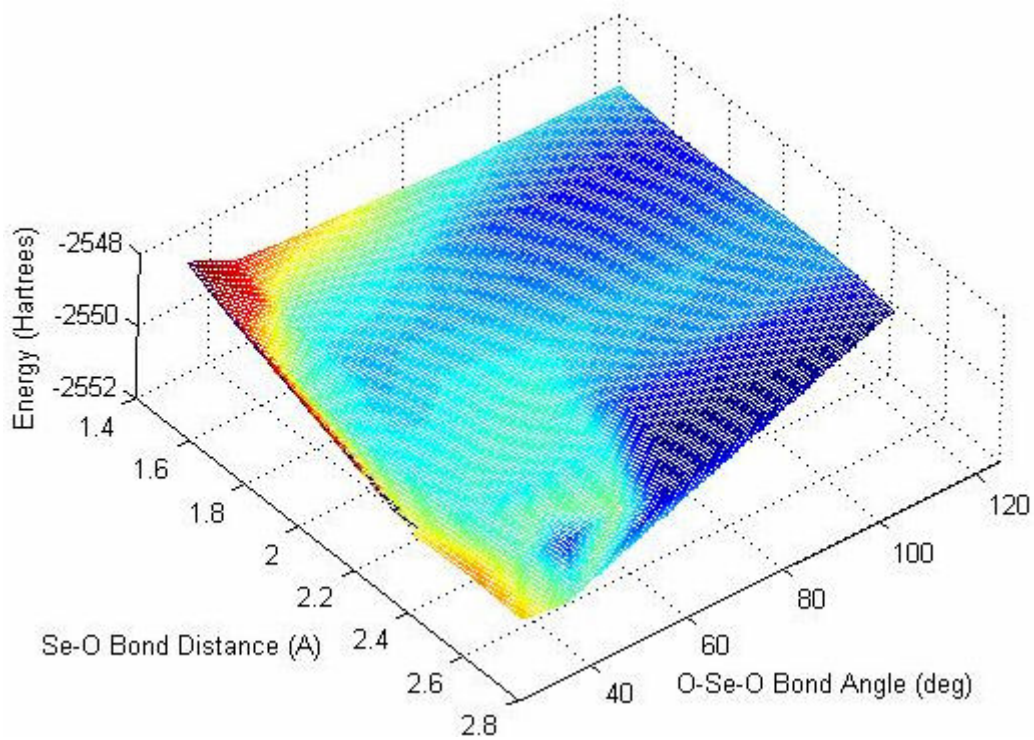


Figure 40: $\text{Se} + \text{O}_2 \rightarrow \text{SeO}_2$ (PES)

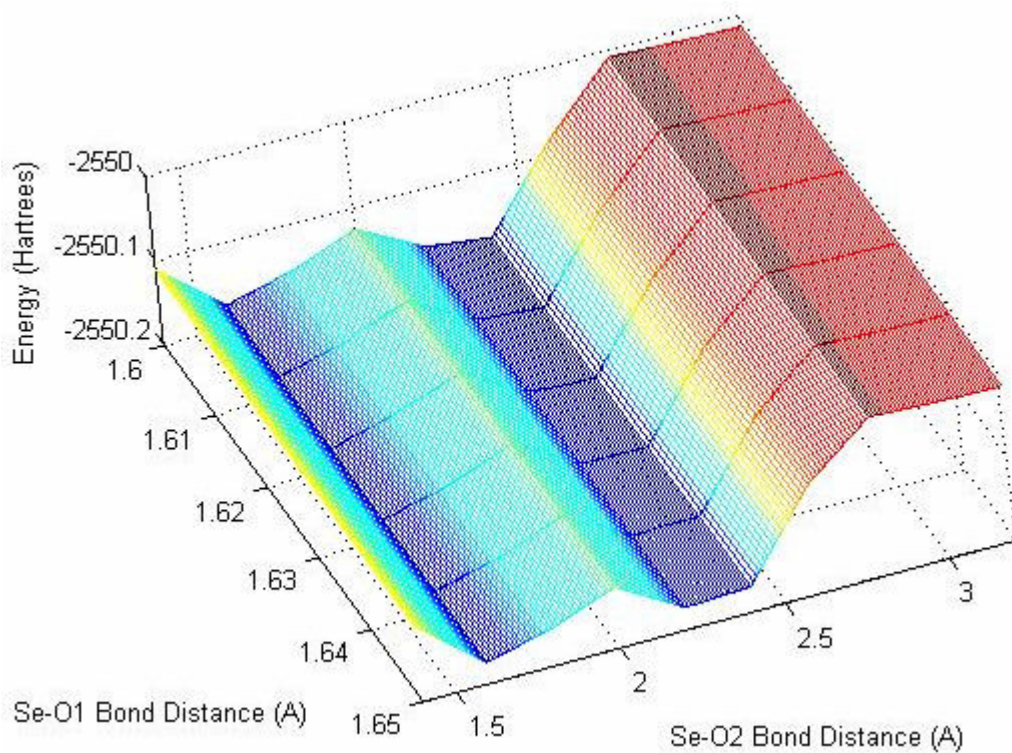


Figure 41: $\text{SeO} + \text{O} \rightarrow \text{SeO}_2$ (PES)

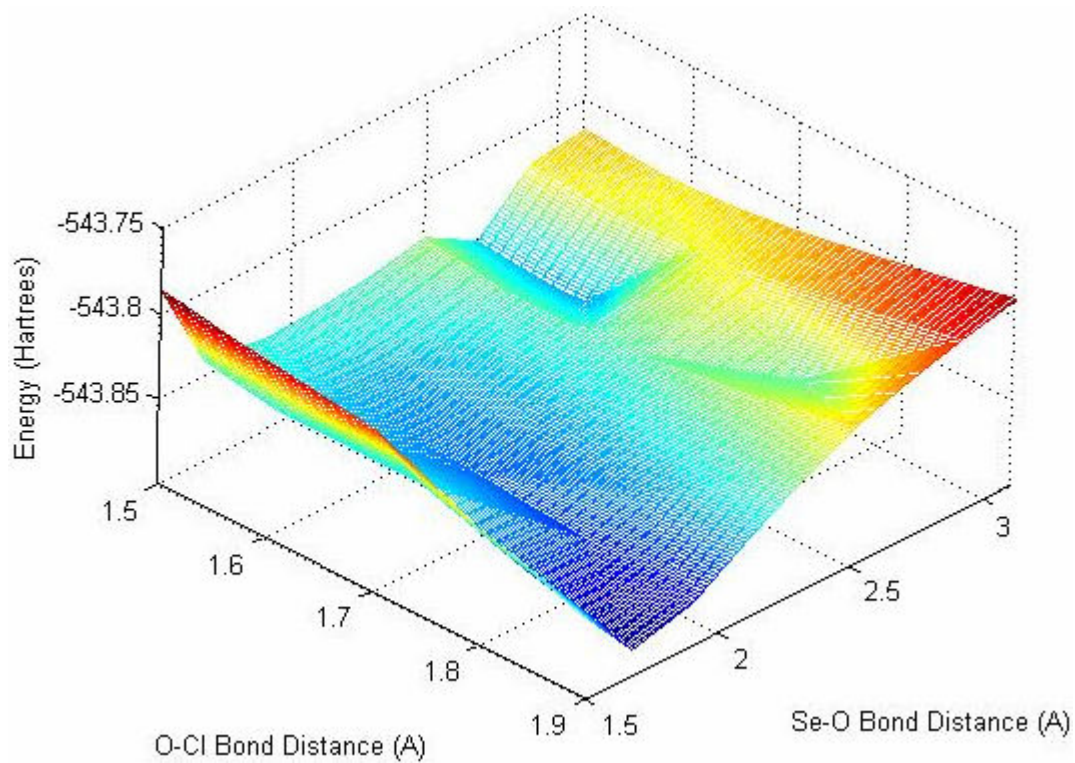


Figure 42: $\text{Se} + \text{OCl} \rightarrow \text{SeO} + \text{Cl}$ (PES)

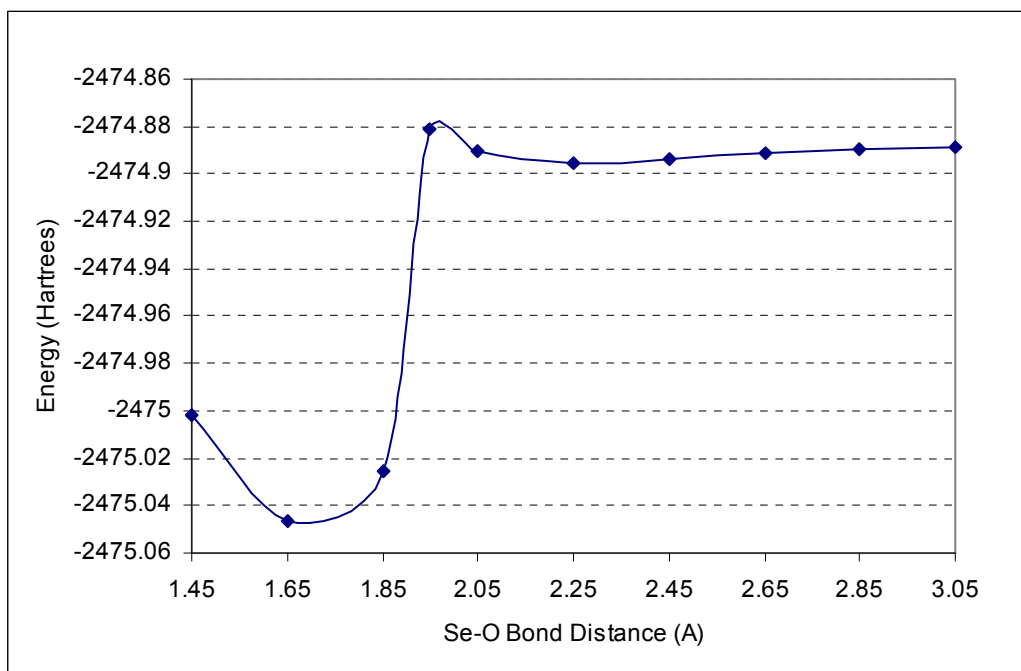


Figure 43: $\text{Se} + \text{O} \rightarrow \text{SeO}$ (PED)

4.5 Overall Discussion

Having examined each reaction individually, exploring the development of each PES, the determination of the kinetic parameters, and the comparison of theoretical equilibrium data to experiment, it is useful to study the overall reaction system as a whole. As the reaction kinetics are the primary factor in determining speciation in the flue gas, it would be most beneficial to compare theoretical rate constants to experimental ones, however, the nature of these compounds, again, makes such a comparison nearly impossible. The relationship of the rate constants to the equilibrium constant within a reaction allows a second-hand comparison of experiment and theory which may still provide valuable insight. In any bimolecular reaction, the rate constants and equilibrium constant are related as shown in (45); only bimolecular reactions are considered because both forward and reverse rate constants are calculated independently of the equilibrium constant.

$$45 \quad \frac{k_f}{k_r} = K_{eq}$$

Therefore, a comparison can be made between the theoretical ratio of the rate constants and the theoretical as well as the experimental equilibrium constant; having all three values on the same order of magnitude is a good sign that the data is accurate. Table 15 shows each of these values (if known) for all of the bimolecular reactions with complete kinetic information. Unfortunately, the two arsenic monoxide formation reactions are affected by the previously discussed issue of incorrect experimental thermodynamic data for the species AsO, which make the theoretical and experimental equilibrium values drastically different. However, when comparing the theoretical kinetic ratio to the theoretical equilibrium constant it is clear that they are on the same order of magnitude across the entire temperature range for both reactions. The arsenic monochloride formation reaction also has this same issue; the theoretical kinetic and thermodynamic data match beautifully but no experimental data, in this case due to an absence of thermodynamic information on AsCl, exists to provide an outside point of comparison. Fortunately, the selenium oxide formation reaction has both completed theoretical kinetic and thermodynamic data as well as a full range of experimental thermodynamic information. It is important to note that for this

reaction all three quantities are of the same order of magnitude throughout. From this data, it can be seen that, from theory, the ratio of the forward and reverse reactions approaching equilibrium will be the same as that predicted thermodynamically, thus the data fulfills another logical requirement. For the case of the SeO formation reaction, the theory also matches the values predicted experimentally thus adding another point of validation to the work. With the inclusion of accurate experimental for AsO and AsCl, it should also be seen that the arsenic reaction data will agree with experimental results.

While these four bimolecular reactions are the only ones for which the kinetic data is complete, several of the incomplete reactions do possess theoretical and experimental thermodynamic data. This data has been previously presented in graphical form but it is useful to include it within a table as well, which has been done in Table 16. Notice again that for the reactions in which AsO is present, the theory and experiment do not match. For all others reactions however, the values never deviate by more than an order of magnitude, further stressing the need to re-evaluate the experimental values for AsO.

Table 15: Completed Reactions Kinetic/Thermodynamic Analysis

As + O ₂ → AsO + O				As + OH → AsO + H			
T (K)	k _f /k _r	K _{eq,Th}	K _{eq, Exp}	T (K)	k _f /k _r	K _{eq,Th}	K _{eq, Exp}
298.15	2.74x10 ⁻⁴	2.97x10 ⁻⁴	1.91x10 ¹⁷	298.15	4.45x10 ⁵	4.61x10 ⁵	1.79x10 ²⁸
600	2.18x10 ⁻²	2.61x10 ⁻²	1.12x10 ⁹	600	3.99x10 ²	5.45x10 ²	7.60x10 ¹³
900	9.21x10 ⁻²	0.114	2.17x10 ⁶	900	39.65	59.26	1.41x10 ⁹
1200	0.189	0.237	9.58x10 ⁴	1200	12.49	19.54	6.07x10 ⁶
1500	0.292	0.369	1.47x10 ⁴	1500	6.25	10.04	2.31x10 ⁵
2000	0.449	0.574	2.26x10 ³	2000	3.12	5.16	8.80x10 ³
As + HCl → AsCl + H				Se + O ₂ → SeO + O			
T (K)	k _f /k _r	K _{eq,Th}	K _{eq, Exp}	T (K)	k _f /k _r	K _{eq,Th}	K _{eq, Exp}
298.15	2.43x10 ⁻²⁶	3.34x10 ⁻²⁶	-	298.15	6.77x10 ⁻¹³	3.69x10 ⁻¹³	2.21x10 ⁻¹³
600	2.27x10 ⁻¹³	3.76x10 ⁻¹³	-	600	2.38x10 ⁻⁶	1.44x10 ⁻⁶	1.26x10 ⁻⁶
900	4.24x10 ⁻⁹	7.44x10 ⁻⁹	-	900	3.41x10 ⁻⁴	2.12x10 ⁻⁴	2.12x10 ⁻⁴
1200	5.79x10 ⁻⁷	1.05x10 ⁻⁶	-	1200	4.08x10 ⁻³	2.58x10 ⁻³	2.74x10 ⁻³
1500	1.11x10 ⁻⁵	2.04x10 ⁻⁵	-	1500	1.81x10 ⁻²	1.15x10 ⁻²	1.28x10 ⁻²
2000	2.12x10 ⁻⁴	3.97x10 ⁻⁴	-	2000	8.01x10 ⁻²	5.17x10 ⁻²	5.93x10 ⁻²

Table 16: Incomplete Reactions Kinetic/Thermodynamic Analysis

As + O → AsO		As + OH → AsH + O		As + OCl → AsO + Cl		
T (K)	K _{eq,Th}	K _{eq, Exp}	K _{eq,Th}	K _{eq, Exp}	K _{eq, Exp}	
298.15	1.41x10 ⁷⁵	3.46x10 ⁹⁸	7.25x10 ⁻²⁵	1.88x10 ⁻²⁷	2.11x10 ³⁶	3.28x10 ⁵⁶
600	4.16x10 ³⁴	1.20x10 ⁴⁶	1.72x10 ⁻¹²	1.12x10 ⁻¹³	7.63x10 ¹⁷	1.11x10 ²⁸
900	1.88x10 ²¹	6.40x10 ²⁸	2.05x10 ⁻⁸	3.83x10 ⁻⁹	6.46x10 ¹¹	4.71x10 ¹⁸
1200	4.00x10 ¹⁴	1.48x10 ²⁰	2.23x10 ⁻⁶	7.09x10 ⁻⁷	5.95x10 ⁸	9.68x10 ¹³
1500	3.96x10 ¹⁰	9.73x10 ¹⁴	3.73x10 ⁻⁵	1.63x10 ⁻⁵	8.97x10 ⁶	1.49x10 ¹¹
2000	3.93x10 ⁶	6.40x10 ⁹	6.22x10 ⁻⁴	3.73x10 ⁻⁴	1.35x10 ⁵	2.30x10 ⁸
SeO + O ₂ → SeO ₂ + O		Se + O ₂ → SeO ₂		SeO + O → SeO ₂		
T (K)	K _{eq,Th}	K _{eq, Exp}	K _{eq,Th}	K _{eq, Exp}	K _{eq, Exp}	
298.15	1.00x10 ⁻¹⁵	4.25x10 ⁻¹⁵	2.29x10 ⁵⁴	1.70x10 ⁵⁴	4.56x10 ⁶⁴	7.66x10 ⁶⁶
600	1.10x10 ⁻⁸	3.93x10 ⁻⁸	5.07x10 ²³	5.33x10 ²³	5.42x10 ²⁸	4.22x10 ²⁹
900	2.29x10 ⁻⁶	7.74x10 ⁻⁶	4.09x10 ¹³	4.82x10 ¹³	8.06x10 ¹⁶	2.28x10 ¹⁷
1200	3.30x10 ⁻⁷	1.08x10 ⁻⁴	3.67x10 ⁸	4.59x10 ⁸	9.82x10 ¹⁰	1.67x10 ¹¹
1500	1.64x10 ⁻⁴	5.29x10 ⁻⁴	3.45x10 ⁵	4.46x10 ⁵	2.78x10 ⁷	3.49x10 ⁷
2000	8.11x10 ⁻⁴	2.58x10 ⁻³	3.23x10 ²	4.32x10 ²	7.86x10 ³	7.29x10 ³
Se + OCl → SeO + Cl		Se + O → SeO				
T (K)	K _{eq,Th}	K _{eq, Exp}	K _{eq,Th}	K _{eq, Exp}		
298.15	3.79x10 ²⁶	2.17x10 ²⁶	1.05x10 ⁶⁹	3.97x10 ⁶⁸		
600	1.26x10 ¹³	1.08x10 ¹³	5.30x10 ³¹	1.35x10 ³¹		
900	4.59x10 ⁸	4.48x10 ⁸	2.78x10 ¹⁹	6.22x10 ¹⁸		
1200	2.77x10 ⁶	2.89x10 ⁶	2.02x10 ¹³	4.22x10 ¹²		
1500	1.29x10 ⁵	1.40x10 ⁵	4.18x10 ⁹	8.40x10 ⁸		
2000	6.02x10 ³	6.80x10 ³	8.65x10 ⁵	1.67x10 ⁵		

Chapter 5: Conclusions

The current energy situation facing the United States has led to a resurgence of interest for alternatives to petroleum. As the most prevalent form of energy in use, coal seems like a natural choice for replacing a portion of the load carried by crude oil; it is well-tested and domestically plentiful. However, concerns about the emissions released during the combustion of coal must be addressed before a truly clean-coal process can be developed.

The most recent aspect of this development revolves around the removal of trace metals such as Hg, As, and Se using a variety of methods. While Hg has been examined previously, it is only now that species of As and Se are beginning to come to the attention of observers. Limited work has been conducted on the removal of species containing these elements, primarily through the use of Ca-based sorbents, however, an effective removal scheme requires that the predominant species be known. Unfortunately, this knowledge can be difficult to determine experimentally as the nature of several of the species themselves make them undetectable to analytical techniques. These two issues, the need to predict the speciation of trace metals in the flue gas and the difficulty in doing so experimentally, are the driving force behind this study.

Because of the inability of experimentation to develop a speciation model, computational chemistry techniques have been employed to first determine the properties of species of interest and then to determine the kinetic and thermodynamic parameters of the reactions in which they participate. This has been achieved using the Gaussian '03 software package utilizing a myriad of methods and basis sets to accurately find which levels of theory work best for a particular species, reaction, or reaction system.

In the initial phase of this process, the validation of the theoretical method, several observations were made which, upon further examination, may lead to a better understanding of the capabilities of particular methods and/or basis sets in handling certain compounds. For instance, the ECP28MWB basis set was better able to predict the geometry of oxide compounds than non-oxide compounds by an order magnitude for both As and Se species. This data, presented in

Table 17, also shows that this basis set more accurately matches the experimental values of vibrational frequency and reaction enthalpy for Se-O species and reactions and is on par with the prediction of vibrational frequencies for non-oxide As species; only in the computation of reaction enthalpy for As reactions does it perform markedly worse for reactions including oxygen. Additionally, the ECP28MWB basis set outperforms the RECP28VDZ basis set in every category when oxygen is present and in most cases is as good as, if not better than, the complete Pople basis set. These observations certainly warrant further study, as it may be that there exists some connection between valence electron configuration and basis function behavior which could lead to a greater understanding of basis set selection for trace metal compounds.

Also, under some circumstances the impact of including triple excitations in the calculational method was quite significant. As the data in Table 18 shows, in most cases the inclusion of the triple excitations produces similar results to those calculated using only the double excitations, but in certain instances, such as the prediction of vibrational frequencies of selenium species using ECP basis sets, the triple excitation value is markedly worse than just the double, averaging 70 cm^{-1} deviation. On the other hand, for the reaction enthalpy predictions of Se reactions, the triple excitations predict average values at least 3 kcal/mol closer to experiment than just the double excitations. Here, the reason for this result is unknown, similar behavior is not seen in the calculations for As, again suggesting that the basis functions are better able to predict properties of certain electron configurations than others. The computation of additional trace metal species, specifically ones with similar valence electron configurations, would certainly be beneficial.

In the determination of the kinetic parameters, several bimolecular reactions, along with one unimolecular decomposition reaction, have been completed; that is forward and backward rate constants and equilibrium constants have been found. Additionally, several other reactions under investigation are in various stages of examination, some having an incomplete PES, others having everything but the transition structure calculated. Due to the absence of experimental kinetic data, the theoretical values obtained for each reaction were compared to experimental equilibrium constants, when data existed. Only one reaction, $\text{Se} + \text{O}_2 \rightarrow \text{SeO} + \text{O}$, has a full compliment of accurate data for theoretical kinetics and thermodynamics and experimental

thermodynamics, however the consistency in the data is incredibly high. The theoretical and experimental equilibrium data for this and all other reactions is recapped in Table 19. Because the equilibrium constant is a ratio of the forward over the reverse rate constant, the tabulated values should give a good estimate of whether a reaction is likely to proceed to products or not at any given temperature. For instance, a value of 1×10^{50} would suggest that the products are more thermodynamically favorable at that temperature.

By examining the equilibrium constant data, a qualitative assessment can be made as to which species would appear at a given temperature range if equilibrium were reached. Looking at the data for the formation of AsH and AsCl, it would seem that both of these species would be more favorable than elemental arsenic at higher temperatures. AsO, on the other hand, seems more stable at lower temperatures as determined by the large theoretical equilibrium constants (theoretical because of the suspected experimental values) for the AsO formation reactions. As for the selenium compounds, SeH₂ is clearly more stable at lower temperature, but the selenium oxides are not quite as clear. The formation of SeO from Se and O₂ is most likely at high temperatures while its formation from Se and either O or OCl, is much more likely at ambient conditions. This is most likely due to the stability of the oxygen molecule at low temperatures when compared to the atomic O or the OCl radical. A similar situation occurs in the formation of SeO₂ from SeO, the combination of the monoxide with diatomic oxygen is favorable at high temperatures while the combination with oxygen atom is more likely at low temperatures. Additionally, the formation of the dioxide from elemental Se and O₂ is also more likely at low temperatures, meaning that at low temperatures SeO₂ is even more stable than O₂. From these observations it is difficult to see the overall picture of the formation of selenium oxides, but it would seem that SeO, being a radical species, is more likely at higher temperatures while SeO₂ is more stable at ambient conditions. Admittedly, these conclusions are preliminary at best, being drawn from only a handful of reactions, however, these predictions would seem to be confirmed by the experimental speciation studies. Yan⁴² determined that under oxidizing conditions SeO would be the dominant species above 1500 K while SeH₂ is the majority, and essentially only, selenium compound between 700-1300 K. However, in this study SeO₂ was shown to exist only at high temperatures, not the ambient conditions suggested by the data. In this same study, AsO is shown to be the predominant arsenic species above 1500 K which is directly in contrast with

the conclusions drawn from the data, but again, the present work only considers a few of all possible reactions which take place in the flue in addition to neglecting the influence of competing C, N, S, etc. reactions. In a later study Yan⁴³ showed that SeO₂ was actually more prevalent at lower temperatures, having a peak at roughly 500 K, before declining slowly as temperature increased and the majority of the Se went into forming SeO. In the case of reducing conditions when oxygen is scarce, SeH₂ is the dominant species from 500 K up, which cannot be confirmed as only one non-oxide selenium reaction was fully studied.

Overall, more reactions must be completed before conclusions can be drawn on the larger picture. Once a greater number of kinetic rate constants have been determined, they can be compiled and combined with other known reaction kinetics using a differential equation solving software package such as CHEMKIN, to build a comprehensive model of the flue gas environment. This will then allow for the determination of speciation under a variety of process conditions which would be difficult to achieve through experimentation. In this way, the predominant trace metal species can be predicted before the combustion process has begun; if changes are expected in the process conditions, the model can be used to predict the new output speciation and the necessary adjustments to the removal methods can be made.

It is believed that this research will be the foundation upon which further work in this area may be based. By beginning to identify the species present in the coal combustion flue gas and understand the kinetics of the reactions taking place, more efficient and effective removal strategies can be developed. Additionally, the computational chemistry approach can be duplicated for non-homogenous reactions such as those involving solid clusters in suspension or fly ash surface reactions. By combining all of these possible mechanisms for the creation of toxic trace metal species, it is hoped that their release into the atmosphere can be greatly reduced and the process of coal combustion for power generation made that much more attractive.

Table 17: Average Deviations: Oxygen vs. no Oxygen

Basis Set		ECP28MWB		6-311++G(3df,3pd)		RECP28VDZ	
Oxygen Present?		w/ O	w/o O	w/ O	w/o O	w/ O	w/o O
Bond Length (Å)	As	0.0086	0.0144	-	0.0068	0.0192	0.0260
	Se	0.0055	0.0406	0.0063	0.0055	0.0334	0.0797
Vib. Freq. (cm ⁻¹)	As	52.81	33.76	-	1.91	100.35	38.63
	Se	14.14	162.11	36.48	67.99	55.47	123.66
ΔH (kcal/mol)	As	6.83	0.32	9.37	0.45	11.98	0.07
	Se	5.18	11.27	4.37	1.98	7.94	11.06

Table 18: Average Deviations by Basis Set

Basis Set		SDD			6-311++G(3df,3pd)		
Excitations		Double	Triple	Both	Double	Triple	Both
Bond Length (Å)	As ^a	0.055	0.056	0.055	0.006	0.008	0.007
	Se ^b	0.181	0.152	0.167	0.004	0.009	0.006
Vib. Freq. (cm ⁻¹)	As ^c	134.74	118.61	126.68	6.60	1.58	4.93
	Se ^d	124.78	122.25	123.51	58.61	-	51.02
ΔH (kcal/mol)	As	11.66	10.29	10.97	7.53	5.01	6.27
	Se	30.07	24.13	27.10	5.86	2.02	3.94
Basis Set		ECP28MWB			RECP28VDZ		
Excitations		Double	Triple	Both	Double	Triple	Both
Bond Length (Å)	As ^a	0.011	0.015	0.013	0.022	0.026	0.024
	Se ^b	0.023	0.032	0.028	0.061	0.077	0.068
Vib. Freq. (cm ⁻¹)	As ^c	51.65	34.92	43.29	62.40	76.59	69.49
	Se ^d	98.01	165.07	122.40	79.82	157.02	104.52
ΔH (kcal/mol)	As	6.76	5.18	5.97	10.35	8.64	9.50
	Se	7.91	4.67	6.29	10.66	6.37	8.51

^aGeometries from AsH, AsH₂, AsH₃, and AsO; bond length only^bGeometries from all Se compounds, Se₂ included only for RECP; bond length only^cFrequencies from AsCl and AsO only^dFrequencies from SeO, SeH₂, SeO₂, SeCl₂

Table 19: Equilibrium Data, All Reactions

	$\text{As} + \text{O}_2 \rightarrow \text{AsO} + \text{O}$		$\text{As} + \text{OH} \rightarrow \text{AsO} + \text{H}$		$\text{As} + \text{OCl} \rightarrow \text{AsO} + \text{Cl}$	
T (K)	$K_{\text{eq,Th}}$	$K_{\text{eq,Exp}}$	$K_{\text{eq,Th}}$	$K_{\text{eq,Exp}}$	$K_{\text{eq,Th}}$	$K_{\text{eq,Exp}}$
298.15	2.97×10^{-4}	1.91×10^{17}	4.61×10^5	1.79×10^{28}	2.11×10^{36}	3.28×10^{56}
600	2.61×10^{-2}	1.12×10^9	5.45×10^2	7.60×10^{13}	7.63×10^{17}	1.11×10^{28}
900	0.114	2.17×10^6	59.26	1.41×10^9	6.46×10^{11}	4.71×10^{18}
1200	0.237	9.58×10^4	19.54	6.07×10^6	5.95×10^8	9.68×10^{13}
1500	0.369	1.47×10^4	10.04	2.31×10^5	8.97×10^6	1.49×10^{11}
2000	0.574	2.26×10^3	5.16	8.80×10^3	1.35×10^5	2.30×10^8
	$\text{As} + \text{O} \rightarrow \text{AsO}$		$\text{As} + \text{OH} \rightarrow \text{AsH} + \text{O}$		$\text{As} + \text{HCl} \rightarrow \text{AsCl} + \text{H}$	
T (K)	$K_{\text{eq,Th}}$	$K_{\text{eq,Exp}}$	$K_{\text{eq,Th}}$	$K_{\text{eq,Exp}}$	$K_{\text{eq,Th}}$	$K_{\text{eq,Exp}}$
298.15	1.41×10^{75}	3.46×10^{98}	7.25×10^{-25}	1.88×10^{-27}	3.34×10^{-26}	-
600	4.16×10^{34}	1.20×10^{46}	1.72×10^{-12}	1.12×10^{-13}	3.76×10^{-13}	-
900	1.88×10^{21}	6.40×10^{28}	2.05×10^{-8}	3.83×10^{-9}	7.44×10^{-9}	-
1200	4.00×10^{14}	1.48×10^{20}	2.23×10^{-6}	7.09×10^{-7}	1.05×10^{-6}	-
1500	3.96×10^{10}	9.73×10^{14}	3.73×10^{-5}	1.63×10^{-5}	2.04×10^{-5}	-
2000	3.93×10^6	6.40×10^9	6.22×10^{-4}	3.73×10^{-4}	3.97×10^{-4}	-
	$\text{Se} + \text{O}_2 \rightarrow \text{SeO} + \text{O}$		$\text{Se} + \text{O} \rightarrow \text{SeO}$		$\text{Se} + \text{OCl} \rightarrow \text{SeO} + \text{Cl}$	
T (K)	$K_{\text{eq,Th}}$	$K_{\text{eq,Exp}}$	$K_{\text{eq,Th}}$	$K_{\text{eq,Exp}}$	$K_{\text{eq,Th}}$	$K_{\text{eq,Exp}}$
298.15	3.69×10^{-13}	2.21×10^{-13}	1.05×10^{69}	3.97×10^{68}	3.79×10^{26}	2.17×10^{26}
600	1.44×10^{-6}	1.26×10^{-6}	5.30×10^{31}	1.35×10^{31}	1.26×10^{13}	1.08×10^{13}
900	2.12×10^{-4}	2.12×10^{-4}	2.78×10^{19}	6.22×10^{18}	4.59×10^8	4.48×10^8
1200	2.58×10^{-3}	2.74×10^{-3}	2.02×10^{13}	4.22×10^{12}	2.77×10^6	2.89×10^6
1500	1.15×10^{-2}	1.28×10^{-2}	4.18×10^9	8.40×10^8	1.29×10^5	1.40×10^5
2000	5.17×10^{-2}	5.93×10^{-2}	8.65×10^5	1.67×10^5	6.02×10^3	6.80×10^3
	$\text{Se} + \text{O}_2 \rightarrow \text{SeO}_2$		$\text{SeO} + \text{O} \rightarrow \text{SeO}_2$		$\text{SeO} + \text{O}_2 \rightarrow \text{SeO}_2 + \text{O}$	
T (K)	$K_{\text{eq,Th}}$	$K_{\text{eq,Exp}}$	$K_{\text{eq,Th}}$	$K_{\text{eq,Exp}}$	$K_{\text{eq,Th}}$	$K_{\text{eq,Exp}}$
298.15	2.29×10^{54}	1.70×10^{54}	4.56×10^{64}	7.66×10^{66}	1.00×10^{-15}	4.25×10^{-15}
600	5.07×10^{23}	5.33×10^{23}	5.42×10^{28}	4.22×10^{29}	1.10×10^{-8}	3.93×10^{-8}
900	4.09×10^{13}	4.82×10^{13}	8.06×10^{16}	2.28×10^{17}	2.29×10^{-6}	7.74×10^{-6}
1200	3.67×10^8	4.59×10^8	9.82×10^{10}	1.67×10^{11}	3.30×10^{-7}	1.08×10^{-4}
1500	3.45×10^5	4.46×10^5	2.78×10^7	3.49×10^7	1.64×10^{-4}	5.29×10^{-4}
2000	3.23×10^2	4.32×10^2	7.86×10^3	7.29×10^3	8.11×10^{-4}	2.58×10^{-3}
	$\text{Se} + \text{H}_2 \rightarrow \text{SeH}_2$					
T (K)	$K_{\text{eq,Th}}$	$K_{\text{eq,Exp}}$				
298.15	2.05×10^{32}	3.49×10^{31}				
600	2.36×10^{13}	1.14×10^{14}				
900	1.37×10^7	9.39×10^6				
1200	1.05×10^4	8.50×10^3				
1500	1.41×10^2	1.27×10^2				
2000	1.90	1.90				

Appendix A: Basis Sets

A.1 Arsenic

As LANL2DZ

AS	0		
S	2	1.00	
		0.963500000	-2.67095490
		0.542700000	2.93878920
S	1	1.00	
		0.140700000	1.00000000
P	2	1.00	
		2.08400000	-0.113710000
		0.322400000	1.03802660
P	1	1.00	
		0.102000000	1.00000000

Effective Core Potentials			

AS	0		
AS-ECP	3	28	
f potential			
5			
1	375.47488030	-28.00000000	
2	72.65547690	-198.36873570	
2	15.91626770	-60.45637980	
2	4.64202510	-22.31882740	
2	1.47891820	-2.16382900	
s-f potential			
5			
0	105.88538700	3.00000000	
1	62.59518460	31.84867770	
2	34.50174310	200.99582150	
2	10.37585940	102.63876040	
2	2.53793470	34.18453590	
p-f potential			
5			
0	37.64714400	5.00000000	
1	17.20346650	24.25057470	
2	18.90757090	48.91749630	
2	6.81534520	66.53322590	
2	2.06118530	19.65776660	
d-f potential			
5			
0	52.07313350	3.00000000	
1	28.00378240	23.34607120	
2	14.70512080	80.78549190	
2	4.79731940	40.26813470	
2	1.10627630	4.83327900	

As SDD

S	3	1.00		
			0.3431474000D+01	0.2650606252D+00
			0.1896866000D+01	-0.8048278597D+00
			0.2944490000D+00	0.1244535898D+01
S	1	1.00		
			0.1118960000D+00	0.1000000000D+01
P	3	1.00		
			0.1296447000D+01	-0.5650244862D+00
			0.9499710000D+00	0.5700034290D+00
			0.2544210000D+00	0.9168341446D+00
P	1	1.00		
			0.8759300000D-01	0.1000000000D+01

As 6-311++G(3df,3pd)

S 6 1.00
 0.3812000000D+06 0.8332661156D-03
 0.5724000000D+05 0.6219771005D-02
 0.1311000000D+05 0.3202985069D-01
 0.3743000000D+04 0.1272894066D+00
 0.1238000000D+04 0.3913181758D+00
 0.4563000000D+03 0.5458074556D+00
 S 3 1.00
 0.4563000000D+03 0.1809701465D+00
 0.1814000000D+03 0.6218005032D+00
 0.7707000000D+02 0.2498802022D+00
 S 1 1.00
 0.2857000000D+02 0.1000000000D+01
 S 1 1.00
 0.1236000000D+02 0.1000000000D+01
 S 1 1.00
 0.4117000000D+01 0.1000000000D+01
 S 1 1.00
 0.1678000000D+01 0.1000000000D+01
 S 1 1.00
 0.2761000000D+00 0.1000000000D+01
 S 1 1.00
 0.1105000000D+00 0.1000000000D+01
 P 3 1.00
 0.2528000000D+04 0.2227089820D-01
 0.5973000000D+03 0.1819891681D+00
 0.1907000000D+03 0.8613260628D+00
 P 3 1.00
 0.7096000000D+02 0.3433804028D+00
 0.2889000000D+02 0.5059805935D+00
 0.1213000000D+02 0.2612803065D+00
 P 3 1.00
 0.1213000000D+02 0.6853616583D-01
 0.6533000000D+01 0.3828209263D+00
 0.3028000000D+01 0.6059914663D+00
 P 1 1.00
 0.1344000000D+01 0.1000000000D+01
 P 1 1.00
 0.5823000000D+00 0.1000000000D+01
 P 1 1.00
 0.2558000000D+00 0.1000000000D+01
 P 1 1.00
 0.8651000000D-01 0.1000000000D+01

D 4 1.00
 0.8605000000D+02 0.2798918392D-01
 0.2449000000D+02 0.1650210844D+00
 0.8442000000D+01 0.4373628739D+00
 0.2981000000D+01 0.5725537623D+00
 D 1 1.00
 0.9790000000D+00 0.1000000000D+01
 SP 1 1.00
 0.2600000000D-01 0.1000000000D+01
 0.1000000000D+01
 D 1 1.00
 0.7920000000D+00 0.1000000000D+01
 D 1 1.00
 0.2640000000D+00 0.1000000000D+01
 D 1 1.00
 0.8800000000D-01 0.1000000000D+01
 F 1 1.00
 0.4200000000D+00 0.1000000000D+01

As ECP28MWB

AS 0		
S	3	1.00
	3.43147400	0.148166000
	1.89686600	-0.449890000
	0.294449000	0.695682000
S	1	1.00
	0.111896000	1.000000000
P	3	1.00
	1.29644700	-0.369954000
	0.949971000	0.373214000
	0.254421000	0.600304000
P	1	1.00
	0.875930000E-01	1.000000000

Effective Core Potentials		

AS 0		
AS-ECP 4 28		
G POTENTIAL		
	1	
2	1.000000000	0.000000000
S-G POTENTIAL		
	1	
2	3.61262500	53.96562000
P-G POTENTIAL		
	1	
2	3.90792600	88.94908800
D-G POTENTIAL		
	1	
2	1.92646700	22.42028800
F-G POTENTIAL		
	1	
2	1.77343400	-4.704815

As RECP28VDZ

AS 0			
SP 4 1.00			
	2.70900000	0.121479000	-0.292000000E-02
	1.57800000	-0.518918000	-0.950540000E-01
	0.435800000	0.428791000	0.424682000
	0.177600000	0.808078000	0.671290000
SP 1 1.00			
	0.698400000E-01	1.00000000	1.00000000

Effective Core Potentials			

AS 0			
AS-ECP 3 28			
f potential			
1			
1	1.64583000	-4.77028000	
s-f potential			
2			
0	20.76160000	13.03398000	
2	2.80084000	43.12429000	
p-f potential			
2			
0	16.05834000	6.44063000	
2	2.29432000	28.12117000	
d-f potential			
2			
0	1.12086000	2.23508000	
2	1.12140000	4.607210	

A.2. Selenium

Se LANL2DZ

SE	0		
S	2	1.00	
		1.03300000	-3.32240950
		0.652100000	3.60034620
S	1	1.00	
		0.166000000	1.00000000
P	2	1.00	
		2.36600000	-0.118552200
		0.383300000	1.04143200
P	1	1.00	
		0.118600000	1.00000000

Effective Core Potentials			

SE	0		
SE-ECP	3	28	
f potential			
5			
1	433.19313360	-28.00000000	
2	83.89521570	-214.38417620	
2	18.58391390	-65.69187820	
2	5.39552860	-24.61539320	
2	1.74743260	-2.44814970	
s-f potential			
5			
0	202.89861930	3.00000000	
1	78.38204870	62.02953900	
2	35.07530370	258.85559840	
2	10.87695430	118.78001530	
2	2.80059410	38.23552790	
p-f potential			
5			
0	44.30118750	5.00000000	
1	20.38742060	24.79734580	
2	23.18899480	63.75756400	
2	7.97776640	79.05128310	
2	2.29881460	22.95201830	
d-f potential			
5			
0	73.36282630	3.00000000	
1	48.38356180	22.47059070	
2	25.62972110	140.54928870	
2	7.17058220	63.57818350	
2	1.36395380	7.07536140	

Se SDD

S	3	1.00		
			0.3588180000D+01	0.4325036071D+00
			0.2239711000D+01	-0.1007425179D+01
			0.3437730000D+00	0.1262942412D+01
S	1	1.00		
			0.1313990000D+00	0.1000000000D+01
P	3	1.00		
			0.1509427000D+01	0.2871287643D+00
			0.8751060000D+00	-0.3733595884D+00
			0.2908260000D+00	-0.8682589971D+00
P	1	1.00		
			0.1002210000D+00	0.1000000000D+01
P	1	1.00		
			0.3251600000D-01	0.1000000000D+01

Se 6-311++G(3df,3pd)

S 6 1.00
 0.4054000000D+06 0.8310049468D-03
 0.6085000000D+05 0.6233137105D-02
 0.1391000000D+05 0.3207119091D-01
 0.3989000000D+04 0.1263607522D+00
 0.1324000000D+04 0.3889923156D+00
 0.4870000000D+03 0.5488832674D+00
 S 3 1.00
 0.4870000000D+03 0.1796295293D+00
 0.1932000000D+03 0.6222683694D+00
 0.8219000000D+02 0.2506693431D+00
 S 1 1.00
 0.3052000000D+02 0.1000000000D+01
 S 1 1.00
 0.1325000000D+02 0.1000000000D+01
 S 1 1.00
 0.4510000000D+01 0.1000000000D+01
 S 1 1.00
 0.1867000000D+01 0.1000000000D+01
 S 1 1.00
 0.3193000000D+00 0.1000000000D+01
 S 1 1.00
 0.1120000000D+00 0.1000000000D+01
 P 3 1.00
 0.2706000000D+04 0.2214596058D-01
 0.6386000000D+03 0.1817996764D+00
 0.2038000000D+03 0.8615484666D+00
 P 3 1.00
 0.7596000000D+02 0.3424286469D+00
 0.3102000000D+02 0.5054080029D+00
 0.1305000000D+02 0.2623689633D+00
 P 3 1.00
 0.1305000000D+02 0.7016263348D-01
 0.6986000000D+01 0.3841879930D+00
 0.3234000000D+01 0.6036768464D+00
 P 1 1.00
 0.1475000000D+01 0.1000000000D+01
 P 1 1.00
 0.7275000000D+00 0.1000000000D+01
 P 1 1.00
 0.2869000000D+00 0.1000000000D+01
 P 1 1.00
 0.9679000000D-01 0.1000000000D+01

D 4 1.00
 0.9901000000D+02 0.2559615332D-01
 0.2841000000D+02 0.1545909260D+00
 0.9863000000D+01 0.4287825684D+00
 0.3514000000D+01 0.5862035114D+00
 D 1 1.00
 0.1171000000D+01 0.1000000000D+01
 SP 1 1.00
 0.3000000000D-01 0.1000000000D+01
 0.1000000000D+01
 D 1 1.00
 0.9150000000D+00 0.1000000000D+01
 D 1 1.00
 0.3050000000D+00 0.1000000000D+01
 D 1 1.00
 0.1016666667D+00 0.1000000000D+01
 F 1 1.00
 0.4800000000D+00 0.1000000000D+01

Se ECP28MWB

SE 0		
S 3 1.00		
3.58818000	0.249630000	
2.23971100	-0.581460000	
0.343773000	0.728938000	
S 1 1.00		
0.131399000	1.000000000	
P 3 1.00		
1.50942700	0.195271000	
0.875106000	-0.253915000	
0.290826000	-0.590487000	
P 1 1.00		
0.100221000	1.000000000	
P 1 1.00		
0.325160000E-01	1.000000000	

Effective Core Potentials		

SE 0		
SE-ECP 4 28		
G POTENTIAL		
1		
2	1.000000000	0.000000000
S-G POTENTIAL		
1		
2	4.23705700	79.66334500
P-G POTENTIAL		
1		
2	2.91033400	31.56099300
D-G POTENTIAL		
1		
2	2.33570100	30.80461000
F-G POTENTIAL		
1		
2	2.25463900	-6.546875

Se RECP28VDZ

SE 0			
SP 4 1.00			
3.71100000	0.557440000E-01	-0.601400000E-02	
1.58600000	-0.510520000	-0.121447000	
0.533900000	0.480755000	0.452607000	
0.208500000	0.810292000	0.669751000	
SP 1 1.00			
0.782100000E-01	1.000000000	1.000000000	

Effective Core Potentials			

SE 0			
SE-ECP 3 28			
f potential			
1			
1	2.09356000	-5.58498000	
s-f potential			
2			
0	20.55644000	13.28081000	
2	3.15490000	51.00011000	
p-f potential			
2			
0	2.58495000	1.79640000	
2	2.58526000	30.43787000	
d-f potential			
2			
0	1.38290000	2.40001000	
2	1.42671000	6.59948000	

A.3. Chlorine

CI LANL2DZ

```
CL 0
S 2 1.00
    2.23100000    -0.490058900
    0.472000000    1.25426840
S 1 1.00
    0.163100000    1.000000000
P 2 1.00
    6.29600000    -0.635641000E-01
    0.633300000    1.01413550
P 1 1.00
    0.181900000    1.000000000
****
```

Effective Core Potentials

```
-----
CL 0
CL-ECP 2 10
d potential
5
1    94.81300000    -10.00000000
2    165.64400000    66.27291700
2    30.83170000    -28.96859500
2    10.58410000    -12.86633700
2    3.77040000    -1.71021700
s-d potential
5
0    128.83910000    3.00000000
1    120.37860000    12.85285100
2    63.56220000    275.67239800
2    18.06950000    115.67771200
2    3.81420000    35.06060900
p-d potential
6
0    216.52630000    5.00000000
1    46.57230000    7.47948600
2    147.46850000    613.03200000
2    48.98690000    280.80068500
2    13.20960000    107.87882400
2    3.18310000    15.34395600
```

CI SDD

S	5	1.00		
			0.4085000000D+05	0.2532000659D-02
			0.6179000000D+04	0.1920700500D-01
			0.1425000000D+04	0.9525702480D-01
			0.4092000000D+03	0.3455890900D+00
			0.1355000000D+03	0.6364011657D+00
S	3	1.00		
			0.1355000000D+03	0.1217669823D+00
			0.5013000000D+02	0.6528591181D+00
			0.2021000000D+02	0.2773340774D+00
S	1	1.00		
			0.6283000000D+01	0.1000000000D+01
S	1	1.00		
			0.2460000000D+01	0.1000000000D+01
S	1	1.00		
			0.5271000000D+00	0.1000000000D+01
S	1	1.00		
			0.1884000000D+00	0.1000000000D+01
P	4	1.00		
			0.2408000000D+03	0.1459368837D-01
			0.5656000000D+02	0.9903809883D-01
			0.1785000000D+02	0.3305322930D+00
			0.6350000000D+01	0.6828126314D+00
P	2	1.00		
			0.6350000000D+01	-0.5617851070D+00
			0.2403000000D+01	0.1351901258D+01
P	1	1.00		
			0.6410000000D+00	0.1000000000D+01
P	1	1.00		
			0.1838000000D+00	0.1000000000D+01

Cl 6-311++G(3df,3pd)

```
S 6 1.00
  0.1058190000D+06 0.7380002465D-03
  0.1587200000D+05 0.5718001910D-02
  0.3619650000D+04 0.2949500985D-01
  0.1030800000D+04 0.1172860392D+00
  0.3399080000D+03 0.3629491212D+00
  0.1245380000D+03 0.5841491951D+00
S 3 1.00
  0.1245380000D+03 0.1341769734D+00
  0.4951350000D+02 0.6242498762D+00
  0.2080560000D+02 0.2917559421D+00
S 1 1.00
  0.6583460000D+01 0.1000000000D+01
S 1 1.00
  0.2564680000D+01 0.1000000000D+01
S 1 1.00
  0.5597630000D+00 0.1000000000D+01
S 1 1.00
  0.1832730000D+00 0.1000000000D+01
P 5 1.00
  0.5897760000D+03 0.2390999685D-02
  0.1398490000D+03 0.1850399756D-01
  0.4514130000D+02 0.8137698928D-01
  0.1687330000D+02 0.2215519708D+00
  0.6741100000D+01 0.7725688983D+00
P 2 1.00
  0.6741100000D+01 -0.1572243813D+01
  0.2771520000D+01 0.9923888817D+00
P 1 1.00
  0.1023870000D+01 0.1000000000D+01
P 1 1.00
  0.3813680000D+00 0.1000000000D+01
P 1 1.00
  0.1094370000D+00 0.1000000000D+01
SP 1 1.00
  0.4830000000D-01 0.1000000000D+01 0.1000000000D+01
D 1 1.00
  0.3000000000D+01 0.1000000000D+01
D 1 1.00
  0.7500000000D+00 0.1000000000D+01
D 1 1.00
  0.1875000000D+00 0.1000000000D+01
F 1 1.00
  0.7000000000D+00 0.1000000000D+01
```

A.4. Hydrogen

H LANL2DZ

H	0		
S	3	1.00	
		19.2384000	0.328280000E-01
		2.89870000	0.231204000
		0.653500000	0.817226000
S	1	1.00	
		0.177600000	1.00000000

H SDD

S	3	1.00	
		0.1924060000D+02	0.3282807697D-01
		0.2899200000D+01	0.2312085421D+00
		0.6534000000D+00	0.8172399161D+00
S	1	1.00	
		0.1776000000D+00	0.1000000000D+01

H 6-311++G(3df,3pd)

S	3	1.00	
		0.3386500000D+02	0.2549381454D-01
		0.5094790000D+01	0.1903731086D+00
		0.1158790000D+01	0.8521614860D+00
S	1	1.00	
		0.3258400000D+00	0.1000000000D+01
S	1	1.00	
		0.1027410000D+00	0.1000000000D+01
S	1	1.00	
		0.3600000000D-01	0.1000000000D+01
P	1	1.00	
		0.3000000000D+01	0.1000000000D+01
P	1	1.00	
		0.7500000000D+00	0.1000000000D+01
P	1	1.00	
		0.1875000000D+00	0.1000000000D+01
D	1	1.00	
		0.1000000000D+01	0.1000000000D+01

A.5. Oxygen

O LANL2DZ

O	0		
S	7	1.00	
		7817.00000	0.117600000E-02
		1176.00000	0.896800000E-02
		273.200000	0.428680000E-01
		81.1700000	0.143930000
		27.1800000	0.355630000
		9.53200000	0.461248000
		3.41400000	0.140206000
S	2	1.00	
		9.53200000	-0.154153000
		0.939800000	1.05691400
S	1	1.00	
		0.284600000	1.00000000
P	4	1.00	
		35.1800000	0.195800000E-01
		7.90400000	0.124200000
		2.30500000	0.394714000
		0.717100000	0.627376000
P	1	1.00	
		0.213700000	1.00000000

O SDD

S	6	1.00		
			0.7816540000D+04	0.2030998165D-02
			0.1175820000D+04	0.1543598605D-01
			0.2731880000D+03	0.7377093334D-01
			0.8116960000D+02	0.2476057763D+00
			0.2718360000D+02	0.6118314472D+00
			0.3413600000D+01	0.2412047821D+00
S	1	1.00		
			0.9532200000D+01	0.1000000000D+01
S	1	1.00		
			0.9398000000D+00	0.1000000000D+01
S	1	1.00		
			0.2846000000D+00	0.1000000000D+01
P	4	1.00		
			0.3518320000D+02	0.1957998252D-01
			0.7904000000D+01	0.1241888891D+00
			0.2305100000D+01	0.3947266476D+00
			0.7171000000D+00	0.6273744399D+00
P	1	1.00		
			0.2137000000D+00	0.1000000000D+01

O 6-311++G(3df,3pd)

S	6	1.00		
		0.8588500000D+04	0.1895150083D-02	
		0.1297230000D+04	0.1438590063D-01	
		0.2992960000D+03	0.7073200310D-01	
		0.8737710000D+02	0.2400010105D+00	
		0.2567890000D+02	0.5947970261D+00	
		0.3740040000D+01	0.2808020123D+00	
SP	3	1.00		
		0.4211750000D+02	0.1138890124D+00	0.3651139738D-01
		0.9628370000D+01	0.9208111006D+00	0.2371529830D+00
		0.2853320000D+01	-0.3274470358D-02	0.8197019412D+00
SP	1	1.00		
		0.9056610000D+00	0.1000000000D+01	0.1000000000D+01
SP	1	1.00		
		0.2556110000D+00	0.1000000000D+01	0.1000000000D+01
SP	1	1.00		
		0.8450000000D-01	0.1000000000D+01	0.1000000000D+01
D	1	1.00		
		0.5168000000D+01	0.1000000000D+01	
D	1	1.00		
		0.1292000000D+01	0.1000000000D+01	
D	1	1.00		
		0.3230000000D+00	0.1000000000D+01	
F	1	1.00		
		0.1400000000D+01	0.1000000000D+01	

Appendix B: Raw Data, Bimolecular Reactions using Transition State Theory

B.1. As + O₂ → AsO + O (QCISD/ECP28MWB)

Level of Theory:	QCISD/ECP28MWB					
Species	SPE (Hartrees)	Q _e	Frequencies (cm ⁻¹)			
As	-6.0450961	4	-			
O ₂	-150.1116213	3	1668.9901			
AsO	-81.1779947	2	860.9576			
O	-74.9689005	3	-			
AsOO	-156.0919143	2	-373.1685	831.8339	831.8454	1285.6764

Forward Reaction					
Temp (K)	E _a (kcal/mol)	A (cm ³ /mol/s)	k ^{TS1} (cm ³ /mol/s)	k ¹	k (cm ³ /mol/s)
298.15	41.700	4.567x10 ¹¹	1.235x10 ⁻¹⁹	1.135	1.402x10 ⁻¹⁹
600	41.543	4.412x10 ¹¹	3.251x10 ⁻⁴	1.033	3.360x10 ⁻⁴
900	41.707	5.264x10 ¹¹	3.919x10 ¹	1.015	3.977x10 ¹
1200	41.953	6.461x10 ¹¹	1.477x10 ⁴	1.008	1.489x10 ⁴
1500	42.226	7.859x10 ¹¹	5.532x10 ⁵	1.005	5.561x10 ⁵
2000	42.701	1.051x10 ¹²	2.267x10 ⁷	1.003	2.274x10 ⁷
Reverse Reaction					
Temp (K)	E _a (kcal/mol)	A (cm ³ /mol/s)	k ^{TS1} (cm ³ /mol/s)	k ¹	k (cm ³ /mol/s)
298.15	36.654	1.564x10 ¹¹	2.115x10 ⁻¹⁶	1.135	2.401x10 ⁻¹⁶
600	36.266	1.352x10 ¹¹	8.335x10 ⁻³	1.033	8.614x10 ⁻³
900	36.223	1.454x10 ¹¹	2.324x10 ²	1.015	2.358x10 ²
1200	36.329	1.655x10 ¹¹	4.001x10 ⁴	1.008	4.035x10 ⁴
1500	36.505	1.907x10 ¹¹	9.148x10 ⁵	1.005	9.197x10 ⁵
2000	36.877	2.398x10 ¹¹	2.238x10 ⁷	1.003	2.245x10 ⁷

298.15 K						
Species	Th. Corr.	$Q_{v,tot}$	Q_t	$Q_{t,corr}$ (m ⁻³)	Q_r	Q_{tot} (cm ⁻³)
As	0.001416	1	2.549x10 ⁷	6.274x10 ³²	1	2.510x10 ²⁷
O ₂	0.006165	1.001	7.112x10 ⁶	1.751x10 ³²	70.7204	3.716x10 ²⁸
AsO	0.004384	1.020	3.407x10 ⁷	8.387x10 ³²	428.383	7.331x10 ²⁹
O	0.001416	1	2.514x10 ⁶	6.189x10 ³¹	1	1.857x10 ²⁶
AsOO	0.009231	1.050	4.345x10 ⁷	1.070x10 ³³	2534.16	5.691x10 ³⁰
600 K						
Species	Th. Corr.	$Q_{v,tot}$	Q_t	$Q_{t,corr}$ (m ⁻³)	Q_r	Q_{tot} (cm ⁻³)
As	0.002850	1	1.464x10 ⁸	1.791x10 ³³	1	7.165x10 ²⁷
O ₂	0.008694	1.023	4.086x10 ⁷	4.997x10 ³²	142.326	2.184x10 ²⁹
AsO	0.007282	1.166	1.958x10 ⁸	2.394x10 ³³	862.083	4.815x10 ³⁰
O	0.002850	1	1.445x10 ⁷	1.767x10 ³²	1	5.301x10 ²⁶
AsOO	0.012944	1.472	2.496x10 ⁸	3.053x10 ³³	5099.78	4.584x10 ³¹
900 K						
Species	Th. Corr.	$Q_{v,tot}$	Q_t	$Q_{t,corr}$ (m ⁻³)	Q_r	Q_{tot} (cm ⁻³)
As	0.004275	1	4.035x10 ⁸	3.291x10 ³³	1	1.316x10 ²⁸
O ₂	0.011495	1.088	1.126x10 ⁸	9.181x10 ³²	213.489	6.396x10 ²⁹
AsO	0.010412	1.375	5.394x10 ⁸	4.399x10 ³³	1293.12	1.565x10 ³¹
O	0.004275	1	3.981x10 ⁷	3.246x10 ³²	1	9.738x10 ²⁶
AsOO	0.017431	2.286	6.879x10 ⁸	5.609x10 ³³	7649.67	1.962x10 ³²
1200 K						
Species	Th. Corr.	$Q_{v,tot}$	Q_t	$Q_{t,corr}$ (m ⁻³)	Q_r	Q_{tot} (cm ⁻³)
As	0.005700	1	8.284x10 ⁸	5.066x10 ³³	1	2.026x10 ²⁸
O ₂	0.014491	1.178	2.311x10 ⁸	1.414x10 ³³	284.652	1.422x10 ³⁰
AsO	0.013632	1.607	1.107x10 ⁹	6.772x10 ³³	1724.17	3.752x10 ³¹
O	0.005700	1	8.171x10 ⁷	4.997x10 ³²	1	1.499x10 ²⁷
AsOO	0.022245	3.510	1.412x10 ⁹	8.636x10 ³³	10199.6	6.183x10 ³²
1500 K						
Species	Th. Corr.	$Q_{v,tot}$	Q_t	$Q_{t,corr}$ (m ⁻³)	Q_r	Q_{tot} (cm ⁻³)
As	0.007125	1	1.447x10 ⁹	7.080x10 ³³	1	2.832x10 ²⁸
O ₂	0.017599	1.283	4.038x10 ⁸	1.975x10 ³³	355.815	2.706x10 ³⁰
AsO	0.016893	1.848	1.934x10 ⁹	9.465x10 ³³	2155.21	7.539x10 ³¹
O	0.007125	1	1.427x10 ⁸	6.984x10 ³²	1	2.095x10 ²⁷
AsOO	0.027212	5.199	2.467x10 ⁹	1.207x10 ³⁴	12749.4	1.600x10 ³³
2000 K						
Species	Th. Corr.	$Q_{v,tot}$	Q_t	$Q_{t,corr}$ (m ⁻³)	Q_r	Q_{tot} (cm ⁻³)
As	0.009500	1	2.971x10 ⁹	1.090x10 ³⁴	1	4.360x10 ²⁸
O ₂	0.022911	1.475	8.288x10 ⁸	3.041x10 ³³	474.42	6.386x10 ³⁰
AsO	0.022369	2.260	3.971x10 ⁹	1.457x10 ³⁴	2873.61	1.893x10 ³²
O	0.009500	1	2.930x10 ⁸	1.075x10 ³³	1	3.226x10 ²⁷
AsOO	0.035656	9.233	5.064x10 ⁹	1.858x10 ³⁴	16999.3	5.833x10 ³³

B.2. As + OH → AsO + H (QCISD(T)/ECP28MWB)

Level of Theory:	QCISD(T)/ECP28MWB					
Species	SPE (Hartrees)	Q _e	Frequencies (cm ⁻¹)			
As	-6.0451172	4	-			
OH	-75.6400013	2	3769.1045			
AsO	-81.1920679	2	906.4318			
H	-0.4998179	2	-			
AsOH	-81.5889682	5	-1270.1521	225.515	434.8917	549.7517

Forward Reaction					
Temp (K)	E _a (kcal/mol)	A (cm ³ /mol/s)	k ^{1ST} (cm ³ /mol/s)	k ¹	k (cm ³ /mol/s)
298.15	55.817	6.502x10 ¹²	7.888x10 ⁻²⁹	2.568	2.025x10 ⁻²⁸
600	55.876	1.307x10 ¹³	5.791x10 ⁻⁸	1.387	8.032x10 ⁻⁸
900	56.020	2.424x10 ¹³	6.033x10 ⁻¹	1.172	7.071x10 ⁻¹
1200	56.175	4.204x10 ¹³	2.469x10 ³	1.097	2.708x10 ³
1500	56.263	6.049x10 ¹³	3.837x10 ⁵	1.062	4.074x10 ⁵
2000	56.260	1.042x10 ¹⁴	7.408x10 ⁷	1.035	7.666x10 ⁷
Reverse Reaction					
Temp (K)	E _a (kcal/mol)	A (cm ³ /mol/s)	k ^{1ST} (cm ³ /mol/s)	k ¹	k (cm ³ /mol/s)
298.15	64.122	1.672x10 ¹³	1.654x10 ⁻³⁴	2.568	4.246x10 ⁻³⁴
600	63.883	2.977x10 ¹³	1.597x10 ⁻¹⁰	1.387	2.216x10 ⁻¹⁰
900	63.590	4.736x10 ¹³	1.711x10 ⁻²	1.172	2.005x10 ⁻²
1200	63.314	7.145x10 ¹³	2.102x10 ²	1.097	2.305x10 ²
1500	63.029	9.149x10 ¹³	5.995x10 ⁴	1.062	6.366x10 ⁴
2000	62.547	1.355x10 ¹⁴	1.981x10 ⁷	1.035	2.050x10 ⁷

298.15 K						
Species	Enth. Corr.	$Q_{v,tot}$	Q_t	$Q_{t,corr}$ (m ⁻³)	Q_r	Q_{tot} (cm ⁻³)
As	0.002360	1	2.549x10 ⁷	6.274x10 ³²	1	2.510x10 ²⁷
OH	0.011891	1	2.756x10 ⁶	6.783x10 ³¹	10.977	1.489x10 ²⁷
AsO	0.005422	1.016	3.407x10 ⁷	8.387x10 ³²	435.526	7.426x10 ²⁹
H	0.002360	1	3.977x10 ⁴	9.789x10 ²⁹	1	1.958x10 ²⁴
AsOH	0.007050	1.969	3.464x10 ⁷	8.527x10 ³²	773.638	6.495x10 ³⁰
600 K						
Species	Enth. Corr.	$Q_{v,tot}$	Q_t	$Q_{t,corr}$ (m ⁻³)	Q_r	Q_{tot} (cm ⁻³)
As	0.004750	1	1.464x10 ⁸	1.791x10 ³³	1	7.165x10 ²⁷
OH	0.015239	1	1.583x10 ⁷	1.936x10 ³²	22.0903	8.557x10 ²⁷
AsO	0.009246	1.148	1.958x10 ⁸	2.394x10 ³³	876.457	4.817x10 ³⁰
H	0.004750	1	2.285x10 ⁵	2.794x10 ³⁰	1	5.589x10 ²⁴
AsOH	0.012883	5.617	1.990x10 ⁸	2.434x10 ³³	1556.88	1.064x10 ³²
900 K						
Species	Enth. Corr.	$Q_{v,tot}$	Q_t	$Q_{t,corr}$ (m ⁻³)	Q_r	Q_{tot} (cm ⁻³)
As	0.007125	1	4.035x10 ⁸	3.291x10 ³³	1	1.316x10 ²⁸
OH	0.018604	1.003	4.363x10 ⁷	3.557x10 ³²	33.1354	2.366x10 ²⁸
AsO	0.013308	1.342	5.394x10 ⁸	4.399x10 ³³	1314.69	1.552x10 ³¹
H	0.007125	1	6.296x10 ⁵	5.134x10 ³⁰	1	1.027x10 ²⁵
AsOH	0.018852	12.796	5.484x10 ⁸	4.472x10 ³³	2335.32	6.682x10 ³²
1200 K						
Species	Enth. Corr.	$Q_{v,tot}$	Q_t	$Q_{t,corr}$ (m ⁻³)	Q_r	Q_{tot} (cm ⁻³)
As	0.009500	1	8.284x10 ⁸	5.066x10 ³³	1	2.026x10 ²⁸
OH	0.022077	1.014	8.956x10 ⁷	5.477x10 ³²	44.1805	4.909x10 ²⁸
AsO	0.017468	1.559	1.107x10 ⁹	6.772x10 ³³	1752.91	3.702x10 ³¹
H	0.009500	1	1.292x10 ⁶	7.904x10 ³⁰	1	1.581x10 ²⁵
AsOH	0.024947	24.690	1.181x10 ⁹	7.224x10 ³³	3113.75	2.777x10 ³³
1500 K						
Species	Enth. Corr.	$Q_{v,tot}$	Q_t	$Q_{t,corr}$ (m ⁻³)	Q_r	Q_{tot} (cm ⁻³)
As	0.011876	1	1.447x10 ⁹	7.080x10 ³³	1	2.832x10 ²⁸
OH	0.025687	1.034	1.565x10 ⁸	7.654x10 ³²	55.2257	8.743x10 ²⁸
AsO	0.021672	1.787	1.934x10 ⁹	9.465x10 ³³	2191.14	7.411x10 ³¹
H	0.011876	1	2.258x10 ⁶	1.105x10 ³¹	1	2.209x10 ²⁵
AsOH	0.031073	42.493	1.967x10 ⁹	9.622x10 ³³	3892.19	7.957x10 ³³
2000 K						
Species	Enth. Corr.	$Q_{v,tot}$	Q_t	$Q_{t,corr}$ (m ⁻³)	Q_r	Q_{tot} (cm ⁻³)
As	0.015834	1	2.971x10 ⁹	1.090x10 ³⁴	1	4.360x10 ²⁸
OH	0.031977	1.084	3.212x10 ⁸	1.178x10 ³³	73.6342	1.881x10 ²⁹
AsO	0.028724	2.177	3.971x10 ⁹	1.457x10 ³⁴	2921.52	1.853x10 ³²
H	0.015834	1	4.635x10 ⁶	1.701x10 ³¹	1	3.401x10 ²⁵
AsOH	0.041316	88.550	4.037x10 ⁹	1.481x10 ³⁴	5189.59	3.404x10 ³⁴

B.3. As + HCl → AsCl + H (QCISD(T)/6-311++G(3df,3pd))

Level of Theory:	QCISD(T)/6-311++G(3df,3pd)					
Species	SPE (Hartrees)	Q _e	Frequencies (cm ⁻¹)			
As	-2234.2457903	4	-			
HCl	-460.3307089	1	3004.4317			
AsCl	-2694.0155153	3	425.5767			
H	-0.4998179	2	-			
AsClH	-2694.5077474	4	-894.2005	279.1836	280.2866	399.7713

Forward Reaction					
Temp (K)	E _a (kcal/mol)	A (cm ³ /mol/s)	k ^{1ST} (cm ³ /mol/s)	k ¹	k (cm ³ /mol/s)
298.15	40.085	6.169x10 ¹²	2.549x10 ⁻¹⁷	1.777	4.530x10 ⁻¹⁷
600	40.808	1.443x10 ¹³	1.969x10 ⁻²	1.192	2.347x10 ⁻²
900	41.579	2.846x10 ¹³	2.275x10 ³	1.085	2.469x10 ³
1200	42.274	4.827x10 ¹³	9.644x10 ⁵	1.048	1.011x10 ⁶
1500	42.881	7.355x10 ¹³	4.156x10 ⁷	1.031	4.283x10 ⁷
2000	43.745	1.267x10 ¹⁴	2.101x10 ⁹	1.017	2.138x10 ⁹
Reverse Reaction					
Temp (K)	E _a (kcal/mol)	A (cm ³ /mol/s)	k ^{1ST} (cm ³ /mol/s)	k ¹	k (cm ³ /mol/s)
298.15	5.209	6.058x10 ¹²	9.195x10 ⁸	1.777	1.634Ex10 ⁹
600	5.433	1.024x10 ¹³	1.074x10 ¹¹	1.192	1.281x10 ¹¹
900	5.706	1.563x10 ¹³	6.434x10 ¹¹	1.085	6.982x10 ¹¹
1200	5.991	2.189x10 ¹³	1.774x10 ¹²	1.048	1.859x10 ¹²
1500	6.281	2.887x10 ¹³	3.510x10 ¹²	1.031	3.618x10 ¹²
2000	6.771	4.194x10 ¹³	7.633x10 ¹²	1.017	7.765x10 ¹²

298.15 K						
Species	Th. Corr.	$Q_{v,tot}$	Q_t	$Q_{t,corr}$ (m ⁻³)	Q_r	Q_{tot} (cm ⁻³)
As	0.001416	1	2.549x10 ⁷	6.274x10 ³²	1	2.510x10 ²⁷
HCl	0.009205	1	8.482x10 ⁶	2.088x10 ³²	19.6061	4.093x10 ²⁷
AsCl	0.003615	1.168	4.528x10 ⁷	1.115x10 ³³	1367.86	5.343x10 ³⁰
H	0.001416	1	3.977x10 ⁴	9.789x10 ²⁹	1	1.958x10 ²⁴
AsClH	0.005748	2.301	4.590x10 ⁷	1.130x10 ³³	1628.57	1.694x10 ³¹
600 K						
Species	Th. Corr.	$Q_{v,tot}$	Q_t	$Q_{t,corr}$ (m ⁻³)	Q_r	Q_{tot} (cm ⁻³)
As	0.002850	1	1.464x10 ⁸	1.791x10 ³³	1	7.165x10 ²⁷
HCl	0.011605	1.001	4.873x10 ⁷	5.960x10 ³²	39.4556	2.354x10 ²⁸
AsCl	0.006812	1.618	2.601x10 ⁸	3.182x10 ³³	2752.7	4.251x10 ³¹
H	0.002850	1	2.285x10 ⁵	2.794x10 ³⁰	1	5.589x10 ²⁴
AsClH	0.010735	7.642	2.637x10 ⁸	3.226x10 ³³	3277.34	3.231x10 ³²
900 K						
Species	Th. Corr.	$Q_{v,tot}$	Q_t	$Q_{t,corr}$ (m ⁻³)	Q_r	Q_{tot} (cm ⁻³)
As	0.004275	1	4.035x10 ⁸	3.291x10 ³³	1	1.316x10 ²⁸
HCl	0.014083	1.011	1.343x10 ⁸	1.095x10 ³³	59.1834	6.551x10 ²⁸
AsCl	0.010085	2.111	7.168x10 ⁸	5.845x10 ³³	4129.05	1.529x10 ³²
H	0.004275	1	6.296x10 ⁵	5.134x10 ³⁰	1	1.027x10 ²⁵
AsClH	0.015867	18.645	7.267x10 ⁸	5.926x10 ³³	4916.01	2.173x10 ³³
1200 K						
Species	Th. Corr.	$Q_{v,tot}$	Q_t	$Q_{t,corr}$ (m ⁻³)	Q_r	Q_{tot} (cm ⁻³)
As	0.005700	1	8.284x10 ⁸	5.066x10 ³³	1	2.026x10 ²⁸
HCl	0.016729	1.035	2.756x10 ⁸	1.686x10 ³³	78.9112	1.376x10 ²⁹
AsCl	0.013383	2.617	1.472x10 ⁹	8.999x10 ³³	5505.4	3.890x10 ³²
H	0.005700	1	1.292x10 ⁶	7.904x10 ³⁰	1	1.581x10 ²⁵
AsClH	0.021045	37.370	1.492x10 ⁹	9.123x10 ³³	6554.68	8.939x10 ³³
1500 K						
Species	Th. Corr.	$Q_{v,tot}$	Q_t	$Q_{t,corr}$ (m ⁻³)	Q_r	Q_{tot} (cm ⁻³)
As	0.007125	1	1.447x10 ⁹	7.080x10 ³³	1	2.832x10 ²⁸
HCl	0.019533	1.071	4.815x10 ⁸	2.356x10 ³³	98.639	2.488x10 ²⁹
AsCl	0.016692	3.129	2.571x10 ⁹	1.258x10 ³⁴	6881.75	8.124x10 ³²
H	0.007125	1	2.258x10 ⁶	1.105x10 ³¹	1	2.209x10 ²⁵
AsClH	0.026241	65.882	2.606x10 ⁹	1.275x10 ³⁴	8193.35	2.753x10 ³⁴
2000 K						
Species	Th. Corr.	$Q_{v,tot}$	Q_t	$Q_{t,corr}$ (m ⁻³)	Q_r	Q_{tot} (cm ⁻³)
As	0.009500	1	2.971x10 ⁹	1.090x10 ³⁴	1	4.360x10 ²⁸
HCl	0.024460	1.150	9.885x10 ⁸	3.627x10 ³³	131.519	5.484x10 ²⁹
AsCl	0.022217	3.987	5.277x10 ⁹	1.936x10 ³⁴	9175.66	2.125x10 ³³
H	0.009500	1	4.635x10 ⁶	1.701x10 ³¹	1	3.401x10 ²⁵
AsClH	0.034921	140.771	5.350x10 ⁹	1.963x10 ³⁴	10924.5	1.208x10 ³⁵

B.4. $\text{Se} + \text{O}_2 \rightarrow \text{SeO} + \text{O}$ (CCSD/RECP28VDZ)

Level of Theory:	CCSD/RECP28VDZ					
Species	SPE (Hartrees)	Q_e	Frequencies (cm^{-1})			
Se	-9.1458557	3	-			
O_2	-150.1101841	3	1685.8283			
SeO	-84.2573107	3	848.3451			
O	-74.9687738	3	-			
SeOO	-159.1674152	5	-1229.461	213.5064	230.8432	418.0222

Forward Reaction					
Temp (K)	E_a (kcal/mol)	A ($\text{cm}^3/\text{mol/s}$)	k^{TS1} ($\text{cm}^3/\text{mol/s}$)	k^{\ddagger}	k ($\text{cm}^3/\text{mol/s}$)
298.15	54.390	3.616×10^{12}	4.871×10^{-28}	2.469	1.202×10^{-27}
600	55.060	9.004×10^{12}	7.909×10^{-8}	1.363	1.078×10^{-7}
900	55.640	1.744×10^{13}	5.367×10^{-1}	1.161	6.232×10^{-1}
1200	56.122	2.844×10^{13}	1.708×10^3	1.091	1.862×10^3
1500	56.543	4.163×10^{13}	2.403×10^5	1.058	2.542×10^5
2000	57.172	6.779×10^{13}	3.833×10^7	1.033	3.958×10^7
Reverse Reaction					
Temp (K)	E_a (kcal/mol)	A ($\text{cm}^3/\text{mol/s}$)	k^{TS1} ($\text{cm}^3/\text{mol/s}$)	k^{\ddagger}	k ($\text{cm}^3/\text{mol/s}$)
298.15	36.750	5.866×10^{11}	6.740×10^{-16}	2.469	1.664×10^{-15}
600	37.181	1.301×10^{12}	3.720×10^{-2}	1.363	5.069×10^{-2}
900	37.548	2.263×10^{12}	1.724×10^3	1.161	2.001×10^3
1200	37.884	3.413×10^{12}	4.298×10^5	1.091	4.688×10^5
1500	38.206	4.722×10^{12}	1.280×10^7	1.058	1.355×10^7
2000	38.728	7.211×10^{12}	4.225×10^8	1.033	4.363×10^8

298.15 K						
Species	Th. Corr.	$Q_{v,tot}$	Q_t	$Q_{t,corr}$ (m ⁻³)	Q_r	Q_{tot} (cm ⁻³)
Se	0.001416	1	2.808x10 ⁷	6.912x10 ³²	1	2.074x10 ²⁷
O ₂	0.006203	1	7.112x10 ⁶	1.751x10 ³²	70.5003	3.704x10 ²⁸
SeO	0.004359	1.021	3.692x10 ⁷	9.088x10 ³²	457.891	1.275x10 ³⁰
O	0.001416	1	2.514x10 ⁶	6.189x10 ³¹	1	1.857x10 ²⁶
SeOO	0.005671	2.907	4.653x10 ⁷	1.145x10 ³³	2229.67	3.712x10 ³¹
600 K						
Species	Th. Corr.	$Q_{v,tot}$	Q_t	$Q_{t,corr}$ (m ⁻³)	Q_r	Q_{tot} (cm ⁻³)
Se	0.002850	1	1.613x10 ⁸	1.973x10 ³³	1	5.920x10 ²⁷
O ₂	0.008728	1.023	4.086x10 ⁷	4.997x10 ³²	141.875	2.175x10 ²⁹
SeO	0.007264	1.172	2.121x10 ⁸	2.594x10 ³³	921.464	8.405x10 ³⁰
O	0.002850	1	1.445x10 ⁷	1.767x10 ³²	1	5.301x10 ²⁶
SeOO	0.010697	10.494	2.673x10 ⁸	3.270x10 ³³	4487	7.698x10 ³²
900 K						
Species	Th. Corr.	$Q_{v,tot}$	Q_t	$Q_{t,corr}$ (m ⁻³)	Q_r	Q_{tot} (cm ⁻³)
Se	0.004275	1	4.446x10 ⁸	3.625x10 ³³	1	1.088x10 ²⁸
O ₂	0.011522	1.085	1.126x10 ⁸	9.181x10 ³²	212.813	6.362x10 ²⁹
SeO	0.010399	1.385	5.845x10 ⁸	4.766x10 ³³	1382.2	2.738x10 ³¹
O	0.004275	1	3.981x10 ⁷	3.246x10 ³²	1	9.738x10 ²⁶
SeOO	0.015841	26.423	7.366x10 ⁸	6.007x10 ³³	6730.5	5.341x10 ³³
1200 K						
Species	Th. Corr.	$Q_{v,tot}$	Q_t	$Q_{t,corr}$ (m ⁻³)	Q_r	Q_{tot} (cm ⁻³)
Se	0.005700	1	9.126x10 ⁸	5.581x10 ³³	1	1.674x10 ²⁸
O ₂	0.014514	1.174	2.311x10 ⁸	1.413x10 ³³	283.751	1.413x10 ³⁰
SeO	0.013623	1.621	1.200x10 ⁹	7.338x10 ³³	1842.93	6.576x10 ³¹
O	0.005700	1	8.171x10 ⁷	4.997x10 ³²	1	1.499x10 ²⁷
SeOO	0.021025	53.839	1.512x10 ⁹	9.248x10 ³³	8974.01	2.234x10 ³⁴
1500 K						
Species	Th. Corr.	$Q_{v,tot}$	Q_t	$Q_{t,corr}$ (m ⁻³)	Q_r	Q_{tot} (cm ⁻³)
Se	0.007125	1	1.594x10 ⁹	7.800x10 ³³	1	2.340x10 ²⁸
O ₂	0.017618	1.278	4.038x10 ⁸	1.975x10 ³³	354.689	2.686x10 ³⁰
SeO	0.016885	1.866	2.096x10 ⁹	1.026x10 ³⁴	2303.66	1.323x10 ³²
O	0.007125	1	1.427x10 ⁸	6.984x10 ³²	1	2.095x10 ²⁷
SeOO	0.026226	95.884	2.642x10 ⁹	1.292x10 ³⁴	11217.5	6.951x10 ³⁴
2000 K						
Species	Th. Corr.	$Q_{v,tot}$	Q_t	$Q_{t,corr}$ (m ⁻³)	Q_r	Q_{tot} (cm ⁻³)
Se	0.009500	1	3.273x10 ⁹	1.201x10 ³⁴	1	3.603x10 ²⁸
O ₂	0.022926	1.467	8.288x10 ⁸	3.041x10 ³³	472.918	6.332x10 ³⁰
SeO	0.022363	2.285	4.303x10 ⁹	1.579x10 ³⁴	3071.55	3.324x10 ³²
O	0.009500	1	2.930x10 ⁸	1.075x10 ³³	1	3.226x10 ²⁷
SeOO	0.034910	207.000	5.423x10 ⁹	1.990x10 ³⁴	14956.7	3.080x10 ³⁵

Appendix C: Raw Data, Unimolecular Reactions using RRKM Theory

C.1. Se + H₂ → SeH₂ (CCSD(T)/6-311++G(3df,3pd))

Level of Theory:	CCSD(T)/6-311++G(3df,3pd)				
Species	SPE (Hartrees)	Q _e	Frequencies (cm ⁻¹)		
Se	-2399.913758	3	-		
H ₂	-1.1725343	1	4402.2834		
SeH ₂	-2401.16864	1	1061.5935	2460.7037	2471.6026
SeH ₂	-2401.050632	1	-881.3094	1224.1598	2160.9502

Reverse Reaction (Collision Efficiency 0.1)					
Temp (K)	E _a (kcal/mol)	B _c Z _{LJ} [M] (s ⁻¹)	∑X	k _{uni} (s ⁻¹)	k (cm ³ /mol/s)
298.15	70.313	2.285x10 ⁸	7.673x10 ⁻⁵	3.687x10 ⁻⁴⁶	9.019x10 ⁻⁴²
600	70.257	1.303x10 ⁸	4.774x10 ⁻⁵	7.190x10 ⁻²¹	3.540x10 ⁻¹⁶
900	70.139	9.301x10 ⁷	4.016x10 ⁻⁵	1.164x10 ⁻¹²	8.599x10 ⁻⁸
1200	69.917	7.578x10 ⁷	4.022x10 ⁻⁵	1.451x10 ⁻⁸	1.429x10 ⁻³
1500	69.599	6.481x10 ⁷	4.296x10 ⁻⁵	4.144x10 ⁻⁶	0.510
2000	68.926	5.312x10 ⁷	5.091x10 ⁻⁵	1.186x10 ⁻³	1.946x10 ⁻²
Reverse Reaction (Collision Efficiency 1.0)					
Temp (K)	E _a (kcal/mol)	B _c Z _{LJ} [M] (s ⁻¹)	∑X	k _{uni} (s ⁻¹)	k (cm ³ /mol/s)
298.15	70.313	2.285x10 ⁹	7.667x10 ⁻⁴	3.684x10 ⁻⁴⁵	9.013x10 ⁻⁴¹
600	70.257	1.303x10 ⁹	4.773x10 ⁻⁴	7.187x10 ⁻²⁰	3.538x10 ⁻¹⁵
900	70.139	9.301x10 ⁸	4.015x10 ⁻⁴	1.164x10 ⁻¹¹	8.597x10 ⁻⁷
1200	69.917	7.578x10 ⁸	4.021x10 ⁻⁴	1.451x10 ⁻⁷	1.428x10 ⁻²
1500	69.599	6.481x10 ⁸	4.296x10 ⁻⁴	4.143x10 ⁻⁵	5.100
2000	68.926	5.312x10 ⁸	5.091x10 ⁻⁴	1.186x10 ⁻²	1.946x10 ⁻³

Appendix D: Raw Data, Thermodynamic Data

D.1. As + O₂ → AsO + O (QCISD/ECP28MWB)

Theoretical				
Temp (K)	ΔS (cal/molK)	ΔH (kcal/mol)	ΔG (kcal/mol)	K _{eq}
298.15	0.870	5.046	4.787	3.099x10 ⁻⁴
600	1.393	5.277	4.442	2.410x10 ⁻²
900	1.677	5.484	3.975	1.083x10 ⁻¹
1200	1.813	5.624	3.449	2.354x10 ⁻¹
1500	1.883	5.721	2.896	3.785x10 ⁻¹
2000	1.944	5.823	1.935	6.145x10 ⁻¹
Experimental				
Temp (K)	ΔS (cal/molK)	ΔH (kcal/mol)	ΔG (kcal/mol)	K _{eq}
298.15	2.904	-22.758	-23.624	2.076x10 ⁻¹⁷
600	3.901	-22.320	-24.660	9.612x10 ⁸
900	4.460	-21.910	-25.924	1.975x10 ⁶
1200	4.754	-21.596	-27.301	9.383x10 ⁴
1500	4.928	-21.380	-28.772	1.557x10 ⁴
2000	5.000	-21.223	-31.223	2.582x10 ³

298.15 K					
	Theoretical			Experimental	
Species	S (cal/molK)	Th. Corr.	Tot. Energy (Hart.)	S (cal/molK)	H (kcal/mol)
As	41.612	0.001416	-6.0436801	41.611	68.619
O ₂	48.960	0.006165	-150.1054563	49.013	0
AsO	55.004	0.004384	-81.1736107	55.036	-13.692
O	36.438	0.001416	-74.9674845	38.491	59.553
600 K					
	Theoretical			Experimental	
Species	S (cal/molK)	Th. Corr.	Tot. Energy (Hart.)	S (cal/molK)	H (kcal/mol)
As	45.087	0.002850	-6.0422461	45.062	70.108
O ₂	54.003	0.008694	-150.1029273	54.159	2.228
AsO	60.571	0.007282	-81.1707127	61.033	-11.081
O	39.912	0.002850	-74.9660505	42.089	61.097
900 K					
	Theoretical			Experimental	
Species	S (cal/molK)	Th. Corr.	Tot. Energy (Hart.)	S (cal/molK)	H (kcal/mol)
As	47.101	0.004275	-6.0408211	47.060	71.587
O ₂	57.176	0.011495	-150.1001263	57.361	4.610
AsO	64.028	0.010412	-81.1675827	64.761	-8.320
O	41.926	0.004275	-74.9646255	44.120	62.608
1200 K					
	Theoretical			Experimental	
Species	S (cal/molK)	Th. Corr.	Tot. Energy (Hart.)	S (cal/molK)	H (kcal/mol)
As	48.530	0.005700	-6.0393961	48.478	73.065
O ₂	59.549	0.014491	-150.0971303	59.751	7.098
AsO	66.536	0.013632	-81.1643627	67.429	-5.539
O	43.356	0.005700	-74.9632005	45.554	64.106
1500 K					
	Theoretical			Experimental	
Species	S (cal/molK)	Th. Corr.	Tot. Energy (Hart.)	S (cal/molK)	H (kcal/mol)
As	49.639	0.007125	-6.0379711	49.578	74.544
O ₂	61.443	0.017599	-150.0940223	61.663	9.670
AsO	68.501	0.016893	-81.1611017	69.492	-2.7653
O	44.464	0.007125	-74.9617755	46.678	65.600
2000 K					
	Theoretical			Experimental	
Species	S (cal/molK)	Th. Corr.	Tot. Energy (Hart.)	S (cal/molK)	H (kcal/mol)
As	51.068	0.009500	-6.0355961	50.996	77.010
O ₂	63.931	0.022911	-150.0887103	64.221	14.116
AsO	71.05	0.022369	-81.1556257	72.129	1.816
O	45.893	0.009500	-74.9594005	48.088	68.086

D.2. As + OH → AsO + H (QCISD(T)/ECP28MWB)

Theoretical				
Temp (K)	ΔS (cal/molK)	ΔH (kcal/mol)	ΔG (kcal/mol)	K_{eq}
298.15	-1.772	-8.306	-7.778	5.027×10^5
600	-1.117	-8.007	-7.337	4.705×10^2
900	-0.527	-7.570	-7.096	5.286×10^1
1200	-0.113	-7.139	-7.003	1.886×10^1
1500	0.165	-6.766	-7.013	1.052×10^1
2000	0.443	-6.289	-7.174	6.081
Experimental				
Temp (K)	ΔS (cal/molK)	ΔH (kcal/mol)	ΔG (kcal/mol)	K_{eq}
298.15	-3.064	-39.527	-38.613	2.019×10^{-28}
600	-1.979	-39.043	-37.856	6.158×10^{13}
900	-1.132	-38.408	-37.389	1.201×10^9
1200	-0.576	-37.830	-37.138	5.809×10^6
1500	-0.234	-37.359	-37.008	2.468×10^5
2000	0.100	-36.807	-37.006	1.107×10^4

298.15 K					
	Theoretical			Experimental	
Species	S (cal/molK)	Enth. Corr.	Tot. Energy (Hart.)	S (cal/molK)	H (kcal/mol)
As	41.612	0.002360	-6.0427572	41.611	68.619
OH	42.562	0.011891	-75.6281103	43.908	9.319
AsO	55.010	0.005422	-81.1866459	55.036	-13.692
H	27.392	0.002360	-0.4974579	27.419	52.103
600 K					
	Theoretical			Experimental	
Species	S (cal/molK)	Enth. Corr.	Tot. Energy (Hart.)	S (cal/molK)	H (kcal/mol)
As	45.087	0.004750	-6.0403672	45.062	70.108
OH	47.429	0.015239	-75.6247623	48.853	11.456
AsO	60.533	0.009246	-81.1828219	61.033	-11.081
H	30.866	0.004750	-0.4950679	30.903	53.602
900 K					
	Theoretical			Experimental	
Species	S (cal/molK)	Enth. Corr.	Tot. Energy (Hart.)	S (cal/molK)	H (kcal/mol)
As	47.101	0.007125	-6.0379922	47.060	71.587
OH	50.280	0.018604	-75.6213973	51.745	13.595
AsO	63.974	0.013308	-81.1787599	64.761	-8.320
H	32.880	0.007125	-0.4926929	32.911	55.093
1200 K					
	Theoretical			Experimental	
Species	S (cal/molK)	Enth. Corr.	Tot. Energy (Hart.)	S (cal/molK)	H (kcal/mol)
As	48.530	0.00950	-6.0356172	48.478	73.065
OH	52.368	0.022077	-75.6179243	53.872	15.810
AsO	66.476	0.017468	-81.1745999	67.429	-5.539
H	34.309	0.00950	-0.4903179	34.345	56.585
1500 K					
	Theoretical			Experimental	
Species	S (cal/molK)	Enth. Corr.	Tot. Energy (Hart.)	S (cal/molK)	H (kcal/mol)
As	49.639	0.011876	-6.0332412	49.578	74.544
OH	54.052	0.025687	-75.6143143	55.593	18.124
AsO	68.438	0.021672	-81.1703959	69.492	-2.765
H	35.418	0.011876	-0.4879419	35.445	58.074
2000 K					
	Theoretical			Experimental	
Species	S (cal/molK)	Enth. Corr.	Tot. Energy (Hart.)	S (cal/molK)	H (kcal/mol)
As	51.068	0.015834	-6.0292832	50.996	77.010
OH	56.320	0.031977	-75.6080243	57.911	22.170
AsO	70.984	0.028724	-81.1633439	72.129	1.816
H	36.847	0.015834	-0.4839839	36.879	60.557

D.3. As + HCl → AsCl + H (QCISD(T)/6-311++G(3df,3pd))

Theoretical				
Temp (K)	ΔS (cal/molK)	ΔH (kcal/mol)	ΔG (kcal/mol)	K_{eq}
298.15	0.600	34.874	34.696	3.686×10^{-26}
600	1.745	35.375	34.328	3.131×10^{-13}
900	2.422	35.873	33.694	6.573×10^{-9}
1200	2.817	36.283	32.902	1.017×10^{-6}
1500	3.054	36.599	32.018	2.161×10^{-5}
2000	3.271	36.975	30.433	4.724×10^{-4}
Experimental (NO AsCl Data)				

298.15 K					
	Theoretical			Experimental	
Species	S (cal/molK)	Th. Corr.	Tot. Energy (Hart.)	S (cal/molK)	H (kcal/mol)
As	41.612	0.001416	-2234.244374	41.611	68.619
HCl	44.572	0.009205	-460.3215039	44.670	-22.063
AsCl	59.392	0.003615	-2694.0119	-	-
H	27.392	0.001416	-0.4984019	27.419	52.103
600 K					
	Theoretical			Experimental	
Species	S (cal/molK)	Th. Corr.	Tot. Energy (Hart.)	S (cal/molK)	H (kcal/mol)
As	45.087	0.002850	-2234.24294	45.062	70.108
HCl	49.448	0.011605	-460.3191039	49.570	-19.952
AsCl	65.414	0.006812	-2694.008703	-	-
H	30.866	0.002850	-0.4969679	30.903	53.602
900 K					
	Theoretical			Experimental	
Species	S (cal/molK)	Th. Corr.	Tot. Energy (Hart.)	S (cal/molK)	H (kcal/mol)
As	47.101	0.004275	-2234.241515	47.060	71.587
HCl	52.351	0.014083	-460.3166259	52.486	-17.782
AsCl	68.994	0.010085	-2694.00543	-	-
H	32.88	0.004275	-0.4955429	32.911	55.093
1200 K					
	Theoretical			Experimental	
Species	S (cal/molK)	Th. Corr.	Tot. Energy (Hart.)	S (cal/molK)	H (kcal/mol)
As	48.53	0.005700	-2234.24009	48.478	73.065
HCl	54.512	0.016729	-460.3139799	54.685	-15.495
AsCl	71.55	0.013383	-2694.002132	-	-
H	34.309	0.005700	-0.4941179	34.345	56.585
1500 K					
	Theoretical			Experimental	
Species	S (cal/molK)	Th. Corr.	Tot. Energy (Hart.)	S (cal/molK)	H (kcal/mol)
As	49.639	0.007125	-2234.238665	49.578	74.544
HCl	56.263	0.019533	-460.3111759	56.453	-13.098
AsCl	73.538	0.016692	-2693.998823	-	-
H	35.418	0.007125	-0.4926929	35.445	58.074
2000 K					
	Theoretical			Experimental	
Species	S (cal/molK)	Th. Corr.	Tot. Energy (Hart.)	S (cal/molK)	H (kcal/mol)
As	51.068	0.009500	-2234.23629	50.996	77.010
HCl	58.612	0.024460	-460.3062489	58.867	-8.927
AsCl	76.104	0.022217	-2693.993298	-	-
H	36.847	0.009500	-0.4903179	36.879	60.557

D.4. As + O → AsO (QCISD(T)/ECP28MWB)

Theoretical				
Temp (K)	ΔS (cal/molK)	ΔH (kcal/mol)	ΔG (kcal/mol)	K_{eq}
298.15	-23.040	-109.330	-102.460	1.283×10^{75}
600	-24.466	-109.930	-95.250	4.966×10^{34}
900	-25.053	-110.361	-87.814	2.113×10^{21}
1200	-25.410	-110.732	-80.240	4.113×10^{14}
1500	-25.665	-111.075	-72.578	3.758×10^{10}
2000	-25.977	-111.618	-59.664	3.311×10^6
Experimental				
Temp (K)	ΔS (cal/molK)	ΔH (kcal/mol)	ΔG (kcal/mol)	K_{eq}
298.15	-25.067	-141.864	-134.390	3.268×10^{98}
600	-26.118	-142.286	-126.615	1.322×10^{46}
900	-26.419	-142.515	-118.737	6.829×10^{28}
1200	-26.604	-142.710	-110.786	1.505×10^{20}
1500	-26.764	-142.909	-102.763	9.400×10^{14}
2000	-26.956	-143.279	-89.368	5.835×10^9

298.15 K					
	Theoretical			Experimental	
Species	S (cal/molK)	Enth. Corr.	Tot. Energy (Hart.)	S (cal/molK)	H (kcal/mol)
As	41.612	0.002360	-6.0427572	41.611	68.619
O	36.438	0.002360	-74.9696608	38.492	59.553
AsO	55.010	0.005422	-81.1866459	55.036	-13.692
600 K					
	Theoretical			Experimental	
Species	S (cal/molK)	Enth. Corr.	Tot. Energy (Hart.)	S (cal/molK)	H (kcal/mol)
As	45.087	0.004750	-6.0403672	45.062	70.108
O	39.912	0.004750	-74.9672708	42.089	61.097
AsO	60.533	0.009246	-81.1828219	61.033	-11.081
900 K					
	Theoretical			Experimental	
Species	S (cal/molK)	Enth. Corr.	Tot. Energy (Hart.)	S (cal/molK)	H (kcal/mol)
As	47.101	0.007125	-6.0379922	47.060	71.587
O	41.926	0.007125	-74.9648958	44.120	62.608
AsO	63.974	0.013308	-81.1787599	64.761	-8.320
1200 K					
	Theoretical			Experimental	
Species	S (cal/molK)	Enth. Corr.	Tot. Energy (Hart.)	S (cal/molK)	H (kcal/mol)
As	48.53	0.009500	-6.0356172	48.478	73.065
O	43.356	0.009500	-74.9625208	45.554	64.106
AsO	66.476	0.017468	-81.1745999	67.429	-5.539
1500 K					
	Theoretical			Experimental	
Species	S (cal/molK)	Enth. Corr.	Tot. Energy (Hart.)	S (cal/molK)	H (kcal/mol)
As	49.639	0.011876	-6.0332412	49.578	74.544
O	44.464	0.011876	-74.9601448	46.678	65.600
AsO	68.438	0.021672	-81.1703959	69.492	-2.765
2000 K					
	Theoretical			Experimental	
Species	S (cal/molK)	Enth. Corr.	Tot. Energy (Hart.)	S (cal/molK)	H (kcal/mol)
As	51.068	0.015834	-6.0292832	50.996	77.010
O	45.893	0.015834	-74.9561868	48.088	68.086
AsO	70.984	0.028724	-81.1633439	72.129	1.816

D.5. As + OH → AsH + O (QCISD/ECP28MWB)

Theoretical				
Temp (K)	ΔS (cal/molK)	ΔH (kcal/mol)	ΔG (kcal/mol)	K_{eq}
298.15	1.95	33.500	32.919	7.396×10^{-25}
600	2.006	33.530	32.326	1.678×10^{-12}
900	2.177	33.660	31.700	2.004×10^{-8}
1200	2.365	33.855	31.017	2.243×10^{-6}
1500	2.514	34.057	30.286	3.865×10^{-5}
Experimental				
Temp (K)	ΔS (cal/molK)	ΔH (kcal/mol)	ΔG (kcal/mol)	K_{eq}
298.15	2.714	37.255	36.446	1.921×10^{-27}
600	2.874	37.320	35.595	1.081×10^{-13}
900	3.094	37.497	34.712	3.720×10^{-9}
1200	3.311	37.731	33.758	7.105×10^{-7}
1500	3.495	37.964	32.721	1.708×10^{-5}

298.15 K					
	Theoretical			Experimental	
Species	S (cal/molK)	Enth. Corr.	Tot. Energy (Hart.)	S (cal/molK)	H (kcal/mol)
As	41.612	0.002360	-6.0427361	41.611	68.619
OH	42.553	0.011965	-75.6226291	43.908	9.319
AsH	49.677	0.008400	-6.6454387	49.741	55.640
O	36.438	0.002360	-74.9665405	38.492	59.553
600 K					
	Theoretical			Experimental	
Species	S (cal/molK)	Enth. Corr.	Tot. Energy (Hart.)	S (cal/molK)	H (kcal/mol)
As	45.087	0.004750	-6.0403461	45.062	70.108
OH	47.419	0.015312	-75.6192821	48.853	11.456
AsH	54.600	0.011794	-6.6420447	54.700	57.787
O	39.912	0.004750	-74.9641505	42.089	61.097
900 K					
	Theoretical			Experimental	
Species	S (cal/molK)	Enth. Corr.	Tot. Energy (Hart.)	S (cal/molK)	H (kcal/mol)
As	47.101	0.007125	-6.0379711	47.060	71.587
OH	50.27	0.018675	-75.6159191	51.745	13.595
AsH	57.622	0.015364	-6.6384747	57.779	60.070
O	41.926	0.007125	-74.9617755	44.120	62.608
1200 K					
	Theoretical			Experimental	
Species	S (cal/molK)	Enth. Corr.	Tot. Energy (Hart.)	S (cal/molK)	H (kcal/mol)
As	48.53	0.009500	-6.0355961	48.478	73.065
OH	52.355	0.022144	-75.6124501	53.872	15.810
AsH	59.894	0.019145	-6.6346937	60.106	62.500
O	43.356	0.009500	-74.9594005	45.554	64.106
1500 K					
	Theoretical			Experimental	
Species	S (cal/molK)	Enth. Corr.	Tot. Energy (Hart.)	S (cal/molK)	H (kcal/mol)
As	49.639	0.011876	-6.0332201	49.578	74.544
OH	54.037	0.025750	-75.6088441	55.593	18.124
AsH	61.726	0.023072	-6.6307667	61.988	65.032
O	44.464	0.011876	-74.9570245	46.678	65.600

D.6. Se + O₂ → SeO + O (CCSD/RECP28VDZ)

Theoretical				
Temp (K)	ΔS (cal/molK)	ΔH (kcal/mol)	ΔG (kcal/mol)	K _{eq}
298.15	2.362	17.640	16.936	3.848x10 ⁻¹³
600	2.904	17.879	16.136	1.325x10 ⁻⁶
900	3.195	18.093	15.217	2.017x10 ⁻⁴
1200	3.337	18.238	14.234	2.556x10 ⁻³
1500	3.412	18.337	13.219	1.185x10 ⁻²
2000	3.473	18.444	11.498	5.540x10 ⁻²
Experimental				
Temp (K)	ΔS (cal/molK)	ΔH (kcal/mol)	ΔG (kcal/mol)	K _{eq}
298.15	3.169	18.203	17.258	2.233x10 ⁻¹³
600	3.592	18.380	16.225	1.230x10 ⁻⁶
900	3.676	18.437	15.129	2.119x10 ⁻⁴
1200	3.629	18.395	14.041	2.771x10 ⁻³
1500	3.550	18.272	12.947	1.299x10 ⁻²
2000	3.323	17.912	11.266	5.873x10 ⁻²

298.15 K					
	Theoretical			Experimental	
Species	S (cal/molK)	Th. Corr.	Tot. Energy (Hart.)	S (cal/molK)	H (kcal/mol)
Se	41.233	0.001416	-9.1444397	42.236	56.25
O ₂	48.953	0.006203	-150.1039811	49.013	0
SeO	56.110	0.004359	-84.2529517	55.926	14.900
O	36.438	0.001416	-74.9673578	38.492	59.553
600 K					
	Theoretical			Experimental	
Species	S (cal/molK)	Th. Corr.	Tot. Energy (Hart.)	S (cal/molK)	H (kcal/mol)
Se	44.707	0.002850	-9.1430057	45.839	57.810
O ₂	53.991	0.008728	-150.1014561	54.159	2.228
SeO	61.690	0.007264	-84.2500467	61.501	17.321
O	39.912	0.002850	-74.9659238	42.089	61.097
900 K					
	Theoretical			Experimental	
Species	S (cal/molK)	Th. Corr.	Tot. Energy (Hart.)	S (cal/molK)	H (kcal/mol)
Se	46.722	0.004275	-9.1415807	48.010	59.418
O ₂	57.159	0.011522	-150.0986621	57.361	4.610
SeO	65.150	0.010399	-84.2469117	64.927	19.858
O	41.926	0.004275	-74.9644988	44.120	62.608
1200 K					
	Theoretical			Experimental	
Species	S (cal/molK)	Th. Corr.	Tot. Energy (Hart.)	S (cal/molK)	H (kcal/mol)
Se	48.151	0.005700	-9.1401557	49.588	61.064
O ₂	59.529	0.014514	-150.0956701	59.751	7.098
SeO	67.661	0.013623	-84.2436877	67.414	22.452
O	43.356	0.005700	-74.9630738	45.554	64.106
1500 K					
	Theoretical			Experimental	
Species	S (cal/molK)	Th. Corr.	Tot. Energy (Hart.)	S (cal/molK)	H (kcal/mol)
Se	49.259	0.007125	-9.1387307	50.838	62.745
O ₂	61.420	0.017618	-150.0925661	61.663	9.670
SeO	69.627	0.016885	-84.2404257	69.374	25.088
O	44.464	0.007125	-74.9616488	46.678	65.600
2000 K					
	Theoretical			Experimental	
Species	S (cal/molK)	Th. Corr.	Tot. Energy (Hart.)	S (cal/molK)	H (kcal/mol)
Se	50.689	0.009500	-9.1363557	52.492	65.622
O ₂	63.907	0.022926	-150.0872581	64.221	14.116
SeO	72.176	0.022363	-84.2349477	71.947	29.563
O	45.893	0.009500	-74.9592738	48.088	68.086

D.7. Se + O → SeO (QCISD(T)/6-311++G(3df,3pd))

Theoretical				
Temp (K)	ΔS (cal/molK)	ΔH (kcal/mol)	ΔG (kcal/mol)	K_{eq}
298.15	-21.653	-100.555	-94.099	9.528×10^{68}
600	-23.088	-101.159	-87.307	6.346×10^{31}
900	-23.679	-101.593	-80.282	3.132×10^{19}
1200	-24.037	-101.965	-73.121	2.078×10^{13}
1500	-24.292	-102.310	-65.872	3.961×10^9
2000	-24.606	-102.852	-53.640	7.274×10^5
Experimental				
Temp (K)	ΔS (cal/molK)	ΔH (kcal/mol)	ΔG (kcal/mol)	K_{eq}
298.15	-24.802	-100.903	-93.508	3.515×10^{68}
600	-26.427	-101.587	-85.731	1.692×10^{31}
900	-27.203	-102.168	-77.684	7.329×10^{18}
1200	-27.729	-102.718	-69.444	4.445×10^{12}
1500	-28.142	-103.257	-61.044	7.842×10^8
2000	-28.632	-104.144	-46.879	1.327×10^5

298.15 K					
	Theoretical			Experimental	
Species	S (cal/molK)	Enth. Corr.	Tot. Energy (Hart.)	S (cal/molK)	H (kcal/mol)
Se	41.233	0.002360	-2399.911427	42.236	56.250
O	36.438	0.002360	-74.9696608	38.492	59.553
SeO	56.018	0.005442	-2475.041332	55.926	14.900
600 K					
	Theoretical			Experimental	
Species	S (cal/molK)	Enth. Corr.	Tot. Energy (Hart.)	S (cal/molK)	H (kcal/mol)
Se	44.707	0.004750	-2399.909037	45.839	57.810
O	39.912	0.004750	-74.9672708	42.089	61.097
SeO	61.531	0.009259	-2475.037515	61.501	17.321
900 K					
	Theoretical			Experimental	
Species	S (cal/molK)	Enth. Corr.	Tot. Energy (Hart.)	S (cal/molK)	H (kcal/mol)
Se	46.722	0.007125	-2399.906662	48.010	59.418
O	41.926	0.007125	-74.9648958	44.120	62.608
SeO	64.969	0.013318	-2475.033456	64.927	19.858
1200 K					
	Theoretical			Experimental	
Species	S (cal/molK)	Enth. Corr.	Tot. Energy (Hart.)	S (cal/molK)	H (kcal/mol)
Se	48.151	0.009500	-2399.904287	49.588	61.064
O	43.356	0.009500	-74.9625208	45.554	64.106
SeO	67.470	0.017475	-2475.029299	67.414	22.452
1500 K					
	Theoretical			Experimental	
Species	S (cal/molK)	Enth. Corr.	Tot. Energy (Hart.)	S (cal/molK)	H (kcal/mol)
Se	49.259	0.011876	-2399.901911	50.838	62.745
O	44.464	0.011876	-74.9601448	46.678	65.600
SeO	69.431	0.021678	-2475.025096	69.374	25.088
2000 K					
	Theoretical			Experimental	
Species	S (cal/molK)	Enth. Corr.	Tot. Energy (Hart.)	S (cal/molK)	H (kcal/mol)
Se	50.689	0.015834	-2399.897953	52.492	65.622
O	45.893	0.015834	-74.9561868	48.088	68.086
SeO	71.976	0.028729	-2475.018045	71.947	29.563

D.8. Se + OCl → SeO + Cl (CCSD/RECP28VDZ)

Theoretical				
Temp (K)	ΔS (cal/molK)	ΔH (kcal/mol)	ΔG (kcal/mol)	K_{eq}
298.15	0.061	-35.899	-35.917	2.132×10^{-26}
600	0.077	-35.892	-35.939	1.233×10^{13}
900	0.08	-35.889	-35.961	5.404×10^8
1200	0.082	-33.502	-33.601	1.317×10^6
1500	0.085	-35.886	-36.013	1.767×10^5
2000	0.084	-35.884	-36.052	8.705×10^3
Experimental				
Temp (K)	ΔS (cal/molK)	ΔH (kcal/mol)	ΔG (kcal/mol)	K_{eq}
298.15	-0.997	-36.551	-36.253	3.762×10^{-26}
600	-0.877	-36.496	-35.970	1.266×10^{13}
900	-0.913	-36.532	-35.710	4.698×10^8
1200	-1.032	-36.650	-35.412	2.816×10^6
1500	-1.158	-36.819	-35.081	1.293×10^5
2000	-1.362	-37.172	-34.448	5.814×10^3

298.15 K					
	Theoretical			Experimental	
Species	S (cal/molK)	Enth. Corr.	Tot. Energy (Hart.)	S (cal/molK)	H (kcal/mol)
Se	41.233	0.002360	-9.1434957	42.236	56.250
OCl	52.780	0.005333	-534.7056402	54.171	24.192
SeO	56.110	0.005303	-84.2520077	55.926	14.900
Cl	37.964	0.002360	-459.6543364	39.484	28.991
600 K					
	Theoretical			Experimental	
Species	S (cal/molK)	Enth. Corr.	Tot. Energy (Hart.)	S (cal/molK)	H (kcal/mol)
Se	44.707	0.004750	-9.1411057	45.839	57.810
OCl	58.344	0.009185	-534.7017882	59.775	26.625
SeO	61.690	0.009165	-84.2481457	61.501	17.321
Cl	41.438	0.004750	-459.6519464	43.236	30.619
900 K					
	Theoretical			Experimental	
Species	S (cal/molK)	Enth. Corr.	Tot. Energy (Hart.)	S (cal/molK)	H (kcal/mol)
Se	46.722	0.007125	-9.1387307	48.010	59.418
OCl	61.800	0.013264	-534.6977092	63.265	29.209
SeO	65.150	0.013250	-84.2440607	64.927	19.858
Cl	43.452	0.007125	-459.6495714	45.435	32.237
1200 K					
	Theoretical			Experimental	
Species	S (cal/molK)	Enth. Corr.	Tot. Energy (Hart.)	S (cal/molK)	H (kcal/mol)
Se	48.151	0.009500	-9.1363557	49.588	61.064
OCl	64.309	0.013634	-534.6973392	65.798	31.862
SeO	67.661	0.017423	-84.2398877	67.414	22.452
Cl	44.881	0.009500	-459.6471964	46.941	33.824
1500 K					
	Theoretical			Experimental	
Species	S (cal/molK)	Enth. Corr.	Tot. Energy (Hart.)	S (cal/molK)	H (kcal/mol)
Se	49.259	0.011876	-9.1339797	50.838	62.745
OCl	66.273	0.021644	-534.6893292	67.806	34.548
SeO	69.627	0.021635	-84.2356757	69.374	25.088
Cl	45.990	0.011876	-459.6448204	48.112	35.387
2000 K					
	Theoretical			Experimental	
Species	S (cal/molK)	Enth. Corr.	Tot. Energy (Hart.)	S (cal/molK)	H (kcal/mol)
Se	50.689	0.015834	-9.1300217	52.492	65.622
OCl	68.822	0.028704	-534.6822692	70.411	39.073
SeO	72.176	0.028697	-84.2286137	71.947	29.563
Cl	47.419	0.015834	-459.6408624	49.594	37.959

D.9. Se + O₂ → SeO₂ (QCISD(T)/6-311++G(3df,3pd))

Theoretical				
Temp (K)	ΔS (cal/molK)	ΔH (kcal/mol)	ΔG (kcal/mol)	K _{eq}
298.15	-27.498	-82.345	-74.147	2.254x10 ⁻⁵⁴
600	-28.131	-81.993	-65.114	5.231x10 ⁻²³
900	-28.176	-81.427	-56.069	4.129x10 ¹³
1200	-28.172	-80.826	-47.020	3.662x10 ⁸
1500	-28.164	-80.2199	-37.974	3.412x10 ⁵
2000	-28.156	-79.212	-22.900	3.180x10 ²
Experimental				
Temp (K)	ΔS (cal/molK)	ΔH (kcal/mol)	ΔG (kcal/mol)	K _{eq}
298.15	-28.488	-82.450	-73.956	1.635x10 ⁻⁵⁴
600	-29.187	-82.730	-65.218	5.707x10 ⁻²³
900	-29.409	-82.902	-56.434	5.063x10 ¹³
1200	-29.549	-83.041	-47.582	4.635x10 ⁸
1500	-29.633	-83.152	-38.703	4.357x10 ⁵
2000	-29.706	-83.273	-23.860	4.050x10 ²

298.15 K					
	Theoretical			Experimental	
Species	S (cal/molK)	Th. Corr.	Tot. Energy (Hart.)	S (cal/molK)	H (kcal/mol)
Se	41.233	0.001416	-2399.912371	42.236	56.250
O ₂	48.994	0.006003	-150.1229808	49.013	0
SeO ₂	62.729	0.008663	-2550.166577	62.761	-26.200
600 K					
	Theoretical			Experimental	
Species	S (cal/molK)	Th. Corr.	Tot. Energy (Hart.)	S (cal/molK)	H (kcal/mol)
Se	44.707	0.002850	-2399.910937	45.839	57.810
O ₂	54.063	0.008550	-150.1204338	54.159	2.228
SeO ₂	70.639	0.013206	-2550.162034	70.810	-22.692
900 K					
	Theoretical			Experimental	
Species	S (cal/molK)	Th. Corr.	Tot. Energy (Hart.)	S (cal/molK)	H (kcal/mol)
Se	46.722	0.004275	-2399.909512	48.010	59.418
O ₂	57.26	0.011378	-150.1176058	57.361	4.610
SeO ₂	75.806	0.018360	-2550.15688	75.962	-18.873
1200 K					
	Theoretical			Experimental	
Species	S (cal/molK)	Th. Corr.	Tot. Energy (Hart.)	S (cal/molK)	H (kcal/mol)
Se	48.151	0.005700	-2399.908087	49.588	61.064
O ₂	59.646	0.014397	-150.1145868	59.751	7.098
SeO ₂	79.625	0.023762	-2550.151478	79.790	-14.878
1500 K					
	Theoretical			Experimental	
Species	S (cal/molK)	Th. Corr.	Tot. Energy (Hart.)	S (cal/molK)	H (kcal/mol)
Se	49.259	0.007125	-2399.906662	50.838	62.745
O ₂	61.547	0.017520	-150.1114638	61.663	9.670
SeO ₂	82.642	0.029276	-2550.145964	82.869	-10.737
2000 K					
	Theoretical			Experimental	
Species	S (cal/molK)	Th. Corr.	Tot. Energy (Hart.)	S (cal/molK)	H (kcal/mol)
Se	50.689	0.009500	-2399.904287	52.492	65.622
O ₂	64.041	0.022850	-150.1061338	64.221	14.116
SeO ₂	86.574	0.038587	-2550.136653	87.006	-3.535

D.10. $\text{SeO} + \text{O} \rightarrow \text{SeO}_2$ (QCISD(T)/6-311++G(3df,3pd))

Theoretical				
Temp (K)	ΔS (cal/molK)	ΔH (kcal/mol)	ΔG (kcal/mol)	K_{eq}
298.15	-29.727	-97.038	-88.175	4.329×10^{64}
600	-30.804	-97.482	-79.000	5.981×10^{28}
900	-31.089	-97.689	-69.709	8.479×10^{16}
1200	-31.201	-97.802	-60.361	9.855×10^{10}
1500	-31.253	-97.875	-50.995	2.693×10^7
2000	-31.295	-97.947	-35.357	7.307×10^3
Experimental				
Temp (K)	ΔS (cal/molK)	ΔH (kcal/mol)	ΔG (kcal/mol)	K_{eq}
298.15	-31.657	-100.653	-91.213	7.321×10^{66}
600	-32.780	-101.110	-81.442	4.638×10^{29}
900	-33.085	-101.339	-71.562	2.389×10^{17}
1200	-33.178	-101.436	-61.623	1.673×10^{11}
1500	-33.183	-101.424	-51.650	3.355×10^7
2000	-33.029	-101.184	-35.126	6.896×10^3

298.15 K					
	Theoretical			Experimental	
Species	S (cal/molK)	Enth. Corr.	Tot. Energy (Hart.)	S (cal/molK)	H (kcal/mol)
SeO	56.018	0.005442	-2475.041332	55.926	14.900
O	36.438	0.002360	-74.9696608	38.492	59.553
SeO ₂	62.729	0.009607	-2550.165633	62.761	-26.200
600 K					
	Theoretical			Experimental	
Species	S (cal/molK)	Enth. Corr.	Tot. Energy (Hart.)	S (cal/molK)	H (kcal/mol)
SeO	61.531	0.009259	-2475.037515	61.501	17.321
O	39.912	0.004750	-74.9672708	42.089	61.097
SeO ₂	70.639	0.015106	-2550.160134	70.810	-22.692
900 K					
	Theoretical			Experimental	
Species	S (cal/molK)	Enth. Corr.	Tot. Energy (Hart.)	S (cal/molK)	H (kcal/mol)
SeO	64.969	0.013318	-2475.033456	64.927	19.858
O	41.926	0.007125	-74.9648958	44.120	62.608
SeO ₂	75.806	0.021210	-2550.15403	75.962	-18.873
1200 K					
	Theoretical			Experimental	
Species	S (cal/molK)	Enth. Corr.	Tot. Energy (Hart.)	S (cal/molK)	H (kcal/mol)
SeO	67.47	0.017475	-2475.029299	67.414	22.452
O	43.356	0.009500	-74.9625208	45.554	64.106
SeO ₂	79.625	0.027562	-2550.147678	79.790	-14.878
1500 K					
	Theoretical			Experimental	
Species	S (cal/molK)	Enth. Corr.	Tot. Energy (Hart.)	S (cal/molK)	H (kcal/mol)
SeO	69.431	0.021678	-2475.025096	69.374	25.088
O	44.464	0.011876	-74.9601448	46.678	65.600
SeO ₂	82.642	0.034026	-2550.141214	82.869	-10.737
2000 K					
	Theoretical			Experimental	
Species	S (cal/molK)	Enth. Corr.	Tot. Energy (Hart.)	S (cal/molK)	H (kcal/mol)
SeO	71.976	0.028729	-2475.018045	71.947	29.563
O	45.893	0.015834	-74.9561868	48.088	68.086
SeO ₂	86.574	0.044920	-2550.13032	87.006	-3.535

D.11. $\text{SeO} + \text{O}_2 \rightarrow \text{SeO}_2 + \text{O}$ (QCISD(T)/ECP28MWB)

Theoretical				
Temp (K)	ΔS (cal/molK)	ΔH (kcal/mol)	ΔG (kcal/mol)	K_{eq}
298.15	-5.828	18.671	20.409	1.095×10^{-15}
600	-4.963	19.056	22.033	9.420×10^{-9}
900	-4.389	19.479	23.429	2.044×10^{-6}
1200	-4.014	19.868	24.684	3.193×10^{-5}
1500	-3.746	20.230	25.849	1.713×10^{-4}
2000	-3.419	20.795	27.633	9.556×10^{-4}
Experimental				
Temp (K)	ΔS (cal/molK)	ΔH (kcal/mol)	ΔG (kcal/mol)	K_{eq}
298.15	-3.686	18.453	19.552	4.651×10^{-15}
600	-2.761	18.856	20.513	3.372×10^{-8}
900	-2.206	19.266	21.251	6.908×10^{-6}
1200	-1.820	19.678	21.862	1.043×10^{-4}
1500	-1.491	20.105	22.341	5.556×10^{-4}
2000	-1.074	20.871	23.019	3.052×10^{-3}

298.15 K					
	Theoretical			Experimental	
Species	S (cal/molK)	Th. Corr.	Tot. Energy (Hart.)	S (cal/molK)	H (kcal/mol)
SeO	56.029	0.004447	-84.2729022	55.926	14.900
O ₂	48.994	0.006003	-150.1229808	49.013	0
SeO ₂	62.757	0.008448	-159.3955242	62.761	-26.200
O	36.438	0.001416	-74.9706048	38.492	59.553
600 K					
	Theoretical			Experimental	
Species	S (cal/molK)	Th. Corr.	Tot. Energy (Hart.)	S (cal/molK)	H (kcal/mol)
SeO	61.566	0.007324	-84.2700252	61.501	17.321
O ₂	54.063	0.00855	-150.1204338	54.159	2.228
SeO ₂	70.754	0.013051	-159.3909212	70.810	-22.692
O	39.912	0.00285	-74.9691708	42.089	61.097
900 K					
	Theoretical			Experimental	
Species	S (cal/molK)	Th. Corr.	Tot. Energy (Hart.)	S (cal/molK)	H (kcal/mol)
SeO	65.012	0.010442	-84.2669072	64.927	19.858
O ₂	57.26	0.011378	-150.1176058	57.361	4.610
SeO ₂	75.957	0.018247	-159.3857252	75.962	-18.873
O	41.926	0.004275	-74.9677458	44.120	62.608
1200 K					
	Theoretical			Experimental	
Species	S (cal/molK)	Th. Corr.	Tot. Energy (Hart.)	S (cal/molK)	H (kcal/mol)
SeO	67.516	0.013656	-84.2636932	67.414	22.452
O ₂	59.646	0.014397	-150.1145868	59.751	7.098
SeO ₂	79.792	0.023674	-159.3802982	79.790	-14.878
O	43.356	0.0057	-74.9663208	45.554	64.106
1500 K					
	Theoretical			Experimental	
Species	S (cal/molK)	Th. Corr.	Tot. Energy (Hart.)	S (cal/molK)	H (kcal/mol)
SeO	69.479	0.016912	-84.2604372	69.374	25.088
O ₂	61.547	0.01752	-150.1114638	61.663	9.670
SeO ₂	82.816	0.029205	-159.3747672	82.869	-10.737
O	44.464	0.007125	-74.9648958	46.678	65.600
2000 K					
	Theoretical			Experimental	
Species	S (cal/molK)	Th. Corr.	Tot. Energy (Hart.)	S (cal/molK)	H (kcal/mol)
SeO	72.026	0.022383	-84.2549662	71.947	29.563
O ₂	64.041	0.02285	-150.1061338	64.222	14.116
SeO ₂	86.755	0.038532	-159.3654402	87.006	-3.535
O	45.893	0.0095	-74.9625208	48.088	68.086

D.12. Se + H₂ → SeH₂ (CCSD(T)/6-311++G(3df,3pd))

Theoretical				
Temp (K)	ΔS (cal/molK)	ΔH (kcal/mol)	ΔG (kcal/mol)	K _{eq}
298.15	-19.995	-49.973	-44.011	1.829x10 ⁻³²
600	-22.18	-50.295	-36.987	2.971x10 ⁻¹³
900	-22.927	-50.238	-29.604	1.545x10 ⁻⁷
1200	-23.173	-49.894	-22.086	1.053x10 ⁻⁴
1500	-23.242	-49.388	-14.525	1.307x10 ⁻²
2000	-23.245	-48.397	-1.907	1.616
Experimental				
Temp (K)	ΔS (cal/molK)	ΔH (kcal/mol)	ΔG (kcal/mol)	K _{eq}
298.15	-21.143	-49.250	-42.946	3.030x10 ⁻³¹
600	-23.394	-50.203	-36.166	1.493x10 ⁻¹³
900	-24.329	-50.883	-28.987	1.094x10 ⁻⁷
1200	-24.761	-51.338	-21.624	8.679x10 ⁻³
1500	-24.945	-51.598	-14.181	1.165x10 ⁻²
2000	-24.962	-51.604	-1.679	1.526

298.15 K					
	Theoretical			Experimental	
Species	S (cal/molK)	Th. Corr.	Tot. Energy (Hart.)	S (cal/molK)	H (kcal/mol)
Se	41.233	0.001416	-2399.912342	42.236	56.250
H ₂	31.130	0.012390	-1.1601443	31.233	0
SeH ₂	52.368	0.016517	-2401.152123	52.326	7.000
600 K					
	Theoretical			Experimental	
Species	S (cal/molK)	Th. Corr.	Tot. Energy (Hart.)	S (cal/molK)	H (kcal/mol)
Se	44.707	0.002850	-2399.910908	45.839	57.810
H ₂	35.994	0.014780	-1.1577543	36.114	2.106
SeH ₂	58.521	0.019828	-2401.148812	58.559	9.713
900 K					
	Theoretical			Experimental	
Species	S (cal/molK)	Th. Corr.	Tot. Energy (Hart.)	S (cal/molK)	H (kcal/mol)
Se	46.722	0.004275	-2399.909483	48.010	59.418
H ₂	38.828	0.017172	-1.1553623	38.982	4.226
SeH ₂	62.623	0.023735	-2401.144905	62.663	12.761
1200 K					
	Theoretical			Experimental	
Species	S (cal/molK)	Th. Corr.	Tot. Energy (Hart.)	S (cal/molK)	H (kcal/mol)
Se	48.151	0.005700	-2399.908058	49.588	61.064
H ₂	40.879	0.019632	-1.1529023	41.061	6.405
SeH ₂	65.857	0.028169	-2401.140471	65.888	16.131
1500 K					
	Theoretical			Experimental	
Species	S (cal/molK)	Th. Corr.	Tot. Energy (Hart.)	S (cal/molK)	H (kcal/mol)
Se	49.259	0.007125	-2399.906633	50.838	62.745
H ₂	42.521	0.022203	-1.1503313	42.734	8.674
SeH ₂	68.538	0.032970	-2401.13567	68.628	19.821
2000 K					
	Theoretical			Experimental	
Species	S (cal/molK)	Th. Corr.	Tot. Energy (Hart.)	S (cal/molK)	H (kcal/mol)
Se	50.689	0.009500	-2399.904258	52.492	65.622
H ₂	44.730	0.026745	-1.1457893	45.029	12.655
SeH ₂	72.174	0.041467	-2401.127173	72.558	26.673

Bibliography

- ¹ Diaz-Somoano, M.; Martinez-Tarazona, M.R.; Retention of arsenic and selenium compounds using limestone in a coal gasification flue gas. *Environ. Sci. Technol.* 38 (2004) 899-903.
- ² Jadhav, Raja A.; Fan, Liang-Shih. Capture of gas-phase arsenic oxide by lime: kinetic and mechanistic studies. *Environ. Sci. Technol.* 35 (2001) 794-799.
- ³ Agnihotri, R.; Chauk, S.; Mahuli, S.; Fan, L.-S. Selenium removal using Ca-based sorbents: reaction kinetics. *Environ. Sci. Technol.* 32 (1998) 1841-1846.
- ⁴ Querol, X.; Fernandez-Turiel, J.L.; Lopez-Soler, A. Trace elements in coal and their behavior during combustion in a large power station. *Fuel.* 74 (1995) 331-343.
- ⁵ Guo, Xin; Zheng, Chu-Guang; Xu, Ming-Hou. Characterization of arsenic emissions from a coal-fired powered plant. *Energy Fuels.* 18 (2004) 1822-1826.
- ⁶ Andren, A.W.; Klein, D.H.; Taimi, Y. Selenium in coal-fired steam plant emissions. *Environ. Sci. Technol.* 9 (1975) 856-858.
- ⁷ Hindmarsh, J. Thomas, McCurdy, Ross F. Clinical and environmental aspects of arsenic toxicity. *Critical reviews in clinical laboratory sciences.* 23 (2006) 315-347.
- ⁸ Onishi, H. Arsenic, in *Handbook of Geochemistry.* Wedepohl, K.H. Editor, Springer Verlag, New York, NY, 1980.
- ⁹ Han, Fengxiang X., Monts; Su, Yi; David L.; et al. Assessment of global industrial-age anthropogenic arsenic contamination. *Naturwissenschaften.* 90 (2003) 395-401.
- ¹⁰ Matschullat, Jorg. Arsenic in the geosphere-a review. *The Science of the Total Environment.* 249 (2000) 297-312.
- ¹¹ Ratnaike, R. N. Acute and chronic arsenic toxicity. *Postgrad Med J.* 79 (2003) 391-396.
- ¹² Chowdhury, U. K.; Biswas, B. K.; Chowdhury, T. R.; et al. Groundwater arsenic contamination in Bangladesh and West Bengal, India. *Environ Health Perspect.* 108 (2000) 393-397.
- ¹³ Uminska, R. Selenium in human environment. *Roczniki Panstwowego Zakladu Higieny.* 41 (1990) 25-34.
- ¹⁴ Vinceti, Marco; Wei, Edward T.; Malagoli, Carlotta; et al. Adverse health effects of selenium in humans. *Reviews on Environmental Health.* 16 (2001) 233-251.
- ¹⁵ Lemly, Dennis A. Aquatic selenium pollution is a global environmental safety issue. *Ecotoxicology and Environmental Safety.* 59 (2004) 44-56.
- ¹⁶ Hoffman, David J. Role of selenium toxicity and oxidative stress in aquatic birds. *Aquatic Toxicology.* 57 (2002) 11-26.
- ¹⁷ Stout, Jordan. H; Trust, Kimberly A.; Cochrane, Jean F.; et al. Environmental contaminants in four eider species from Alaska and arctic Russia. *Environmental Pollution.* 119 (2002) 215-226.
- ¹⁸ Gamberg, M.; Braune, B. M. Contaminant residue levels in Arctic wolves (*Canis lupus*) from the Yukon Territory, Canada. *Science of the Total Environment.* 243/244 (1999) 329-338.
- ¹⁹ Simons, Jack. An experimental chemist's guide to ab initio quantum chemistry. *J. Phys. Chem.* 95 (1991) 1017-1029.
- ²⁰ Gaussian 03, Revision C.02, Frisch, M. J.; Trucks, G. W.; Schlegel, H. B.; Scuseria, G. E.; Robb, M. A.; Cheeseman, J. R.; Montgomery, Jr., J. A.; Vreven, T.; Kudin, K. N.; Burant, J. C.; Millam, J. M.; Iyengar, S. S.; Tomasi, J.; Barone, V.; Mennucci, B.; Cossi, M.; Scalmani, G.; Rega, N.; Petersson, G. A.; Nakatsuji, H.; Hada, M.; Ehara, M.; Toyota, K.; Fukuda, R.; Hasegawa, J.; Ishida, M.; Nakajima, T.; Honda, Y.; Kitao, O.; Nakai, H.; Klene, M.; Li, X.; Knox, J. E.; Hratchian, H. P.; Cross, J. B.; Bakken, V.; Adamo, C.; Jaramillo, J.; Gomperts, R.; Stratmann, R. E.; Yazyev, O.; Austin, A. J.; Cammi, R.; Pomelli, C.; Ochterski, J. W.; Ayala, P. Y.; Morokuma, K.; Voth, G. A.; Salvador, P.; Dannenberg, J. J.; Zakrzewski, V. G.; Dapprich, S.; Daniels, A. D.; Strain, M. C.; Farkas, O.; Malick, D. K.; Rabuck, A. D.; Raghavachari, K.; Foresman, J. B.; Ortiz, J. V.; Cui, Q.; Baboul, A. G.; Clifford, S.; Cioslowski, J.; Stefanov, B. B.; Liu, G.; Liashenko, A.; Piskorz, P.; Komaromi, I.; Martin, R. L.; Fox, D. J.; Keith, T.; Al-Laham, M. A.; Peng, C. Y.; Nanayakkara, A.; Challacombe, M.; Gill, P. M. W.; Johnson, B.; Chen, W.; Wong, M. W.; Gonzalez, C.; and Pople, J. A.; Gaussian, Inc., Wallingford CT, 2004.
- ²¹ Leach, Andrew R. *Molecular Modeling Principles and Applications (Second Edition).* Pearson Education Limited. London, UK, 2001.
- ²² Hohenberg, P.; Kohn, W. Inhomogeneous Electron Gas. *Physical Review.* B136 (1964) 864-871.
- ²³ Foresman, James B.; et al. *Exploring Chemistry with Electronic Structure Methods (Second Edition).* Gaussian, Inc. Pittsburgh, PA, 1993.
- ²⁴ Levine, Ira. A. *Quantum Chemistry (Fifth Edition).* Prentice Hall. Upper Saddle River, NJ, 2000.
- ²⁵ Eyring, H. The activated complex in chemical reactions. *J. Chem. Phys.* 3 (1935) 107.

-
- ²⁶ E. Wigner. Crossing of potential thresholds in chemical reactions. *Z. Phys. Chem. B* 19 (1932) 203.
- ²⁷ Steinfeld, Jeffery I.; Francisco, Joseph S.; Hase, William L. *Chemical Kinetics and Dynamics* (Second Edition). Prentice Hall. Upper Saddle River, NJ, 1999.
- ²⁸ Beyer, T.; Swinehart, D.F. Algorithm 448. Number of Multiply-Restricted Partitions [A1]. *Commun. ACM* 16 (1973) 379.
- ²⁹ Lide, David R. *CRC Handbook of Chemistry and Physics*. CRC Press, Boca Raton, FL. 2005
- ³⁰ Janszky, J.; Bartram, R.H.; Rossi, A.R.; Corradi, G. Effective-core-potential calculations of sulfur, selenium, and tellurium dioxides and dihydrides. *Chem. Phys Letters*. 124-1 (1986), 26-30.
- ³¹ Batsanov, S.S. Calculation of van der Waals radii of atoms from bond distances. *J. of Molec. Structure*. 468 (1999), 151-159.
- ³² Jordan, A.S.; Robertson, A. Jr. Thermodynamic properties of AsH₃ and its subhydrides. *Journal of Materials Science: Materials in Electronics*. 4 (1993) 215-224.
- ³³ Kruse, H.; Winter, R.; Fink, E.H.; Wildt, J.; Zabel, F. b1Σ⁺ Emissions from group V-VII Diatomic Molecules: b0⁺→X₁0⁺, X₂1 Band Systems of AsCl and AsBr. *Chem. Phys. Letters*. 111-1,2 (1984) 100-104.
- ³⁴ Crowther, Sarah A. The 313nm band system of SeO₂. *J. Molec. Spec.* 225 (2004) 196-205.
- ³⁵ Rautiainen, J. Mikko; Way, Todd; Schatte, Gabriele; Passmore, Jack; Laitinen, Risto S.; Suontamo, Reijo J.; Valkonen, Jussi. A Computational and Experimental Study of the Structures and Raman and ⁷⁷Se NMR Spectra of SeX₃⁺ and SeX₂ (X = Cl, Br, I): FT-Raman Spectrum of (SeI₃)[AsF₆]. *Inorg. Chem.* 44 (2005) 1904-1913.
- ³⁶ Herzberg, Gerhard. *Molecular Spectra and Molecular Spectroscopy: II. Infrared and Raman Spectra of Polyatomic Molecules*. D. Van Nostrand Company, Inc. Toronto, Canada, 1945.
- ³⁷ Shaulov, Yu.; Mosin, A.M. Thermodynamic functions of arsenic chloride, arsenic dichloride, and arsenic trichloride. *Zh. Fizich. Khimii*. 41 (1973) 1135-1136.
- ³⁸ Pankratov, A.N.; Uchaeva, I.M. A semiempirical quantum chemical testing of thermodynamic and molecular properties of arsenic compounds. *J. Mol. Struct.* 498 (2000) 247-254.
- ³⁹ Oppermann, H.; Schmidt, P.; Quoc, H. Dao; Popovkin, B.A.; Berdonosov, P.S.; Dolgikh, V.A. *Z. Anorg. Allg. Chem.* 629 (2003) 523-531.
- ⁴⁰ Barin, I.; Knacke, O.; Kubaschewski, O. *Thermochemical properties of inorganic substances*; Springer-Verlag: Berlin, (1977) p.861.
- ⁴¹ Thermodynamics Research Center, NIST Boulder Laboratories, M. Frenkel Director. "Thermodynamics Source Database" in NIST WebBook, NIST Standard Reference Database Number 69, Eds. P.J. Linstrom and W.G. Mallard, June 2005, National Institute of Standards and Technology, Gaithersburg MD, 20899 (<http://webbook.nist.gov>).
- ⁴² Yan, Rong; et al. Possible interactions between As, Se, and Hg during coal combustion. *Combustion and Flame*. 120 (2000) 49-60.
- ⁴³ Yan, Rong; et al. Fate of selenium in coal combustion: volatilization and speciation in the flue gas. *Environ. Sci. Technol.* 35 (2001) 1406-1410.